PARTIAL-DATA INTERPOLATION DURING ARCING OF AN X-RAY TUBE IN A COMPUTED TOMOGRAPHY SCANNER

JAISINGH RAJWADE

Bachelor of Engineering (B.E.) – Industrial Electronics
University of Pune, India
November 1997

Master of Science in Electrical Engineering
Cleveland State University
August 2001

Submitted in partial fulfillment of requirements for the degree

DOCTOR OF ENGINEERING

at the

CLEVELAND STATE UNIVERSITY
April 2011

This dissertation has been approved
for the Department of Electrical and Computer Engineering
and the College of Graduate Studies by

_____

Dissertation Committee Chairperson, Daniel J. Simon

_____

Electrical Engineering/Date

_____

Zhiqiang Gao

_____

Electrical Engineering /Date

_____

Ana Stankovic

_____

Electrical Engineering /Date

_____

Vijaya Konangi

_____

Electrical Engineering /Date

_____

James A. Lock

_____

Physics/Date

Dedicated to my wife Radhika and kids Anoushka and Veer, a constant source of joy in my life.

ACKNOWLEDGEMENTS

Many thanks go to my advisor, Dr. Dan Simon, for his tireless efforts and guidance during the entire duration of my program of study at CSU. Dr Simon was also my adviser for my masters program, and has been a very special influence in my academic career. Special thanks to my industrial advisor and mentor, Lester Miller, on whose original idea this research is based and who guided me through the entire project. Lester has been my supervisor, guide and friend for all my years at Philips Healthcare and all this would not have been possible without his guidance.

I would also like to thank my employers, the CT engineering management and staff at Philips Healthcare for their support of this research at their facility in Highland Heights, Ohio. Among these I would like to make a special mention of Cliff Van Vliet and Chuck Rooks, my supervisors, for their constant support in allocating time and resources for my dissertation work. I would also like to thank my colleagues Richard Thompson and Randy Luhta, who guided me for a significant part of this project. There were a large number of my friends and colleagues at Philips, both local and from our worldwide divisions that helped in many ways during the whole process that I cannot name individually due to lack of space but still cannot thank enough for their support.

I want to specially thank my wonderful wife Radhika for taking care of our family while I worked through this over the last nine years and supporting me at each step. And lastly, I thank my parents who, despite being far away were always there to push me along whenever I slowed down.

PARTIAL-DATA INTERPOLATION DURING ARCING OF AN X-RAY TUBE IN A COMPUTED TOMOGRAPHY SCANNER

JAISINGH RAJWADE

ABSTRACT

X-ray tubes are used in computed tomography (CT) scanners as the energy source for generation of images. These tubes occasionally tend to arc, an undesired phenomenon where high current surges through the tube. During the time that the x-ray tube recovers to full voltage after an arc, image data is being collected. Normally this data, acquired at less than full voltage, is discarded and interpolation is performed over the arc duration. However, this is not ideal and some residual imperfections in images, called artifacts, still remain. Proposed here is an algorithm that corrects for improper tube voltage, allowing previously discarded data to be used for imaging. Instead of throwing away all data during the arc period, we use some of the data that is available as the voltage is rising back to its programmed value. This method reduces the length of the interpolation period, thus reducing artifacts. Results of implementation on a CT scanner show that there is an improvement in image quality using the partial-data interpolation method when compared to standard interpolation and that we can save up to 30% of data from being lost during an arc. With the continuous drive from the imaging field to have faster scanners with short image acquisition times, adverse effects due to arcing are becoming more significant and the improvement proposed in this research is increasingly relevant.

TABLE OF CONTENTS

Page

NOMENCLATURE

CT: Computed Tomography

MRI: Magnetic Resonance Imaging

PET: Positron Emission Tomography

DSP: Digital Signal Processor

IP: Integration Period

CTDI: Computed Tomography Dose Index

KV: Kilovolts

LAN: Local Area Network

LIST OF TABLES

Table Page

LIST OF FIGURES

Figure Page

CHAPTER 1

INTRODUCTION

X –ray tubes are the energy source for generation of images on a Computed Tomography (CT) scanner. X-rays pass through the patient, undergo attenuation through the patient's body and the attenuated rays are collected on detectors located on the other side of the patient. These detectors convert the attenuated rays into electrical data, which are then converted to images using mathematical computations. This is the principle of computed tomography. Figure 1 shows a basic block diagram (adapted from [1]), of the CT subsystems and their interaction.

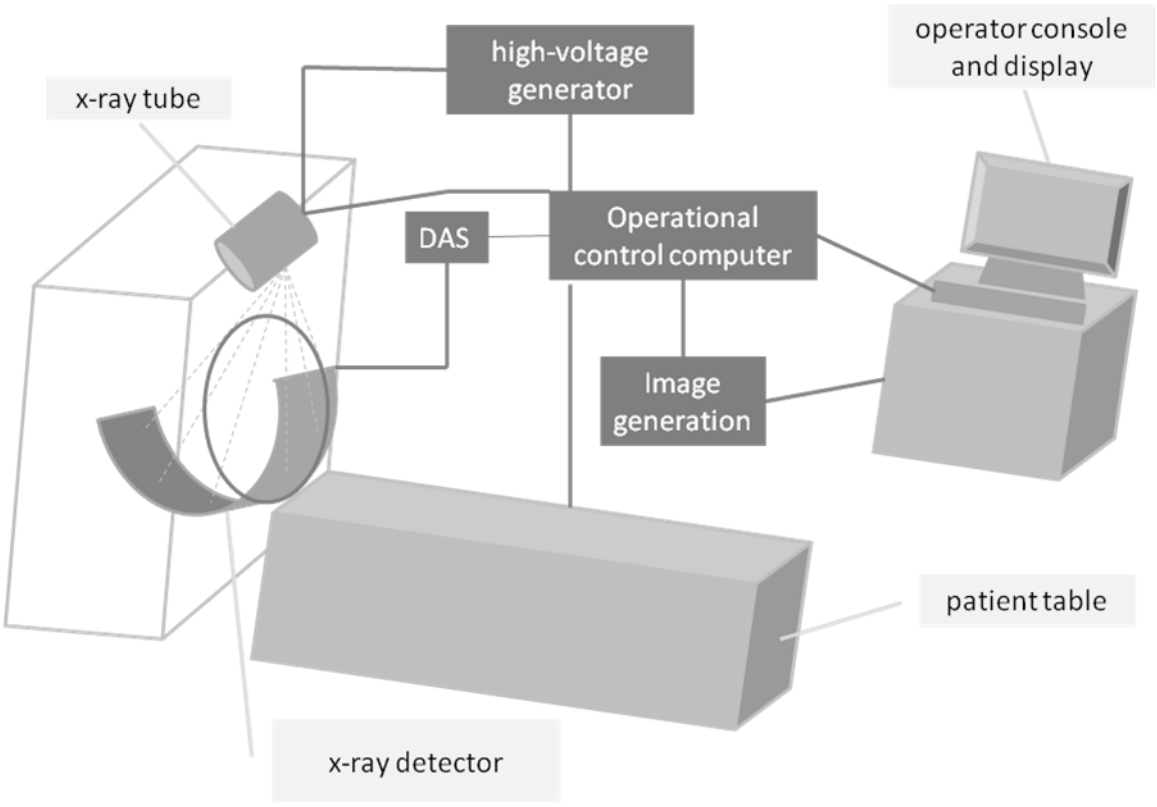

Figure 1: CT Block Diagram, Adapted From [1]

The X-ray tube and high voltage generator (power supply) together make up the X-ray system, the tube being controlled by the generator. The power supply provides the high voltage potential across the vacuum in the tube which causes the electrons from the cathode to accelerate towards the anode. The impact of the electron beam when it collides with the high density anode material results in the generation of X-rays. The generator is also the component that detects an arc event inside the tube and the detector system sees data relating to the event during a scan.

1.1 Goals

The purpose of this research was to implement and evaluate a new algorithm of interpolation in reconstruction of images on a CT scanner during arc events of the X-ray Tube. Specific aims are as follows:

a) Simulate arcs and study differences on images with and without interpolation

When a CT scan is performed, the system is performing an X-ray exposure. The X-ray beams pass through the patient and are collected as attenuated energy on the detector system. The detector system converts these attenuated X-ray energies into coefficients or Hounsfield units (a quantitative scale for describing attenuation coefficient measurement) in a data file. The reconstruction algorithms are then performed on this data to reconstruct images for the user. The data from the detector system, or raw data as unprocessed data is sometimes called, has information about the scan in its file header, which contains details like the time and position of the X-ray beam when the data is collected. This header also contains a status bit that has information about the arc (high when arc occurred, low when no arc or vice versa since this can vary on design definitions), corresponding to a data frame duration. A data frame is the data that is collected at each time sample, which is dependent on the rotation and sampling speeds of the scanner and data acquisition

systems respectively. Every data frame header has an arc status, which will be set active for the duration of the arc, which can be measured by the number of data frames that it remains active for. The typical reconstruction algorithm will discard data that corresponds to this arc (all data whose headers have a set or high arc status) and interpolate over the duration of the arc that is depicted in the data header.

My initial studies consisted of taking this raw data and inserting arcs (by setting the arc status high) at random points and then reconstructing the image with this data, thus giving an image that would be obtained with real arcing in the scanner. A large number of these simulations were performed to understand the effect of arcing on images with respect to magnitude, duration and other factors. The arc images were compared with images of the same data without arcs to give an accurate representation of the differences.

b) Identify cases where images during arcs are not of good quality even after using interpolation

After obtaining data from arc simulation, effort was made towards identifying criteria that cause artifacts in the images. Artifacts are misrepresentations of tissue structures seen in medical images. They are caused by a variety of mechanisms such as data acquisition errors, x-ray tube arcing, inability of reconstruction algorithms to represent the anatomy, and the physics of energy-body interaction. Physicians learn to recognize these artifacts to avoid confusing them with real pathology. However, it is the

aim of all imaging equipment manufacturers to minimize artifacts in images to provide accurate information to the physicians for diagnosis.

The reconstruction simulations were done using the reconstruction routine used by the development team at Philips Healthcare which is implemented in the Matlab® platform. This was used as is since it accurately shows how an image is reconstructed in the Philips CT scanners. Note that the goal of this dissertation was not to write a new reconstruction algorithm, but to provide a translation algorithm or method to generate data during an arc event in cases where there would be no data available. So the new method proposed is actually supplying data to the reconstruction algorithm in a situation where it would be interpolating data due to occurrence of arcs. This is why existing reconstruction methods were used to do simulations and verifications.

The reconstruction results that were obtained from the simulated arc images were analyzed to identify potential use for a better method. It was essential to find cases that actually show the difference in images due to interpolation performed on the data by the reconstruction algorithm. As will be shown in the images in the simulations in Chapter 2, the difference images show undesired streaks, which are caused by the arcs in the images (or places where data is discarded and the time period interpolated over). The ultimate acceptability of the images are defined by medical practitioners that use the scanners, but we are able to see from the difference images that interpolation of data during arc occurrences is undesirable. The purpose of this study is to simply compare the images generated by interpolation with those generated after using the new algorithm proposed here. We do not need to delve into the anatomical details as much as the relative

improvement from using the new method. To put it in layman's terms, the cleaner (smaller difference) the difference image, the better its quality.

c) Implement a method of real-time measurement of voltage using the detector system

Even though the voltage feedback of the power supply is available from the system electronics, it is not fast enough in time (due to hardware propagation delays) to be able to provide real-time correlation to data at the detectors. The data is reconstructed at the end of the scan, but the voltage must be detected at the time that it is rising during recovery from the arc, so that I can implement the translation method to get equivalent desired voltage data that will then be provided to the reconstruction algorithm. Apart from the time delay, it is also more convenient to have the voltage detection as part of the detector data since that is where the correction algorithm is implemented. This therefore requires calculating the voltage from relative measurements made on the scanner detector system, which is a real-time voltage measurement method. I used a material with known attenuation characteristics (copper in my case) to make a relative measurement on the detectors and relate it to the voltage level. This voltage detection also comprised a significant part of the project and is a published and known effective method of voltage detection and will be discussed in detail in Chapter 3. Even though it is a known method, it is not typically implemented in CT scanners since there is not a need for real-time voltage feedback from the detectors. The electronics of the power supply provide feedback to the control circuit to maintain constant voltage. I had to use this method

because it is required to make voltage feedback available for the algorithm implementation at the same time that data is being collected by detectors.

d) Implement the partial-data algorithm to generate images during arcs

A new method of using real voltage magnitudes and attenuation ratios during or following an arc from the detector system has been derived. This data is translated to the X-ray spectrum at the various voltage values. The actual CT numbers or Hounsfield coefficients collected correspond to the anatomical properties of the object being scanned. The algorithm does a translation of the measured data at the real voltage to that which is commanded or desired during the particular scan. The dissertation implements this method of using corrected data during an arc to minimize data loss and improve image quality. Since the method uses measured data for a part of the arc duration and then standard interpolation for the rest, I have called it partial-data interpolation.

1.2 Literature Review

Reconstruction of images from projections was attempted as early as 1940. In a patent granted in 1940, Gabriel Frank described the basic idea of today's tomography [1, Chapter 1]. However, these attempts were made without the benefits of the modern computer. Since the introduction of the first laboratory CT scanner in 1967 by Hounsfield [1, Chapter 1], there has been tremendous development in the implementations of the

reconstruction algorithm. Image reconstruction in CT is typically performed using the back projection algorithm [1, Chapter 3].

The basic principle behind image reconstruction is the Fourier transformation of planar images called projections. The steps involved in the creation of images can be listed as follows:

1. Projection of Original Image Data
2. Transformation of Data into Fourier Domain
3. Filtering of Data
4. Transformation of Data Back into Spatial Domain
5. Back-Projection.

Back-projection refers to the algorithm used to reconstruct images from data collected at electronic detectors on the other side of the patient's body or part being imaged. The data consists of attenuated X-ray signals which correspond to the body part that the X-rays passed through. These attenuation values are then correlated to the properties of the body part and the algorithm generates images based on these values [2].

CT Image reconstruction has come a long way since its advent in 1967. Over the years, several researchers at the major medical device manufacturers including GE, Siemens, Philips and Toshiba have developed various modifications and improvements to the basic reconstruction algorithms and methods. The following are reviews of studies based on interpolation, back projection and other reconstruction algorithms. The literature review spans different efforts made in the implementation of the image reconstruction

algorithm used in CT scanners and in tomography in general. Some arc related publications and patents related to arc handling in CT scanners have also been reviewed.

The author in [3] proposes the use of fan-parallel projection data directly in a reconstruction algorithm as opposed to the commonly used method of rebinning the fan beam data to parallel projections and then using a pixel-dependent weight factor in the back projection algorithm and an axial interpolation. The paper investigates an algorithm involving arcsine calculations to reconstruct an image directly from the fan parallel data which does not require axial interpolation or weight factoring in back projection. The arcsine back projection step requires an arcsine calculation as opposed to an arctangent calculation in fan-beam back projection. The author provides some imaging results using his new algorithm, which demonstrate similar image quality to that used in parallel reconstruction. Hence, according to the author, this algorithm achieves a significant saving in the computationally expensive pixel dependent back projection and better resolution by eliminating resolution compromising axial interpolation.

In [4], the authors present a stochastic relaxation algorithm for reconstruction of a CT image from projection data obtained from four different directions. They use an energy function to describe the states of the system. The algorithm is designed to work in a way to minimize the energy of the system. They view CT reconstruction as an optimization problem, where a cost function (energy in this case) is to be minimized. The optimization problem is setup as a network with two layers − the reconstruction layer and the energy layer. The units of the reconstruction layer correspond to pixels of an image, and the output of each unit represents the gray level of the corresponding pixels. The

units of the energy level correspond to projection data, and each of the projection units corresponds to a column of pixel units. The output of the energy layer is a value that describes the current state of the reconstruction layer. The authors performed experiments in which the proposed algorithm was applied to images with 48×48 pixels. The results showed that the reconstruction by stochastic relaxation worked well with CT image reconstruction.

In [5], the authors investigate the improvement to single circle scan reconstruction images with the use of supplementary information. Their work is based on the fact that a single circle scan using the Feldkamp reconstruction method does not yield complete information to reconstruct an object. There are missing radon data along the rotation axis, which correspond to integration planes mostly in the orthogonal orientation relative to the rotating axis. The authors try to improve this single circle scan reconstruction by filling in the missing radon data with supplementary information on the object obtained with additional scan paths. Their choice of this additional scan path is a line scan orthogonal to the plane of the circle scan. They performed experiments using single scan plus a second circle scan, making use of a priori information of the object, and also used topograms to compare results. They found significant improvement in single circle scan cone beam image reconstructions using the supplementary information from the methods mentioned above. They also provided some images in the paper to illustrate their findings.

In [6], the authors have applied and verified a proposed new algorithm for CT Image reconstruction, which they call the New Fast Radon Transform (NFRT). The NFRT addresses the difficulties found in the filtered back-projection algorithm, which include

conversion between radial coordinates and a raster scan format and the interpolation required to calculate the inverse which requires long computation times. The basic principle behind the NFRT is to virtually divide a square image into two angular parts, i.e. image space below and above +/− 45 degrees. More details of the algorithm itself are not covered in this paper. The NFRT results are compared with images obtained using the regular filtered back-projection algorithm which is used in everyday CT scanners. They found that their Inverse Fast Radon Transform (IFRT) method had images with a considerably lower peak signal to noise ratio and the NFRT has the ability to be faster due to the absence of interpolation and the direct conversion between raster scan and polar grids.

In [7], the authors propose a method for finding and using the detection system response in the projection matrix of a statistical reconstruction algorithm in Positron Emission Tomography (PET)/CT imaging. The quantitative accuracy of PET reconstruction is limited by factors like spatial resolution of the imaging system and the number of photons collected. The authors propose using accurate system modeling and anatomical information in a clinically feasible reconstruction algorithm to reduce quantitative errors. They used CT anatomical data during the PET reconstruction as opposed to after reconstruction, thus supplying approximate boundary information of emission uptake regions in the body, providing a priori image smoothness information. The improvements were combined with the Fourier Rebinning Technique (FORE) in an algorithm using a general system response function for reconstructing fully 3-

Dimensional PET data. Simulated results showed improved tumor bias and variance characteristics with the new algorithm.

In [8], the authors have performed an experiment to evaluate the dosimetric consequences of artifacts during radiotherapy planning of a prostrate patient containing a hip prosthesis. The motivation for this research was to study the effect of inserts in human bodies that have high atomic numbers (thus cause higher attenuation of X-rays), such as prostheses and dental fillings. Such inserts are known to cause streak artifacts in CT images, which severely degrade ability to differentiate tumor volumes during radiotherapy planning. They used different reconstruction algorithms to obtain CT images for the patient with a hip prosthesis. They found that none of the images were artifact-free. However, they also found that the magnitude of the artifacts was not large enough to disturb the radiation dose for the calculations made for therapy.

In [9], an original method for constructing the time-frequency representation of signals from the squared magnitudes of their Fourier transforms is presented. The method uses alpha-norm minimization and elaborates an iterative optimization method with adaptive estimation of the convergence parameter. The basis for this paper is the mathematical formulation used in tomography which has been successfully applied to time-frequency analysis, which represents an important imaging modality of the structure of signals. Based on the interrelation between CT and time-frequency analysis, new methods have been developed for time-frequency analysis.

In this paper, the authors explain that limited-angle approach can contribute to time-frequency analysis. Their new method can also be used for CT image reconstruction even

though it is a little computationally expensive. The authors demonstrate that the method can successfully suppress undesirable interference terms for signals with simple time-frequency configurations without unacceptable degradation of time-frequency localization.

In [10], a Fourier based model for 2-Dimensional projection in CT is presented. The authors discuss the basis and window functions for some projection techniques in the paper. They emphasize that the outcome of an iterative reconstruction depends largely on the projection operator as compared to the back-projection procedure. They also evaluate procedures using the Fourier models and basis/window function concepts as linear operators/filters in signal processing terms. They challenge the concept that voxel and ray driven procedures are related to the interpolation functions, emphasizing that these procedures differ only in the design of the innermost loop of the projector or back-projector.

In [11], the authors propose techniques for successful cardiac CT Angiography (CTA) in a multi-slice (64-slice in this case) CT scanner. The objective of their new algorithm is to maintain constant image quality over the entire range of clinically relevant heart rates from 50 to 140 beats per minute. Their method, called adaptive multi-segment reconstruction makes it possible to assess the coronary arteries as well as cardiac function during the same scan sequence while employing the identical scan protocol for heart rates between 50 and 140 bpm. The normally employed pitch is set uniformly and does not depend on the patient's heart rate. This results in a relative temporal resolution that is almost totally independent of the heart rate. The coronary artery anatomy as well as

cardiac function can be assessed from a single scan with the same scan protocol. There is no need for additional exposure. The authors feel that improving temporal resolution is not the only factor for successful cardiac CTA. The techniques presented in this paper lead to a significant improvement in reconstruction robustness, especially in cardiac patients with pathologic arrhythmias and changes in heart rate. Patient workflow is optimized by reducing the number of reconstructed phases necessary for coronary artery analysis. Coronary artery imaging free of artifacts is possible, even in patients with certain arrhythmias and large changes in heart rate. When combined with automatic detection of the cardiac phases with the least amount of cardiac motion, adaptive multi-segment reconstruction ensures a high degree of detail for the assessment of stenosis, plaque, and stents while minimizing motion blurring. The phase determination is performed by automatic motion intensity analysis of the raw data over the full length of the heart along the z-axis with a step determination of 1 ms. Patient examination and assessment are facilitated and the time required is significantly reduced by the application of these automatic optimization concepts.

In [12], a method for artifact reduction in CT images is patented. The method comprises an inexact reconstruction algorithm to create a first data image, segmenting the first data image to provide a second image with high attenuation objects separated from low attenuation objects, re-projecting the second image to form a second set of data, reconstructing a third image from the second data set using an inexact reconstruction algorithm and then subtracting those portions of the third image that are outside the high

attenuation object from the first image. The invention relates to reducing artifacts in a CT image reconstructed from an inconsistent data set such as cone beam data.

In [13], the author has patented a method of data rebinning, which is a method for producing an enhanced tomographic image of an object. It includes steps of obtaining fan beam projection data of the object from a tomographic scan, rebinning the fan beam projection data into a quantity of parallel projection data points, applying interpolation to the quantity of parallel projection data points to increase the quantity of parallel projection data points and generating a tomographic image from the increased quantity of parallel projection data points. The methods and apparatus of the invention provide rebinning fan data into parallel data for improved image reconstruction. Additional information is obtained and utilized in each scan to increase the quality of the reconstructed images. The additional information can be obtained and used even in the case of non-uniformly sampled projection data. The methods and apparatus of the invention also provide increased helical speed coverage by using thicker slice collimation, without degradation of image quality, and increased volume coverage while maintaining z-resolution in a reconstructed slice.

In [14], the authors have proposed new methods of implementing the Convolution Back Projection and Fourier Inversion methods of image reconstruction. They have used a hierarchical bus-based system (HBBS) to ease the bus-congestion of a shared bus used to connect processors in a shared memory multiprocessor system. These multiprocessor systems are used because the back projection and Fourier inversion methods are highly compute-intensive applications for single processor systems. An HBBS supports larger

number of processors and also has highly specialized instructions and architecture of DSP devices which contribute to its better performance. Additionally, the authors have developed a parallel algorithm in this paper for the back projection and Fourier methods using overlapped communication and computations.

Their results show that an 8-node hierarchical bus based system executes the two algorithms about 100 times faster than the standard multiprocessor system.

In [15], the authors present a reconstruction technique for CT images from a geometrically unconstrained set of ray sums. This paper is interesting due to the fact that the authors are testing for a technology that is not yet in existence but believe will be used in the future. The proposed device would be a flexible band with tiny X-ray emitters and detectors attached to make it a lightweight, flexible and portable X-ray system. This device would be wrapped around an appendage to obtain images. The purpose of the authors study was to evaluate the feasibility of reconstructing a CT image from such a device, for which they built a simulation test bed to simulate CT ray sums of a test image. This data was then used in their reconstruction method, which involves slotting each ray sum onto a grid of data that represents a parallel beam CT scanner data. Once the data is in that form, they performed regular CT back projection to generate images. So they introduced a method of reconstruction which is not constrained to any particular geometry and their test results showed that the method was effective and image quality was as good as that produced by regular CT scanner image reconstruction .

In [16], the authors analyzed the processing of an inconsistent data function by the filtered back-projection algorithm in its continuous form. They demonstrate that an image

reconstructed by the back projection algorithm can be represented as the sum of a pseudo inverse solution and a residual image generated from an inconsistent component of the measured data. It shows that when the original data function is in the range of the radon transform, the image reconstructed using the back projection algorithm corresponds to the pseudo inverse solution.

In [17], the authors have patented a voltage detection method that was devised to measure X-ray tube voltage in a CT system. The basic method used is placing filtration material over two detectors on the scanner, and feeding the ratio of the signals produced by these two detector elements to a calculation algorithm which produces a signal indicative of the X-ray tube voltage. The authors discovered that for any given X-ray tube and differential filter, an exponential relationship exists between tube voltage and the ratio of the two detector signals. The relationship is determined by a calibration procedure in which an exponential curve is fit to a set of ratios measured at different, known X-ray tube voltages. They were able to achieve voltage measurements accurate to +/− 0.5%.

In [18], a review of methods of speeding up of the reconstruction algorithm implementation has been performed. The paper focuses on faster computation using parallel computing, including first and second generations of parallel computing (centralized computers and LAN based computers) and also on distributed client server topology to a peer to peer (P2P) enhanced network models. The author's main message is that single PC reconstruction is insufficient and risky for fast implementation, and the

benefits of parallel computing including reliability and low cost can be realized by integrating geographically distributed systems over the internet.

In [19], a new architecture called the cell broadband engine (CBE), which has been recently optimized for distributed computing, has been used to perform the generally computationally expensive iterative reconstruction algorithms used in cone-beam CT. A CT algorithm called the ordered subset convex (OSC), which achieves high image quality, has been used to perform the image reconstruction using the CBE. The researchers tried to maximize the OSC image reconstruction speed for statistical cone-beam CT, which they also believe has the potential to significantly reduce image noise and thereby improve dose usage of the scanner. The result of the study showed that only four OSC iterations were sufficient to achieve high image quality and the authors concluded that this method has high potential to be available with the high performing CBE.

Reference [20] is a patent that is a design of an arc suppressor for an x-ray tube consisting of a combination of coils and diodes which limit the arc current within the tube. The authors have proposed a parallel connected coil and diode between the high voltage supply and the target of the x-ray tube as the building block of this suppressor. When an arc occurs, the sudden increase in current flow is converted and stored in a magnetic field leaving only a small current to contribute to arcing inside the tube. The coils are sized such that the arc current is sufficiently limited to protect the tube from damage. The diodes permit the energy stored in the magnetic field to be converted to a current flow through the coil and diode such that the energy is dissipated as heat by the

resistance of the coil thus limiting the energy passing to the tube. These diode-coil blocks can be staggered into multiple stages depending on what the power supply design permits to add even more current suppression during arcing.

Reference [21] is another patent that provides a method to protect the x-ray tube during arcing. The authors have presented a CT apparatus which, in addition to the standard CT blocks of an x-ray tube and detectors, also includes an interlock unit configured to monitor generation of an arc in the x-ray tube. When an arc in the tube is detected, the interlock unit stops the emission of x-rays by suspending the generation of voltage output from the high voltage supply. When a predetermined period of time elapses from the stop of x-ray emission, the interlock unit restarts the emission. The authors also talk about using an interpolation method during the period of x-ray suspension. This interpolation is based on data that was collected before the arc. This interpolation serves to eliminate artifacts due to arcing.

In [22], the authors have patented a method for tube-spit (or arc) detection and correction. They propose a method of arc detection by analyzing the data read by the detectors, a software based implementation as opposed to hardware arc improvement methods which are expensive. Their method of tube-spit detection is to find any occurrences of almost zero-signal read by the detectors. After detecting an occurrence of tube-spit, they propose interpolation as a correction for that duration. They have mentioned linear interpolation and LaGrange interpolation as some of the interpolation methods that could be used for correction.

Despite these numerous methods implemented in image reconstruction over the last few years, there have been limited studies done in interpolation methods during X-ray tube arcing. This is partly due to the fact that the current basic interpolation methods as those mentioned in [21] and [22] were found to work well in most cases in scanners made so far. However, with the more recent scanner technology moving towards faster rotation speeds and reconstruction times, the short arc durations will now have more significant effect on image quality. In these conditions the traditional interpolation will be inadequate, and any small increase in recorded data during arcing will contribute to improving images significantly. It is with these new and futuristic applications that this study proposes a targeted interpolation method.

1.3 Contributions of this Research

This chapter (Chapter 1) introduces the fundamentals of computed tomography and the goals of this study. It also reviews material published in the field of study and work that relates to reconstruction and arcing in CT scanners. Chapter 2 explains how arcing is currently handled in some CT systems and also reviews effects of arcing on images when using current methods of arc handling such with standard interpolation techniques. Simulations are performed in this chapter to illustrate these effects with different rates of arcing using two different human body sections. Chapter 3 reviews the theory and implementation of the voltage detection method used during this research. This is not a new contribution of this research but was a significant part of it since it was

necessary for the implementation of the algorithm developed in this study. Chapter 4 details the data collected for the development of the proposed partial-data algorithm and gives an overview of the basic flow of the algorithm.

The new contribution of this research is the introduction of an algorithm to handle tube arcing using data that is available during the arc event. Use of this partial-data interpolation method results in improvement in image quality during tube arcing. This derivation and method of implementation are detailed in Chapter 5. Chapter 6 shows the implementation and results of the partial-data algorithm and Chapter 7 draws conclusions from the results and looks at future applications for the new method.

CHAPTER 2

ARC DETECTION, SIMULATION AND IMAGE STUDIES

In this chapter we review how CT systems detect and handle arcing with respect to image reconstruction and look into details of x-ray tube and power supply interaction during an arc. This is covered in section 2.1. In section 2.2, we compare images generated by simulation of arcing on a system. We take data from scans made on head and pelvic phantoms, and then set the arc status active in some of the data frames in the data headers from these scans, then perform standard image reconstruction on the data. We then have images that show effects of different durations of arcing which we compare with images from scans without any arcing. This is to illustrate the effects of arcing on imaging that we are trying to address with the new method proposed in this research.

2.1 Arc Detection in the CT X-ray System

Figure 2 shows a common system used in CT scanners to detect arcing in tubes. It consists of the power supply detecting an arc and passing on the information to the

detection system, which then handles it using interpolation or other methods to minimize detrimental effects on image quality.

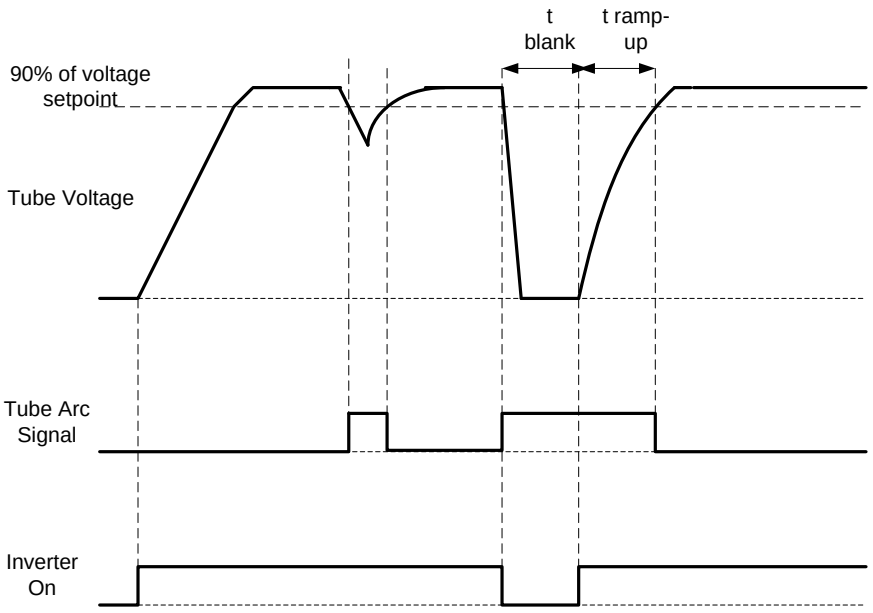

Figure 2: Arc Detection and Reporting in X-ray Power Supply

The ‘tube arc signal’ becomes active every time the voltage drops below the 90% set point. It remains active until the voltage is above the 90% value again. This signal tells the image reconstruction system when and for how long to perform interpolation during the scan. The ‘inverter on’ signal shows if and for how long the event has caused the inverter to shut down. It is an indicator of the severity of the arc. Both these signals are generated in the power supply and passed on to relevant control systems in the scanner.

The inverter charges the output capacitors of the supply. It is turned off when an arc is detected due to the high current surge that causes the voltage to drop. Once the arc

event is over the inverter is turned on again to charge the capacitors. This is the second part of the arc signal still being active until the voltage is able to ramp up to the desired value. One thing that can be seen in Figure 2 is that the inverter turns off only for the second arc event. This is because the magnitude and slope (rate of fall of voltage) of the first arc event was within the threshold of the inverter recovery capability. The system by design tries to recover from an arc as soon as one is detected. If it can accomplish this before the voltage drops below an amount that the inverters cannot supply, it will not switch off the inverters. These thresholds and switching schemes are meant to protect the components of the tube and power supply.

If an arc occurs during a patient scan, the shutdown of tube power results in a momentary loss of X-rays, thus a loss of imaging data. The momentary period is determined by the time it takes for the power supply's voltage source to recover, which may be on the order of several milliseconds. This lost data leads to artifacts in the consequent image generated from the scan.

Typical image computation or reconstruction algorithms will usually just detect these arc events, and interpolate data during the shutdown period to continue with the patient scan [21], [22]. This method can be quite acceptable from an imaging point of view depending on how long the shutdown period of the system may be and the number of arcs that occur during it. However, these thresholds are small in scanners that have high rotation and reconstruction speeds and frequently the artifacts get so bad that the image is not acceptable and the patient must be scanned again [1].

Typical X-ray generators have a large capacitive bank at their output stage to feed the power required by the tube. As mentioned earlier, an arc is a short circuit across the X-ray tube, which results in a large current draw in the tube, which in turn results in a rapid discharging of the capacitors. The inverter bridges that feed the capacitors then have a small ramp up time before the capacitors are fully charged again and capable of supplying the required power to the tube. This delay is when the voltage across the tube has dropped very low and has a ramp-like profile before the voltage rises up to a usable value again. This usable value is typically considered to be approximately 90% of the maximum requested voltage. The voltages used for imaging in CT scanners are in the range of 80 to 140 kilovolts (kV).

2.2 Simulation to find limitations of current interpolation methods

The approach to studying arcing effects on images is to first get data for a good image, then set arc status active (during certain data frames) in the data which is then fed to the reconstruction software which will discard data that corresponds to the arcs. These simulations give a good idea as to the effects of arcing on images. Several such simulations have been performed using a head and pelvis phantom and are shown in figures 3 through 11.

Figure 3 shows slice number 7 taken from a 40 slice Philips Brilliance™ CT scanner. This image is without any simulated arcs. Number of slices is determined by the number of rows of detectors that are part of the detector assembly.

Figure 3: Pelvis Phantom without Arcs

Figure 4 shows the same phantom image with two arcs in the data. This is simulated by setting the arc status active in the data header in 2 data frames at random points, which cause the reconstruction algorithm to discard the data for those two data

time periods. Figure 5 shows the mathematical difference of the data from figures 3 and 4.

Figure 4: Pelvis Phantom Showing Two Arcs

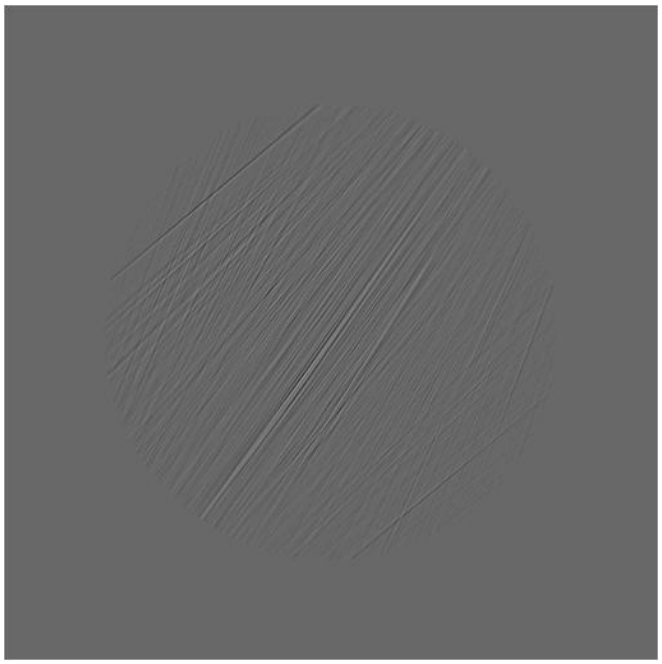

Figure 5: Difference of Pelvis Phantom Image with Two Arcs and without Arcs

Several such experiments were done using head and pelvis phantoms. I have summarized a view of three different slices of a head phantom and a pelvis phantom in figures 6 through 11. The first columns show slices without any arcs, the second column is corresponding slices with a specific number of arcs, and the third column shows the difference of the first two columns. This third column is the mathematical difference, which actually shows the artifact caused by the arcing more clearly to the layman's eye. As can be clearly seen in the figures, the more the arcs, the more pronounced the streaks.

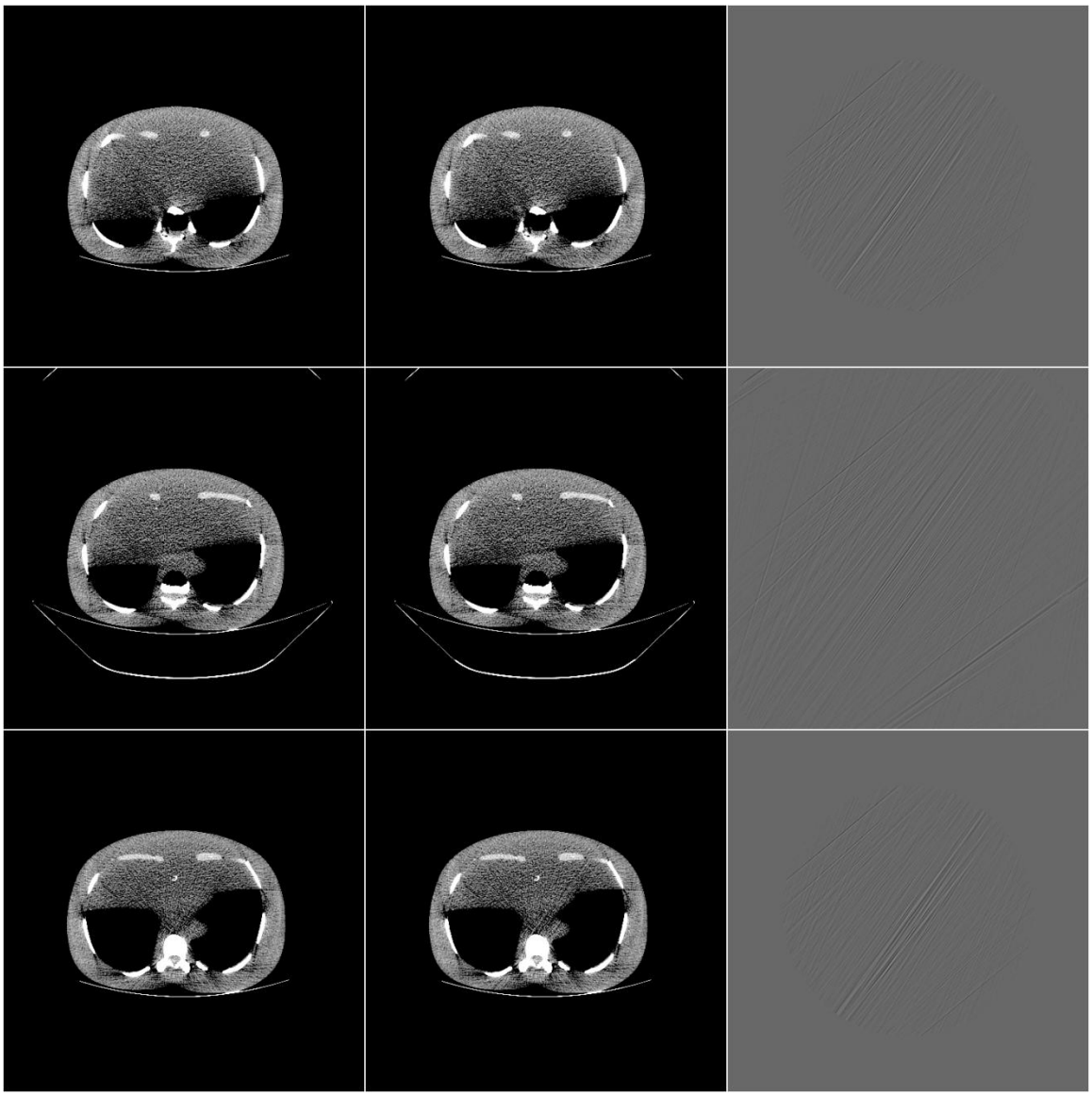

Figure 6: Pelvis Phantom Images with Two Arcs

Column 1 = Images with no arcs, Column 2 = Images with 2 arcs
Column 3 = Difference image of columns 1 and 2
Row 1 = Slice number 7, Row 2 = Slice number 20
Row 3 = Slice number 34

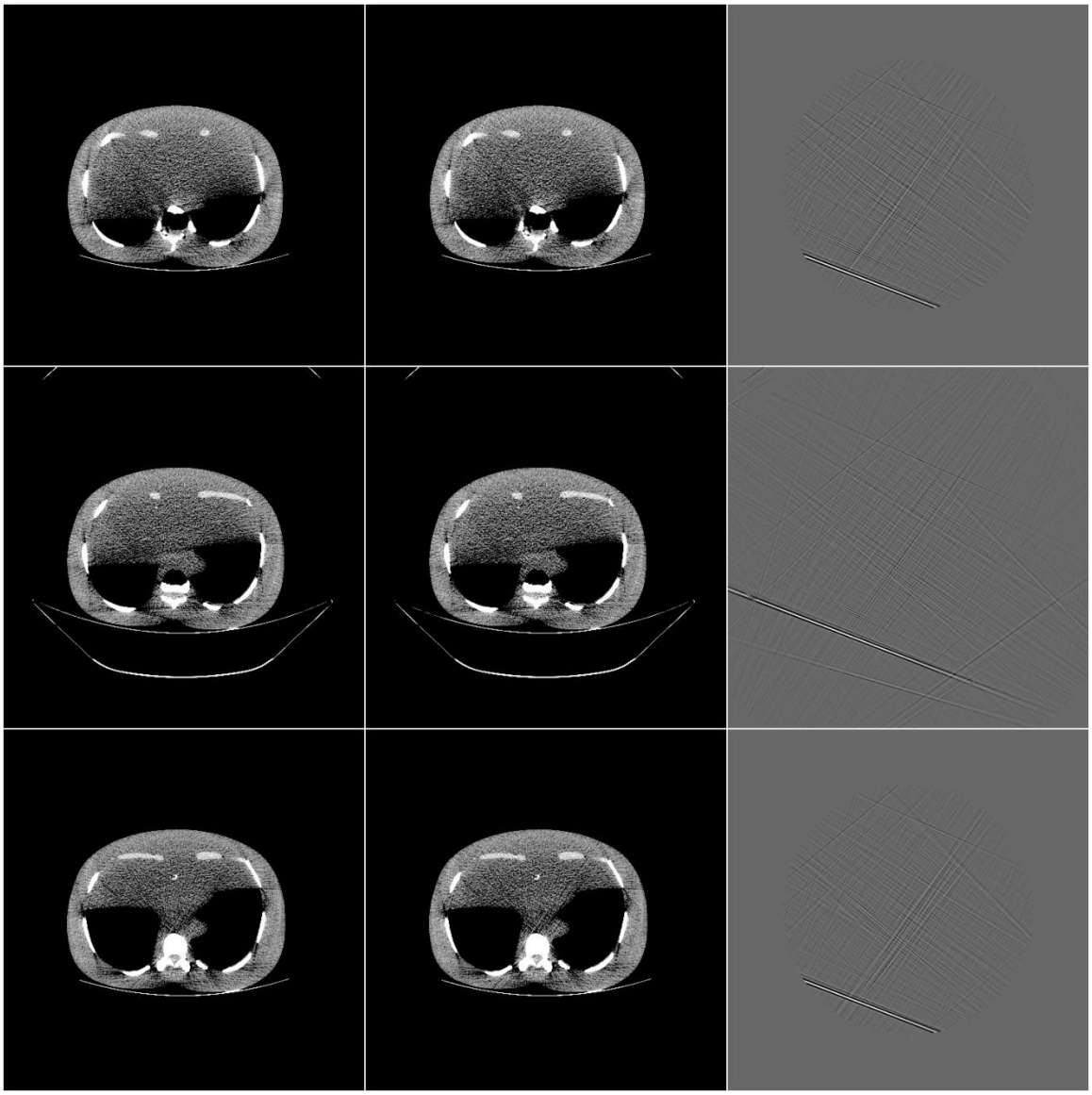

Figure 7: Pelvis Phantom Images with Four Arcs

Column 1 = Images with no arcs, Column 2 = Images with 4 arcs
Column 3 = Difference image of columns 1 and 2
Row 1 = Slice number 7, Row 2 = Slice number 20
Row 3 = Slice number 34

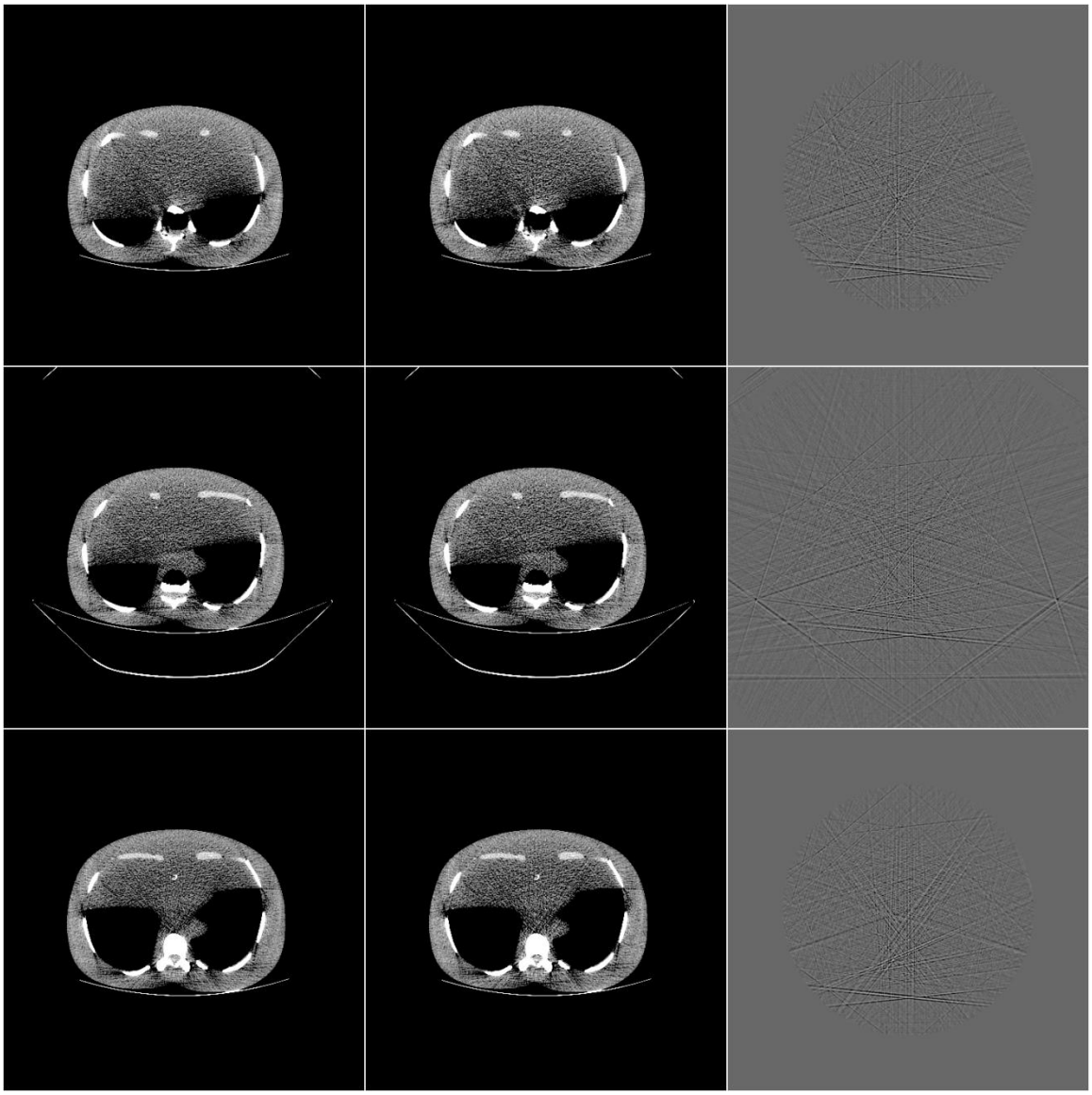

Figure 8: Pelvis Phantom Images with Ten Arcs

Column 1 = Images with no arcs, Column 2 = Images with 10 arcs
Column 3 = Difference image of columns 1 and 2
Row 1 = Slice number 7, Row 2 = Slice number 20
Row 3 = Slice number 34

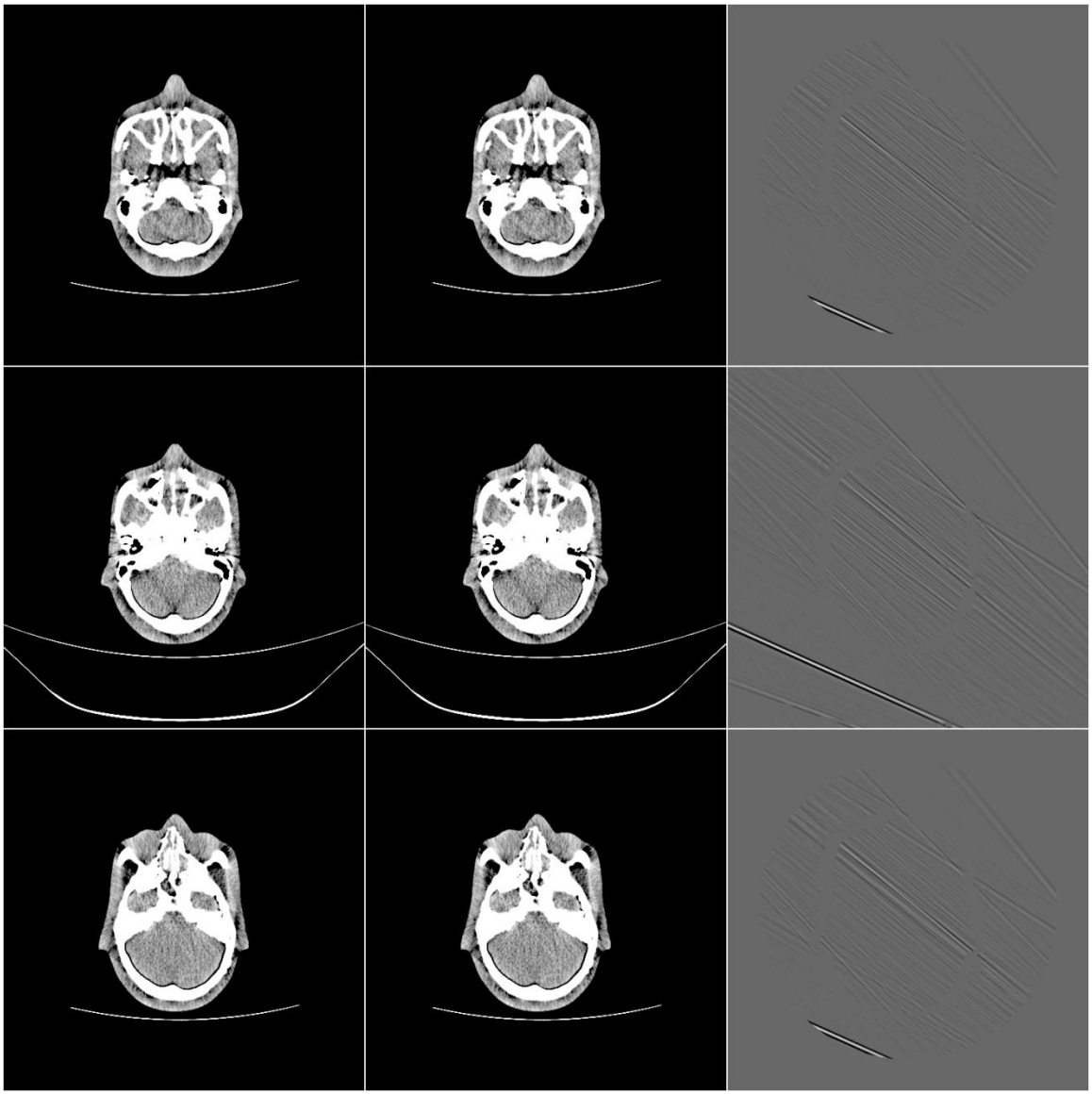

Figure 9: Head Phantom Images with Two Arcs

Column 1 = Images with no arcs, Column 2 = Images with 2 arcs
Column 3 = Difference image of columns 1 and 2
Row 1 = Slice number 7, Row 2 = Slice number 20
Row 3 = Slice number 34

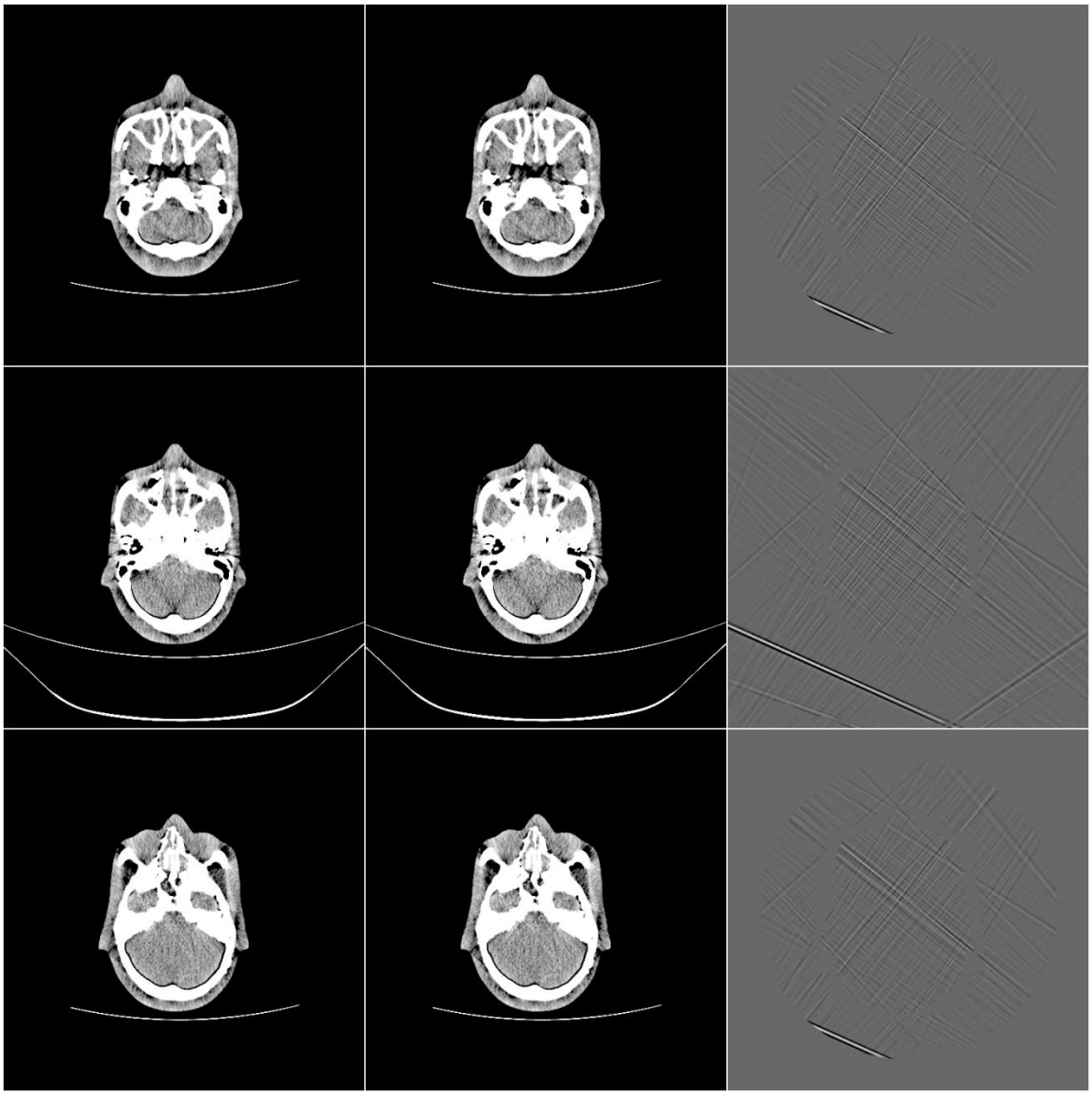

Figure 10: Head Phantom Images with Four Arcs

Column 1 = Images with no arcs, Column 2 = Images with 4 arcs
Column 3 = Difference image of columns 1 and 2
Row 1 = Slice number 7, Row 2 = Slice number 20
Row 3 = Slice number 34

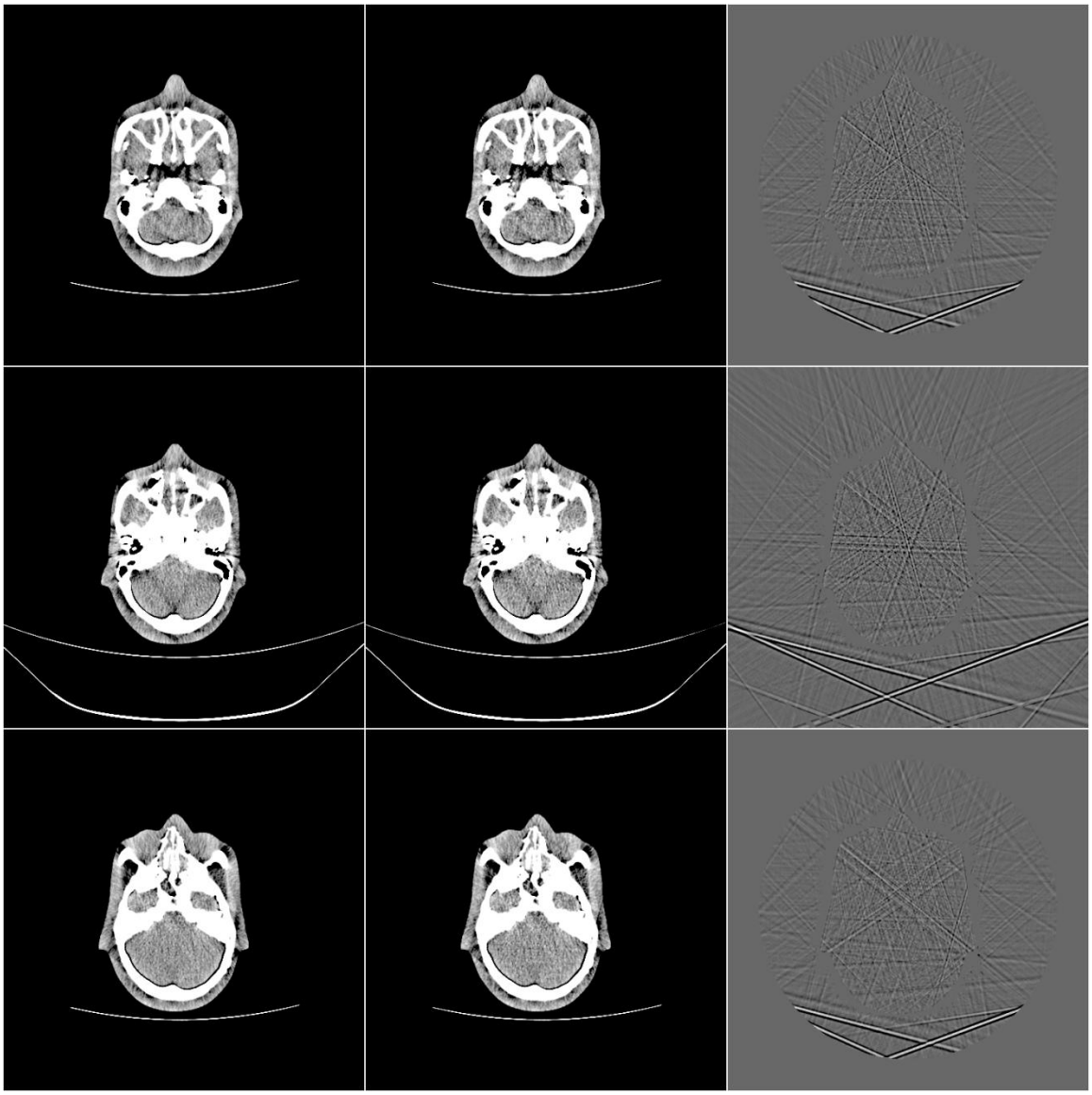

Figure 11: Head Phantom Images with Ten Arcs

Column 1 = Images with no arcs, Column 2 = Images with 10 arcs
Column 3 = Difference image of columns 1 and 2
Row 1 = Slice number 7, Row 2 = Slice number 20
Row 3 = Slice number 34

CHAPTER 3

REAL-TIME VOLTAGE DETECTION

This chapter focuses on the voltage measurement method which, even though not an original contribution of this research is a very important tool in achieving the goals set forth for this study. Section 3.1 introduces the fundamentals behind the method and section 3.2 provides data obtained in this research which is used in the implementation of the voltage measurement, which feeds the partial-data method presented in the subsequent chapter.

3.1 Principle

This method for determining voltage on x-ray systems follows a simple filtering and ratio principle. It uses the fact that the voltage applied across an x-ray tube has a direct relation to the energy of the x-rays and the attenuation caused by any material when the x-rays are incident on it. Attenuation ratios are collected from detectors that are covered by a known thickness of copper and detectors that have no copper covering. These ratios are collected at different voltages and the relationship is determined between attenuation and voltage

for that particular thickness of copper. The same thickness of copper is then used on detectors while making scans at unknown voltages. The attenuation ratios are then converted to voltage values from the previously determined relationship. Figure 12 illustrates the placement of copper on the detector array to make the voltage measurements.

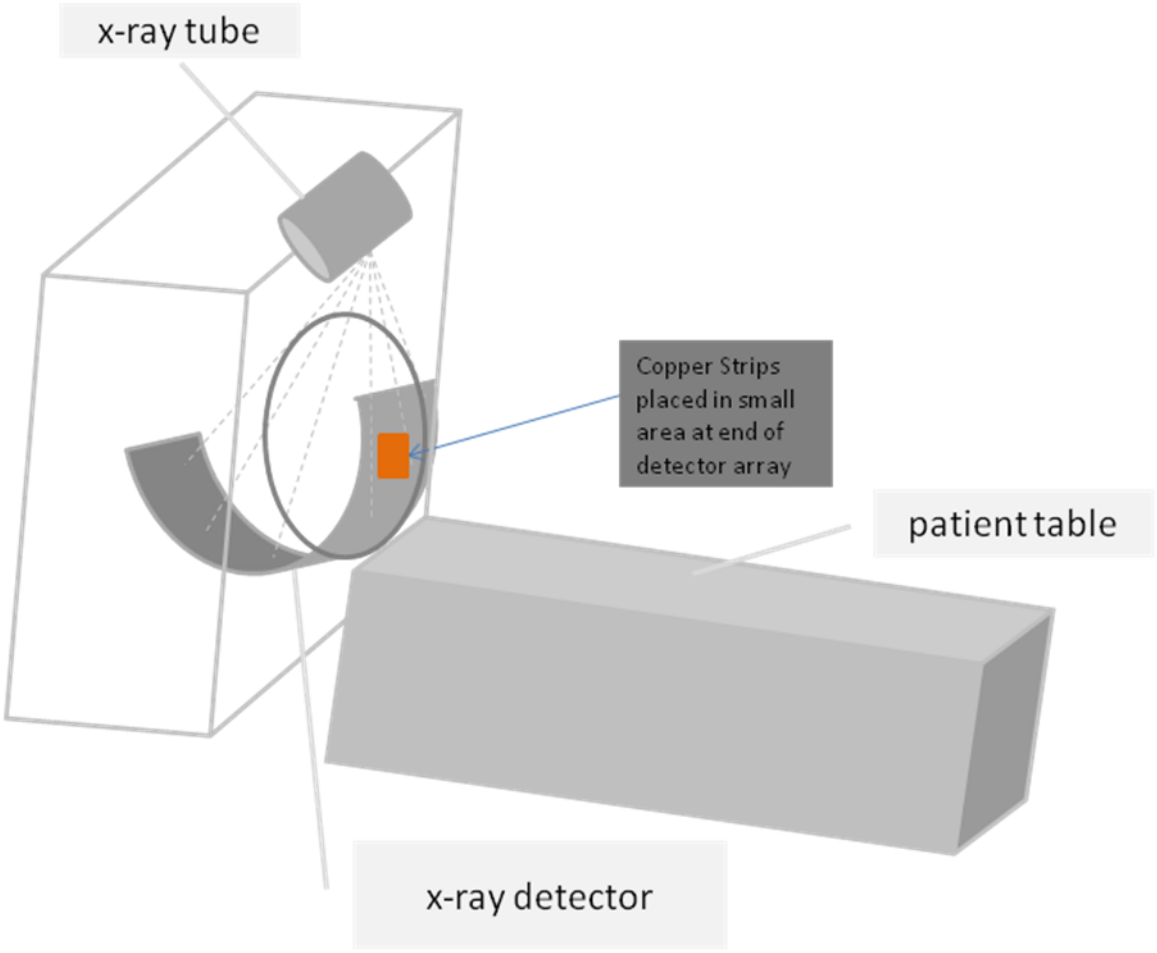

Figure 12: Placement of Copper Strips for Voltage Measurement

Please note that the copper strips in this case have been placed on the scanner detectors only for convenience, since we are only looking at a small section of the images for our

measurements and ignoring the area covered by the copper. In a system implementation, this copper filter will need to be placed outside the field of view, preferably on a small detector array placed in the collimator to make voltage measurements.

3.2 Implementation

Attenuation ratio in general x-ray physics is represented as follows:

$$\frac{I}{I_o} = e^{-\mu t} \quad (1)$$

where

I_o = Original intensity of the x-ray beam

I = Intensity of the x-ray beam at distance (or thickness) t

e=Euler's number

μ= Effective attenuation coefficient for polychromatic x-ray beam

t= Thickness of attenuating material

Based on equation (1), the expression for μt (logged attenuation ratio) is derived as follows:

$$\mu t = -\ln\left(\frac{I}{I_o}\right) \quad (2)$$

Note that we are using the logged attenuation ratio for simplicity of implementation in the algorithm because the scanner data is available in this form. Since we use μ to denote attenuation coefficients for both copper and water in this document, I will henceforth refer to them as μ_c for copper and μ_w for water to avoid confusion.

The implementation of the voltage detection in this case consisted of using attenuation calculations from simulations generated by a Matlab® x-ray simulation program and comparing them to attenuations measured from a real CT scanner. The simulations allowed for an extended range of voltages that are not standard on the scanner, which is needed to detect unknown voltages for this application.

A simulation program in Matlab was developed in 2007 by Ulrich Neitzel, a scientist working for Philips Healthcare's X-ray tube division in Hamburg, Germany. He used a program called Spektr (2004 (C) Copyright by Jeffrey H. Siewerdsen, Princess Margaret Hospital, Toronto, Canada), which is a routine that generates X-ray spectrums based on the material and construction used in X-ray tubes. Spektr is widely used by different X-ray tube manufacturers to perform theoretical spectrum analyses on the output of different tubes based on different construction materials. Dr Nietzel used Spektr to apply to the specific tube being used on the system that I worked on for this project, and generated a program that allows us to analyze X-ray attenuation through different materials of our choice.

Using this program, I calculated the effects of different thicknesses of copper on the signal level seen by the detectors in a CT scanner. Copper was chosen because it is a good X-ray attenuating material, it is easy to make into thin sheets to place on the CT detectors, and it is relatively inexpensive and readily available. Other materials like tin or molybdenum could also be used for this purpose [17]. The simulation program makes calculations using the properties of all materials inside the X-ray tube and the scanner that are in the path of the X-rays all the way until they reach the detectors. It generates a spectrum of the X-rays coming out of a tube and then uses the different materials in the beam path to attenuate these rays on their way to the detectors, just like they will in a real scanner.

I also made measurements on a scanner with different thicknesses of copper placed over the detectors (Figure 12) and was able to prove that the simulation program is a very good representation of the real scanner. The measurement was done by placing rectangular pieces of 1 mm copper sheets over the detectors on the scanner and making scans. More copper strips were added in 1 mm increments to get relationships for different thicknesses up to 5 mm. The data was then analyzed and the area which showed the attenuation due to the copper sheet was noted by specific detector locations. I then took the attenuation values at points under this copper covered area and calculated the ratio with values that were not under the sheets. The relationship of the attenuation ratios to the voltage is shown in the chart in Figures 13 and 14. Figure 15 shows the difference of the two charts which highlights the closeness of the simulated data to the measured values.

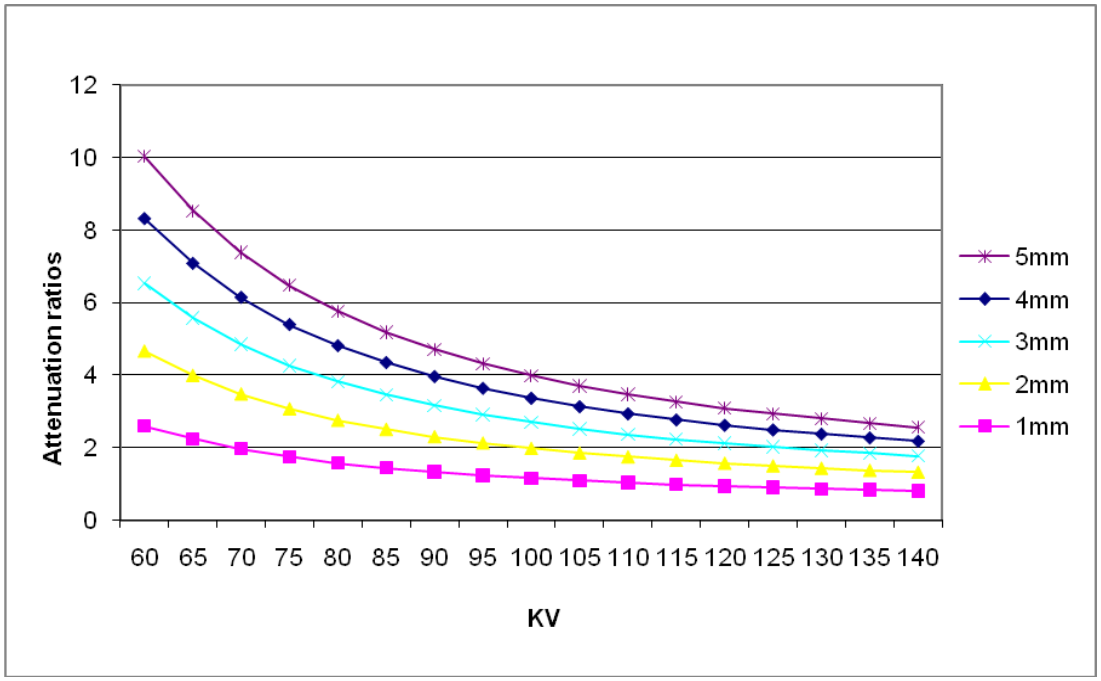

Figure 13: Relationship between Voltage and Attenuation Ratio $\mu_c t$ (simulated) for Different Values of Copper Thickness

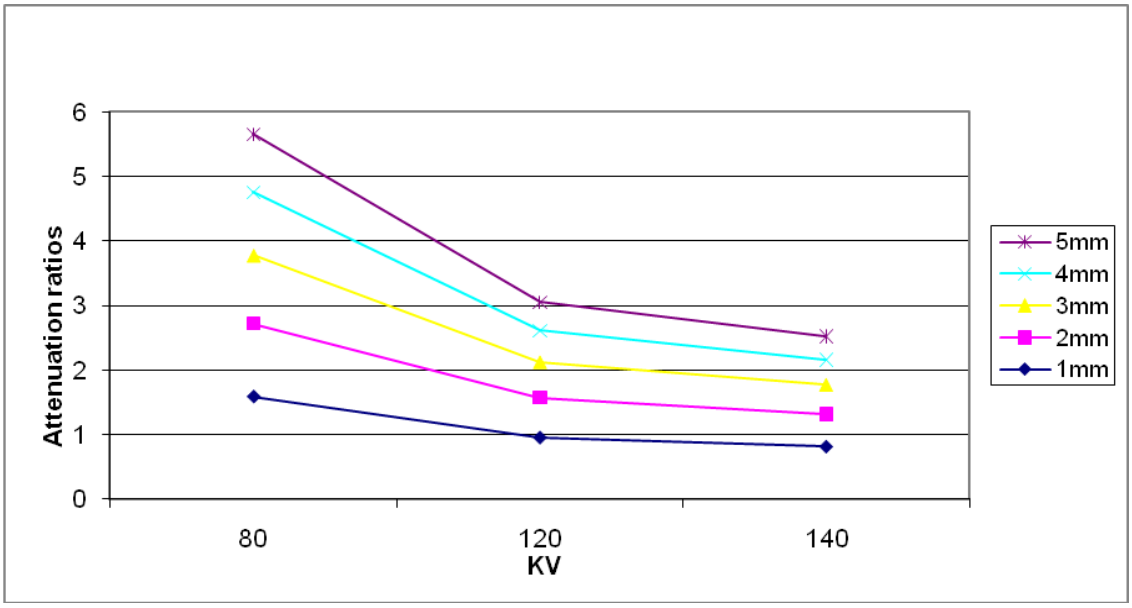

Figure 14: Relationship between Voltage and Attenuation Ratio $\mu_c t$ (Measured) for Different Values of Copper Thickness

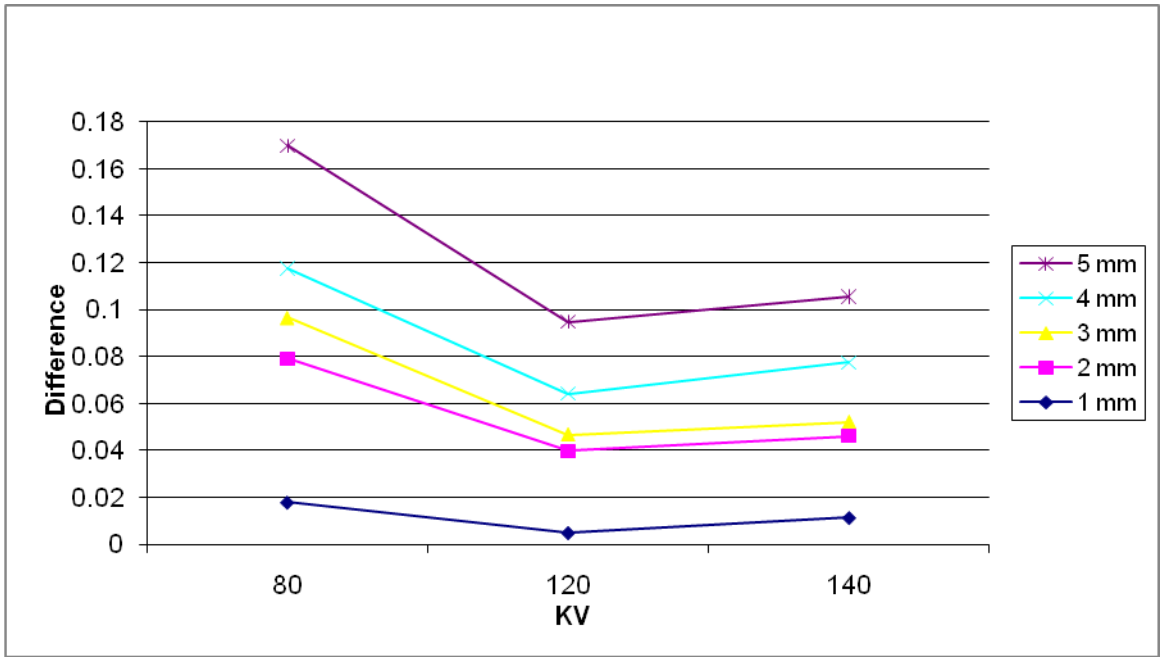

Figure 15: Difference between Measured and Simulated Attenuation Ratio ($\mu_c t$) for Different Values of Copper Thickness

I chose to use 2 mm of copper to stay in a low attenuation range to keep the signal level above 1% for a good signal to noise ratio and at the same time have a good variation for different voltages. Figure 16 shows the simulated, measured and fitted curves for 2 mm of copper, which highlights the closeness of the simulated data to the measured data.

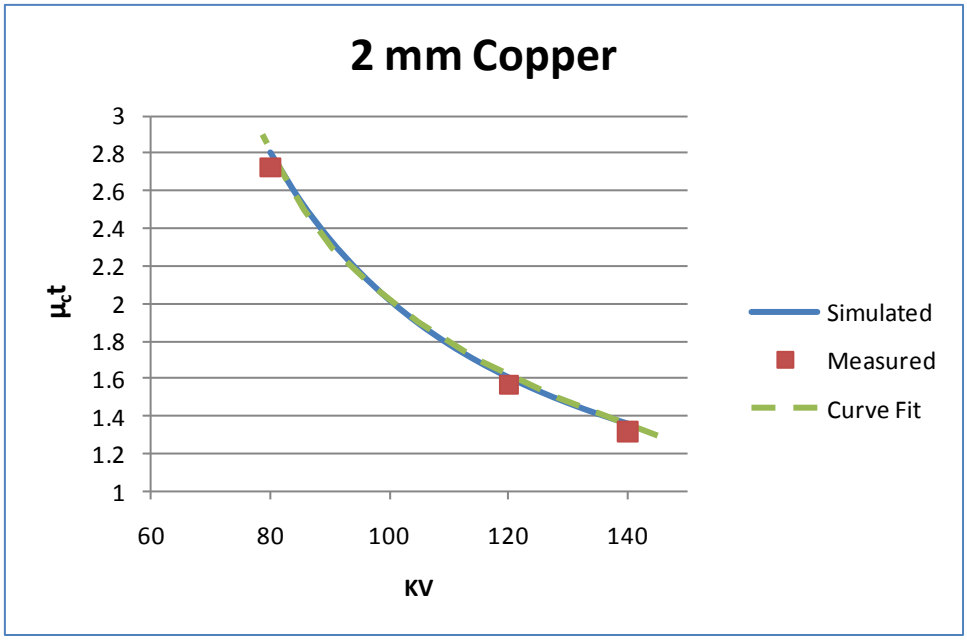

Figure 16: Relationship between voltage and $\mu_c t$ (simulated, measured and curve fit (equation 3)) for 2 mm copper thickness

The 2 mm thickness of copper proved to be a good balance between providing a good ratio curve and also being light enough to stick on the scanner to rotate at extremely high speeds without falling off. Based on the above charts, the $\mu_c t$ values for the different voltages for 2 mm of copper were the following:

Voltage = [60 65 70 75 80 85 90 95 100 105 110 115 120 125 130 135 140] kV;

Corresponding $\mu_c t$ = [4.7224 4.0532 3.5396 3.1225 2.802 2.5484 2.3408 2.167 2.019 1.8929 1.7848 1.6914 1.6097 1.5376 1.4734 1.4159 1.3642];

Using the polynomial fit function in Matlab, I ran calculations and found that the fourth order polynomial provided the best fit to the curves above. I also found that a fourth order polynomial gave the best representation of the curve with the lowest error.

This equation represents the real data with an accuracy of approximately 3%. Equation (3) was the result of the voltage to μ_c relation (for 2 mm of copper):

$$v = 1.7443(\mu_c t)^4 - 24.755(\mu_c t)^3 + 132.3188(\mu_c t)^2 - 327.8174(\mu_c t) + 396.9295 \quad (3)$$

This equation is used to calculate the voltages along the rising curve after the arc during arcing scans for the partial-data algorithm in chapter 5.

CHAPTER 4

DATA COLLECTION AND METHODOLOGY

In this chapter we look at measurements and data collected for the next steps in the study and give a simplistic overview of the algorithm implementation before presenting the partial-data interpolation in the following chapter. Section 4.1 looks at the data points simulated and measured on different water thicknesses, while section 4.2 gives the implementation overview.

4.1 Water Data

Once the voltage to attenuation ratio relationship is derived, we have a way to detect the rising voltage during an arc on a scanner. The next step was to simulate attenuation ratios for different thicknesses of water at different voltage levels. As mentioned earlier, water is representative of a large portion of the human body and serves as a good baseline for attenuation that would be derived when a human is scanned.

Using the same simulation program that was used for copper, but replacing material properties to those of water, simulations were performed to collect data. The results are

shown in figure 17. It shows the simulation of attenuation ratios for water of different thickness levels.

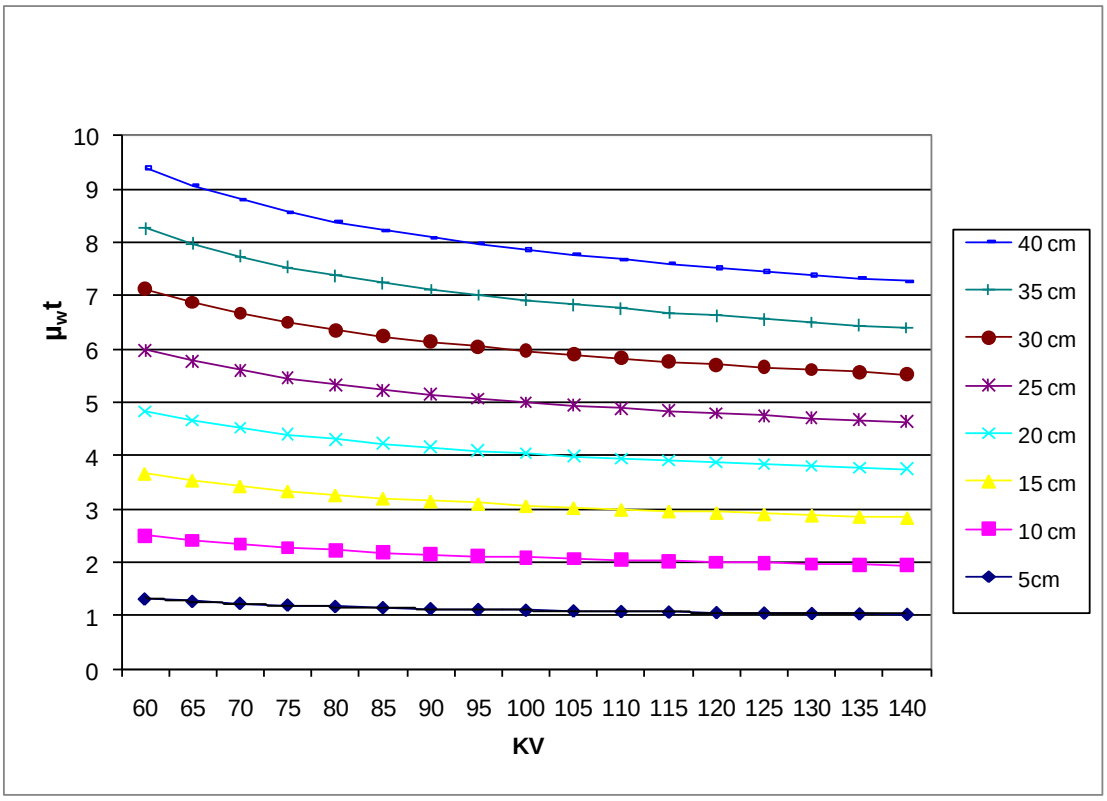

Figure 17: Relationship between Voltage and Attenuation Ratio (μ_wt) for Different Thicknesses of Water (Simulated)

Radiology phantoms are commonly used in the medical arena to test imaging systems due to their likeness to the human body. The most frequently used phantoms are water, plexiglas, aluminum and copper [23]. Figure 17 shows that a relationship exists between the different voltage levels and their X-ray attenuation ratio with water, and an algorithm can be developed to translate body caused attenuations to the desired voltage levels during the implementation of the interpolation method.

After the simulation data was collected, I made scans on a CT scanner using two different thicknesses of water in a paper cup and compared the data to the results obtained from the simulations. Figure 18 shows the measured values for two thicknesses of water on a scanner and figure 19 illustrates the difference between the simulations and measurements, which shows the simulated data can be used for deriving relationships to be used in the algorithm.

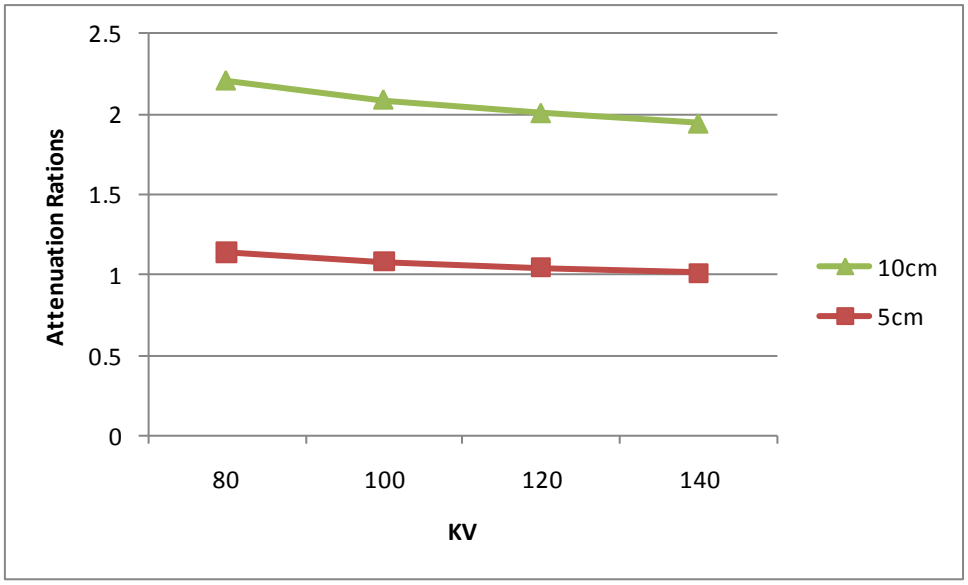

Figure 18: Relationship between $\mu_w t$ and Voltage for Water (Measured)

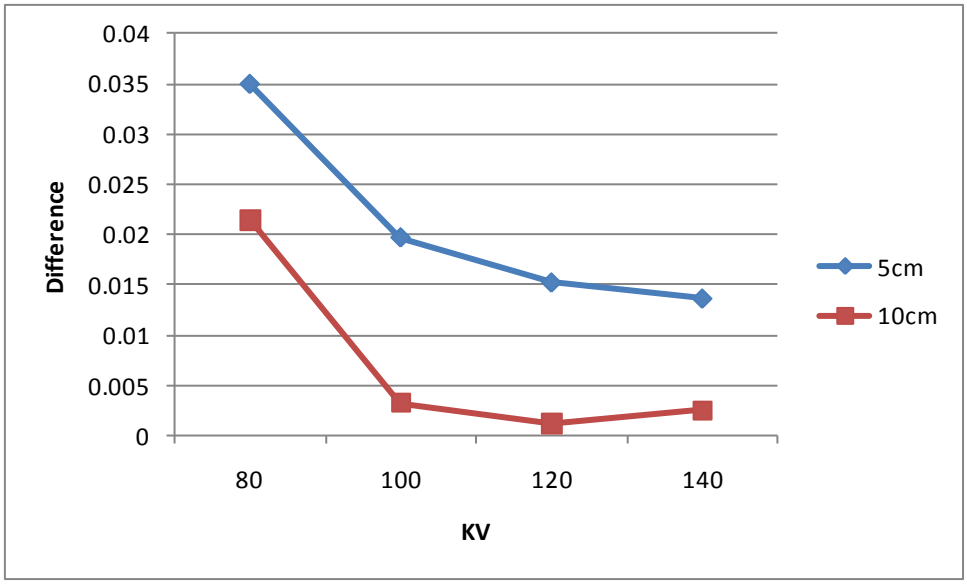

Figure 19: Difference between Measured and Simulated $\mu_w t$ for Water

The advantage of using simulated data lies in the fact that we can get data for any number of thicknesses and voltages easily, which is not always possible using measured data due to practical limitations on a scanner.

4.2 Partial-Data Interpolation Methodology

The proposed implementation of the partial-data interpolation method is illustrated in figures 20 and 21. Figure 20 shows the standard interpolation commonly used in CT scanners at present. It uses simple linear interpolation of the data during the arc duration.

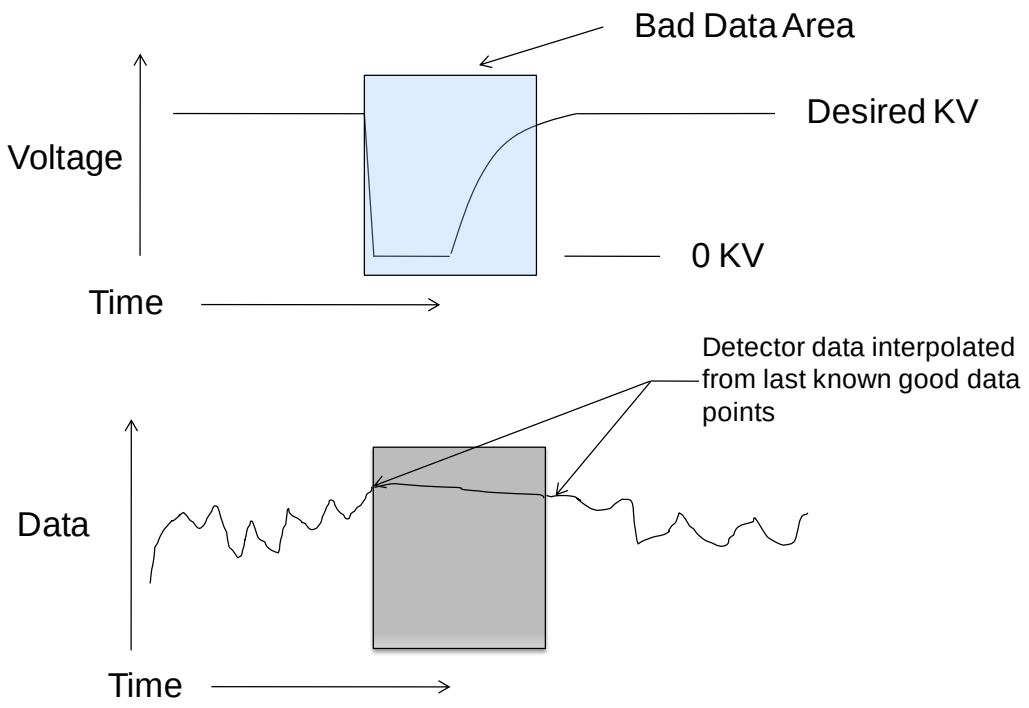

Figure 20: Standard Arc Handling in CT Scanners Today

Figure 21 shows the proposed concept of the partial-data method. We can see that the tail end of the arc, during which the voltage is rising to the programmed level (120 KV in this case) is the region where data is collected while measuring the voltage. This data, which is essentially image information at voltages that are on the rising slope (below 120 KV), is then translated using the partial-data relationships as derived in the previous and following chapters, to provide image data that is equivalent to that of the object being scanned at 120 KV.

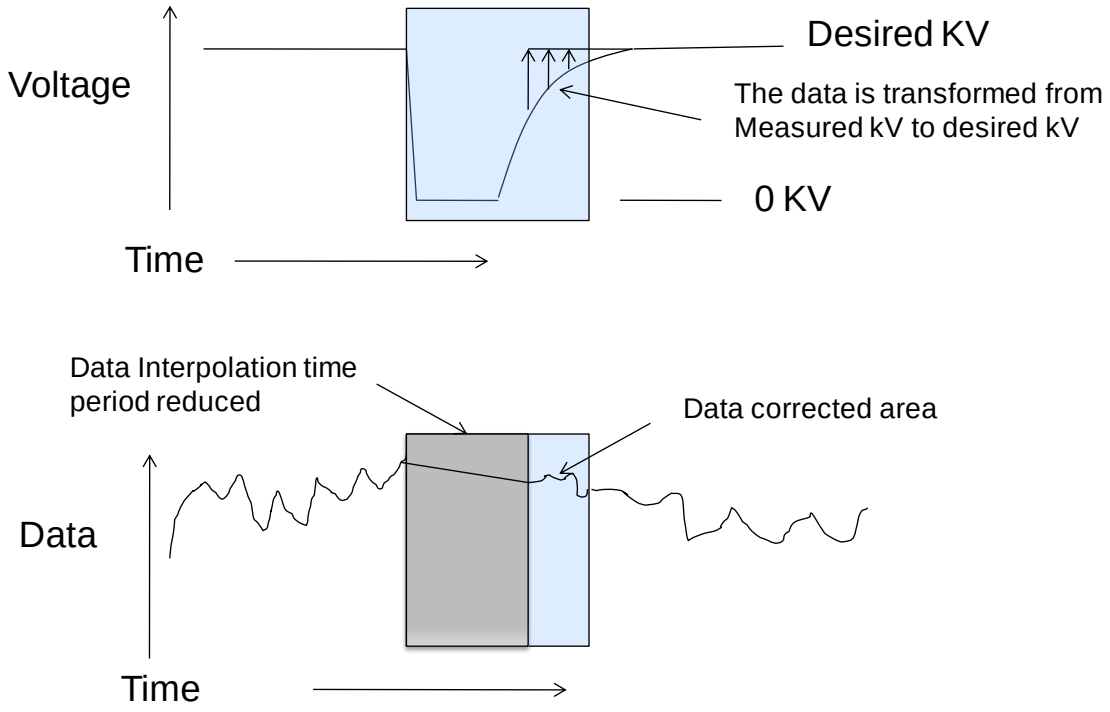

Figure 21: Proposed Implementation for Partial-Data Interpolation

Figure 20 shows a standard arc handling method where data is interpolated over the entire arc duration. Figure 21 shows the proposed method of partial-data interpolation where we use the new algorithm to translate or correct measured data to its equivalent at the programmed voltage during the tail part of the arc event and then perform standard interpolation over the remaining duration. Though it may seem from the figure that since the voltage is constant over the entire duration simple linear interpolation would offer a perfect correction, it is important to note that the part of the object being imaged is not necessarily uniform. There is definitely a benefit to using real data for correction, which will correspond to the objects relevant attenuation characteristics.

To summarize, the basic principle of the partial-data interpolation method is a substitution or addition of real data during part of the arc interpolation to enhance the quality of the resulting image. The advantage of this is that instead of assuming or guessing (using standard interpolation) what the attenuation ratios will be during the period of an arc, we now use real information in conjunction with the previous interpolation routine. Note that there is still a need for interpolation because the part where the voltage drops to zero (the early part of the arc) does not have any X-ray production, thus no data at all.

We can see that the proposed partial-data interpolation is performed in-line with the standard interpolation and is a complementary method rather than a replacement for the standard interpolation.

CHAPTER 5

THE PARTIAL-DATA ALGORITHM

After having simulated and compared data with real measurements, the data obtained is then used to derive mathematical relationships between the various variables of interest. Once we have the equation to measure real-time voltage during a scan, and more particularly during an arcing scan, we need to derive the relationship between voltages and thicknesses of water to the attenuation ratio, $\mu_w t$. We start by first finding the relationship between $\mu_w t$ and voltage in terms of some unknown variables *a*, *b* and *c*.

Using some knowledge about the general relationship of voltage to the attenuation ratio and several rounds of trial and error, I formulated equation (4) as a best representation to fit the data collected.

$$\mu_w t = \left(\frac{a}{(v-b)^{0.5}}\right) + c \qquad (4)$$

where *v* is the voltage and *a, b* and *c* are constants to be determined. The inverse relationship between μ and voltage is a known one and has been shown in [24]. I used trial and error to arrive at the structure for equation (4). For each thickness shown in

figure 17 (5 cm through 40 cm), *a*, *b* and *c* were determined using the Newton-Raphson method in Mathcad®. Then each *a*, *b* and *c* were fitted to first and second order polynomials in terms of *t*. I then replaced *a, b* and *c* in terms of thickness *t*, in equation (4) to get μ_w as shown in equation (5).

The equation was initially formulated only with one variable based on the knowledge that voltage has an exponential relationship with μ (the 0.5 exponent choice was based on prior experience of working with attenuation ratios and tube voltage relationships) which was then followed by selection of more variables to best fit the data that had been collected. Note that this is only one way of representing the voltage to attenuation ratio relationship; others could also be derived using different approaches of curve fitting.

Equation (4) was solved using the MathCAD solver, using values from the simulations and forming 3 equations to solve for *a, b* and *c*, which gave us the following values:

For the following water thicknesses (in cm):

t = [5 10 15 20 25 30 35 40]

The corresponding *a, b* and *c* values obtained were:

a= [3.029 5.88 8.836 11.5 15.09 18.376 21.757 25.234]

b= [33.129 32.7 32.08 32.391 30.73 30.069 29.435 28.824]

c= [0.733 1.375 1.998 2.641 3.192 3.766 4.326 4.873]

Then using the polynomial fit function in Matlab to solve for *a*, *b* and *c* in terms of thickness, *t*, I found that the *a* and *b* curves were best fit with second order polynomials and *c* with a first order polynomial to get the following solutions:

$$a = 0.0026t^2 + 0.5191t + 0.3801$$

$$b = -0.0015t^2 - 0.0620t + 33.5132$$

$$c = 0.1181t + 0.2064$$

Replacing these values of *a*, *b* and *c* in the original equation (4) above, we get

$$\mu_w = \left(\frac{(0.0026\,t^2 + 0.5191t + 0.3801)}{(KV + 0.0015\,t^2 + 0.0620t - 33.5132)^{0.5}}\right) + 0.1181t + 0.2064 \qquad (5)$$

where *t* is the thickness of the relevant part of the scanned object. This equation was found to provide results with an average accuracy of approximately 2.5% when compared with the data. Equation (5) gives the relation between $\mu_w t$, voltage and *t*. It can be used to solve for any one of the three variables when given the remaining two. Now that the full equation has been derived, we can go on to lay out the algorithm steps.

The partial-data algorithm process can be implemented in the following steps. These steps are also illustrated in figure 22.

A. Scan an object during an arc event and collect measured image data (I_m), data from a detector covered with copper (I_c) and data from an unblocked reference

detector (I_0). The data contains the $\mu_c t_c$ (copper) and $\mu_w t_w$ (water) needed for subsequent calculations.

B. Solve for voltage measured at a particular point (kV_m) on the rising voltage curve using equation (3). We have $\mu_c t_c$ (measured) at the copper strip covered detectors.

C. Equate the $\mu_m t_m$ to $\mu_w t_w$ based on our approximation that the body equals water. $\mu_m t_m$ (measured) = f (v (estimated), t) as shown in equation (5).

D. Using the $\mu_w t_w$ from the image detector data and kV_m obtained from step B, use equation (5) to solve for t (estimated) using an iterative method. This is the thickness of water (t_{w2} in Figure 8) at the voltage kV_m and $\mu_w t_w$.

E. Use this thickness of water to solve the following (also using equation (5)): $\mu_w t_w$ (corrected) = f (v (programmed), t (estimated)). kV_{set} shows the programmed voltage in Figure 8.

   This is the translated $\mu_w t_w$ provided to the reconstruction system to fill in the missing data during the arc.

F. Repeat steps B through E for all points measured on the rising voltage curve.

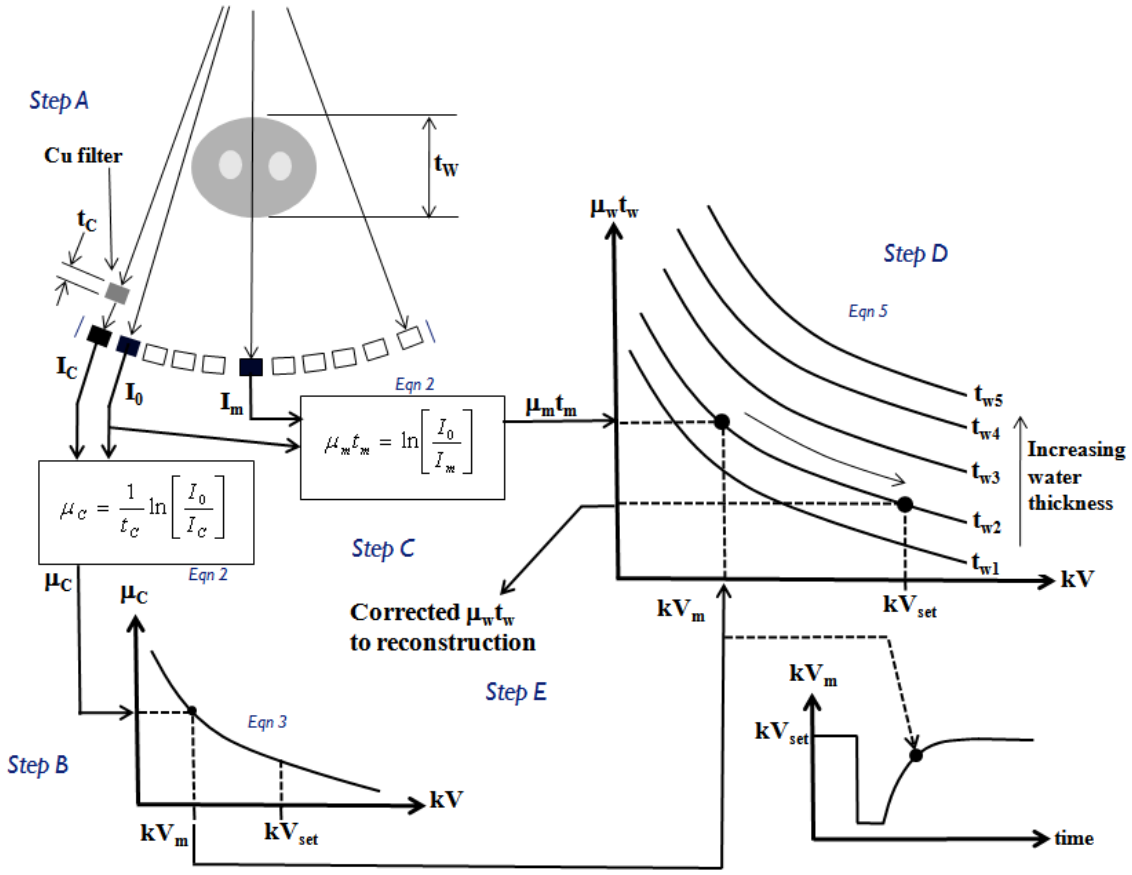

Figure 22: Complete Process Implementation

The algorithm implementation requires that the arc status be detected, select the last few views to correct, then reset the corrected views. The corrected views will contain good data and we do not want those to be interpolated during the reconstruction steps. Figures 23 through 26 show this manipulation of the arc status for the algorithm, where we can see the hardware line status during arcs before and after the correction done in the partial data algorithm implementation. Figure 23 shows the status of the hardware bit in the data header from a scan performed on a system with special code installed to simulate an arc every 100 milliseconds. Since the total length of the scan was about 300ms, we can see 3 arcs during the entire 2400 views. The vertical axis shows the hexadecimal values

of different reads made during the reconstruction process. For our specific purpose, it is sufficient to know that the three spikes we see are representative of the arc status being high during the data points that they correspond to.

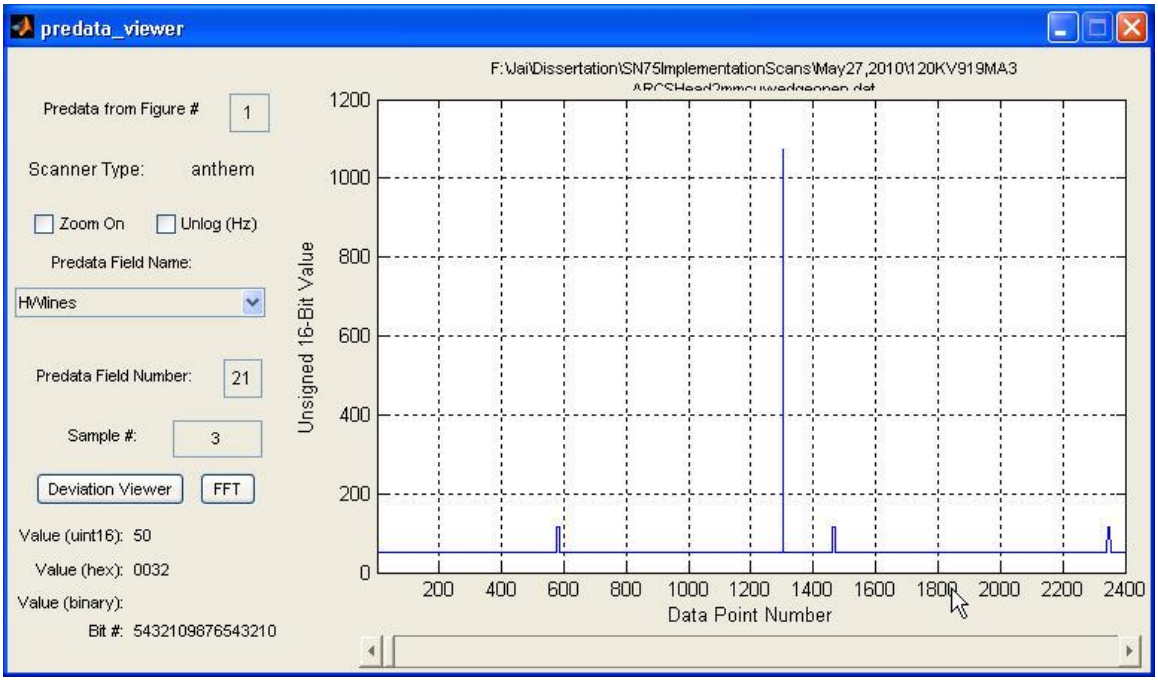

Figure 23: Arc Status During Three Arc Events

Views are the number of acquisitions that take place during a complete rotational scan of 360 degrees of rotation around the patient. This is a selectable number based on how much data is desired from the scan (the higher the number of views means that each view is of a shorter duration). The tall line is a rotation index marker, which is a count of rotations during the particular scan. So the one high value shows that one rotation took place during this scan. Also, each arc event covers a number of views, shown in detail in figure 24.

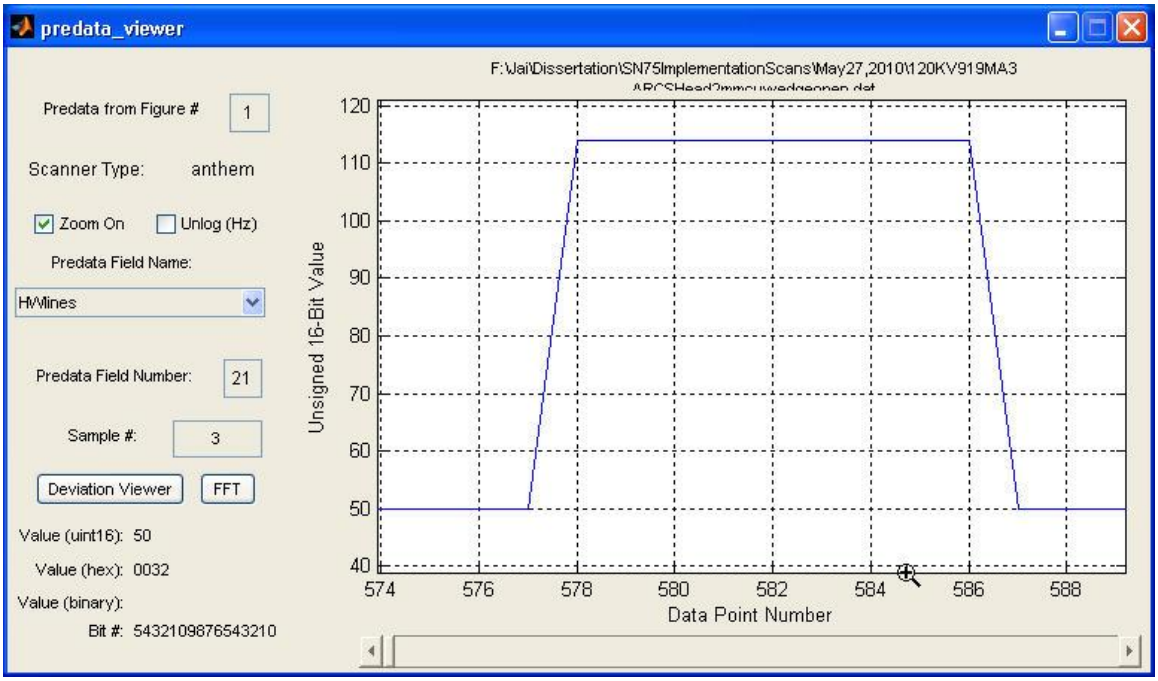

Figure 24: Uncorrected Arc Status Showing Arc Lasting for Ten Views

Here we can see that the arc event lasts 10 views, from view number 577 to 587. This bit stays active till the voltage has fully recovered to the programmed value and the level it was at before the arc event.

Figure 25 shows the hardware line status of the same scan data file header after being processed through the partial data algorithm. The widths of the three arc events can be seen to be narrower than the previous case (better seen in the smaller number of views zoomed in figure 26), which shows the corrected status after the partial data correction.

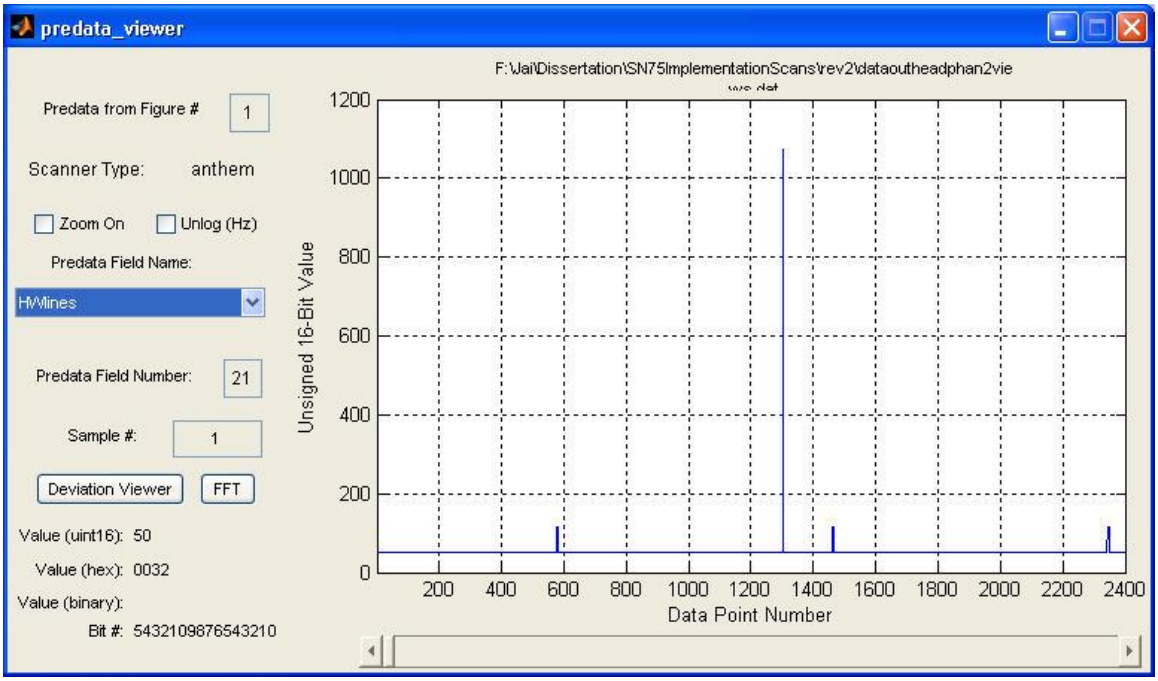

Figure 25: Arc Status After Correction is Applied

Figure 26 shows the number of views during one arc event after correction using the partial data algorithm. We can see that the same arc event is now high only for 8 views as opposed to 10 from the original data header in figure 24. This is because the 2 views have been corrected using the translation developed in this method and after correction, the arc status corresponding to the corrected views are reset before performing image reconstruction on the data.

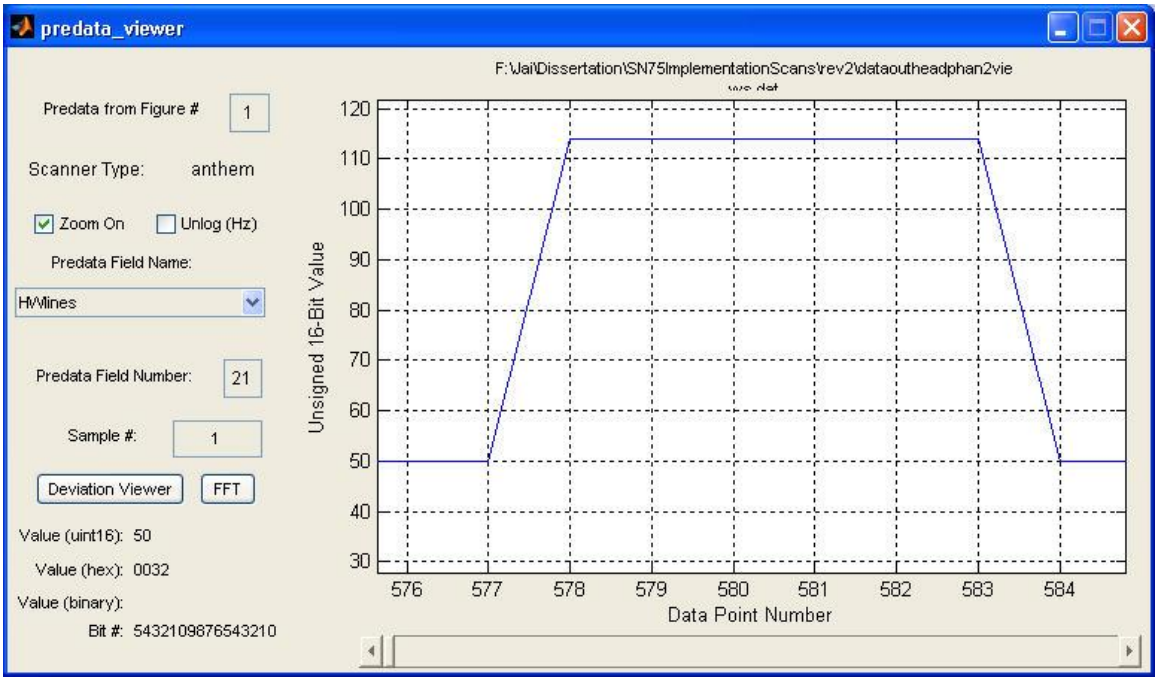

Figure 26: Arc Status for One Arc, after Partial-data Correction

The reconstruction step then only performs interpolation on the remaining 8 views and the resulting images include the translated data that has been collected during the tail end of the arc. The method to find which points to correct during the arc period was based on selecting a certain threshold of voltage value, which in our case was approximately 60% of programmed value and then correcting data only above that voltage level. I used 60% because I found through experimentation that the signal below 60% was very low and close to the common noise levels in the data, which would make it very difficult to differentiate from noise. When the voltage is low the signal to noise ratio becomes very low and makes for unclear images. The implementation of the correction part of the process is described in a simplified flowchart shown in figure 27, which leads

into the implementation and results of the partial-data interpolation algorithm in the following chapter.

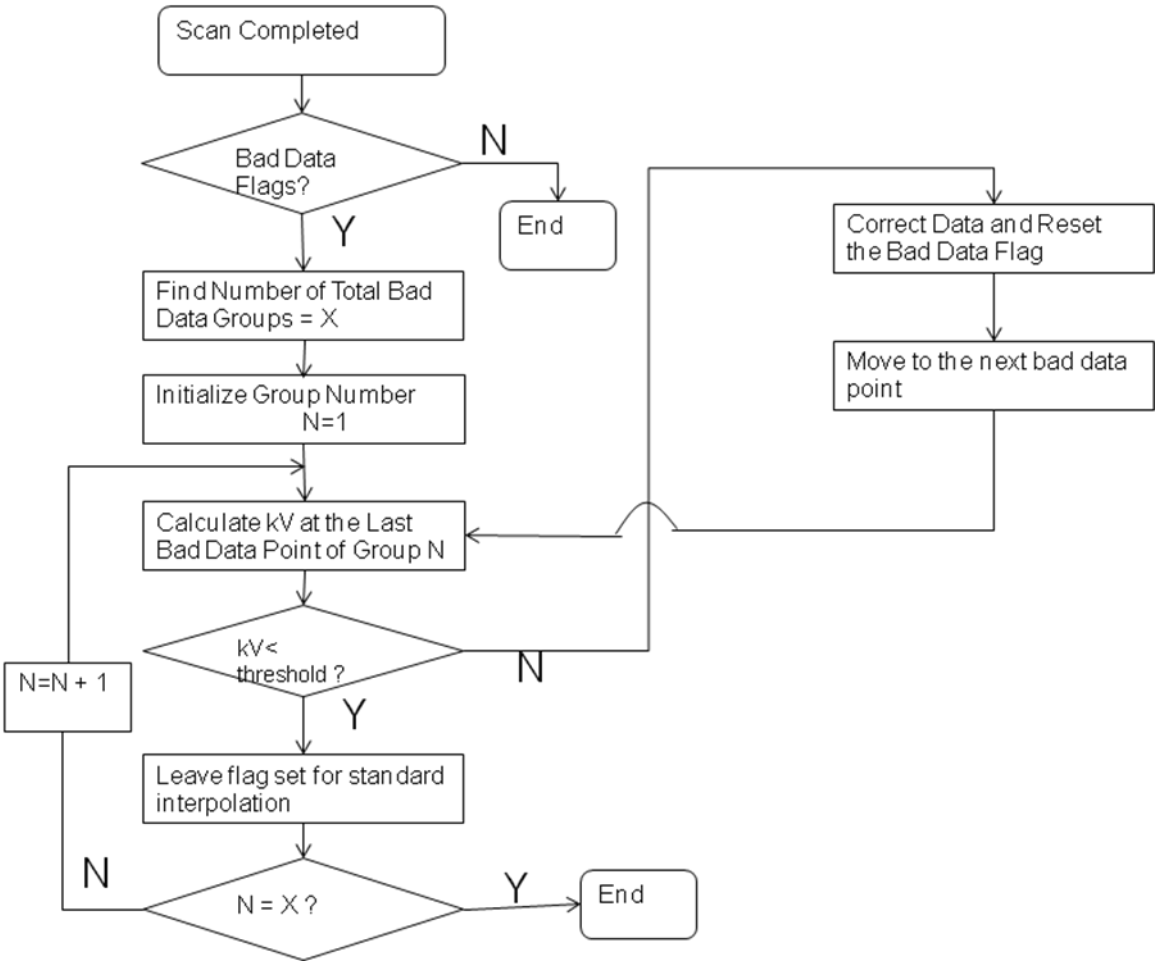

Figure 27: Correction Algorithm Implementation Flowchart. Each Data Group Represents an Arc.

CHAPTER 6

IMPLEMENTATION AND RESULTS

The final implementation of the algorithm was coded in Matlab, which was run on data from a scan on a scanner with special arc simulation code, using copper strips on the detectors to measure real-time voltage. The code had a routine to detect arc active status in the data header and apply the algorithm on data views corresponding to the tail end of the arc duration (only corresponding to the rising voltage detected by the copper). The corrected view arc status was then reset, and then the output data was run through a regular reconstruction sequence, which performed linear interpolation on the remaining arc bits. Thus, the result of our algorithm is a combination of standard interpolation and partial-data correction.

The partial-data algorithm was implemented on data that was collected on a Philips Brilliance iCT ™, 256 slice scanner using arc simulation software, which actually causes the tube voltage to shut-off during a scan and rise again just like during a real arc. Copper strips of 2 mm thickness (two strips of 1 mm each) were placed in the x-ray path to detect the rising voltage level, and the data was then processed using both the standard interpolation and partial data algorithms. All were axial scans performed at 120 KV, 919 mA, and 0.27 seconds duration at 220 RPM. The special code was made to cause an arc

status every 60 ms, so 3 arcs were simulated during the 270 ms scan period. The power supply, on seeing this arc status, would respond like it does to a real arc, by shutting down the voltage production for 500 micro-seconds (us) and then bringing up the voltage to the requested value (another 500 us), thus creating an arc period of 1millisecond.

Figure 28 shows the setup used in the implementation and validation of the partial-data algorithm. It shows the copper strips placed over a small number of detectors at one end of the array, which serve to measure real-time voltage in this case. The phantom is the object being imaged and the images obtained of the two different objects scanned are shown in figures 30 through 34.

The algorithm is implemented after collecting data from the scan. The data in this case includes those detectors covered by the copper, thus providing information that can be used to determine voltage during the arc portions of the scan.

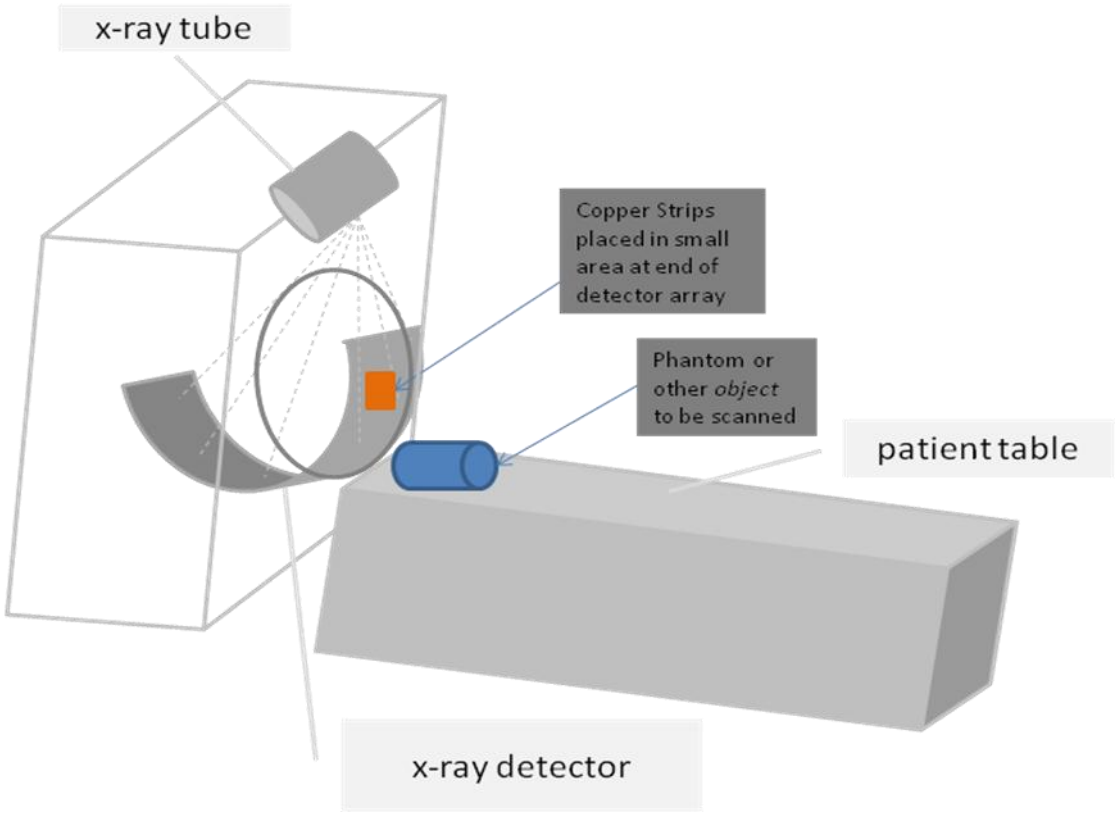

Figure 28: Experimental Setup

Note that the copper strips in this case have been placed on the scanner detectors only for convenience, since we are only looking at a small section of the images for our measurements and ignoring the area covered by the copper. In a system implementation, this copper filter will need to be placed outside the field of view, preferably on a small detector array placed in the collimator to make voltage measurements. Figure 29 shows another setup to implement the algorithm, with the phantom being replaced by a human body to show how it would look during system implementation.

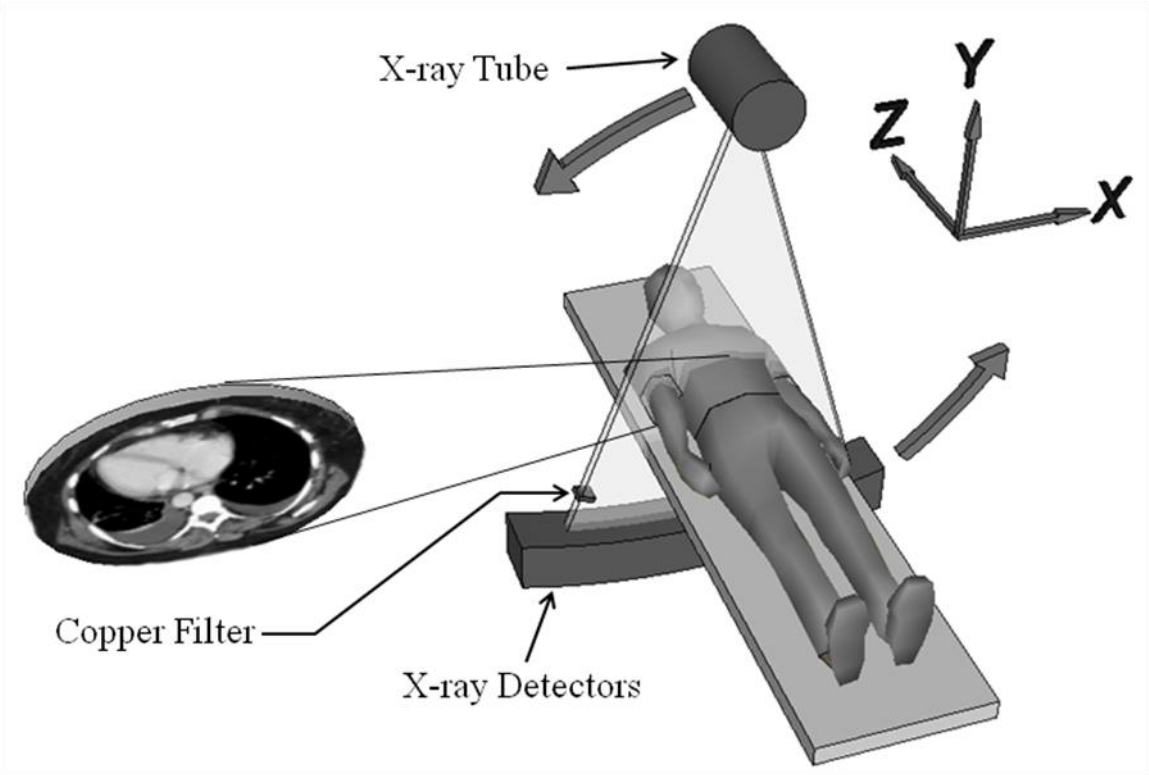

Figure 29: Location of copper filter at edge of CT detector array and unblocked by scanned object

Figure 30 shows a snapshot of the original and corrected data during the arcing. We can see three arc events where the peaks depict the detector levels during the arc. The lower line shows the data corrected by the partial data algorithm.

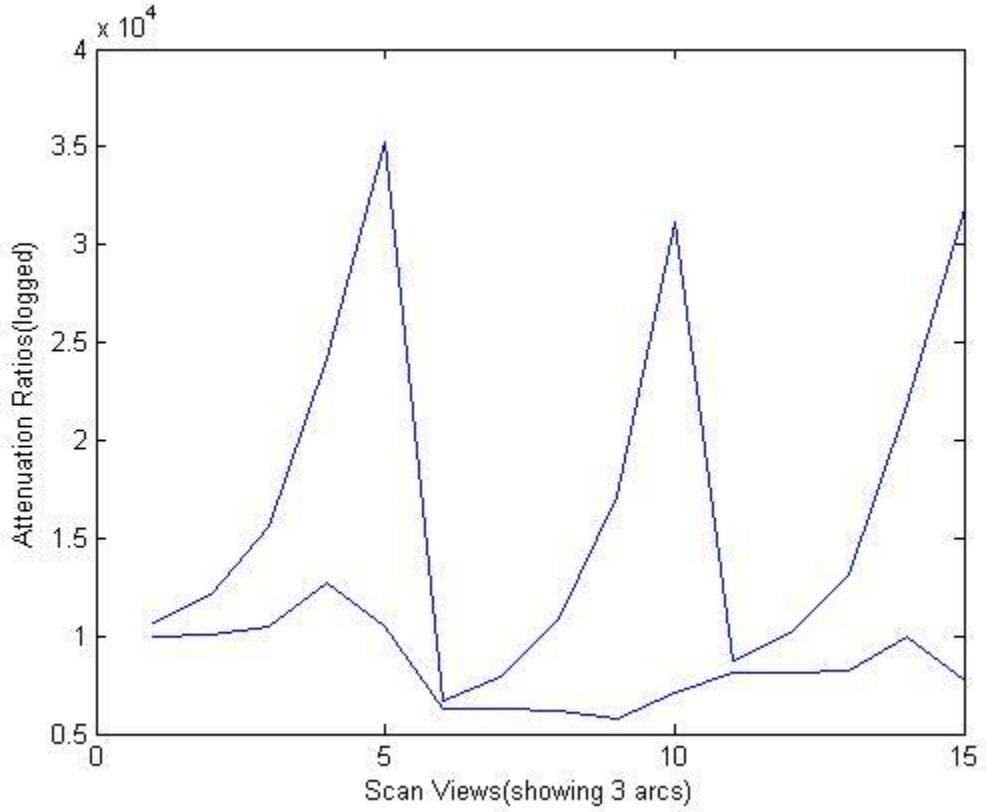

Figure 30: Actual (Upper Line) and Corrected Detector Levels (Lower) during Three Arcs

The partial data algorithm was implemented in Matlab code, which processed the data from the scanner, using the arc status in the data file header to select views to be corrected during arcing. The resulting images are shown in figures 31 through 35. All statistical units are in Hounsfield units (HU), which is a quantitative scale for describing attenuation coefficient measurement.

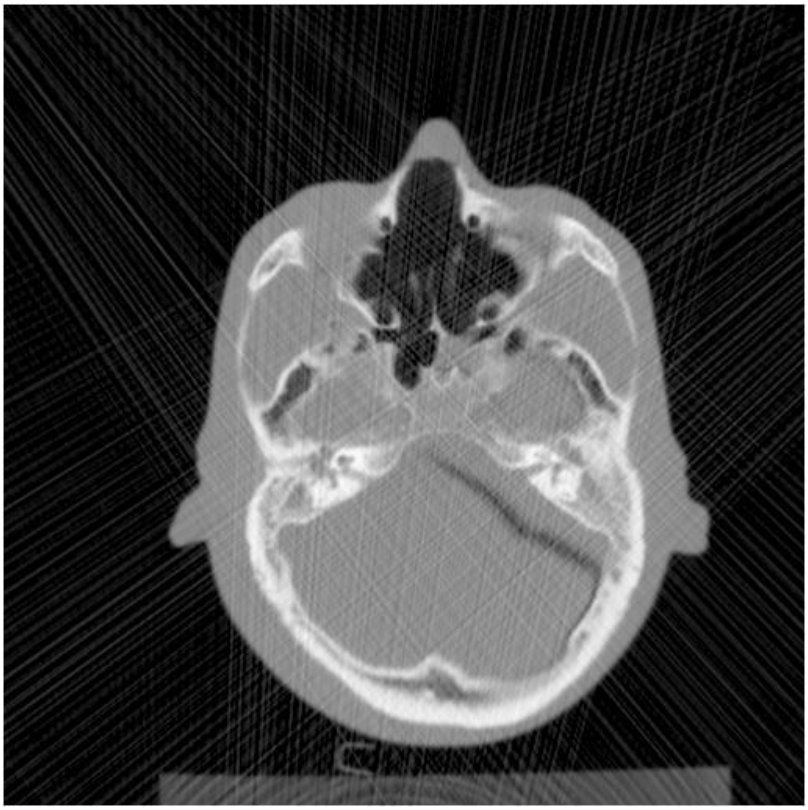

Figure 31: Head Phantom Image without Interpolation (Three Arcs During Scan)

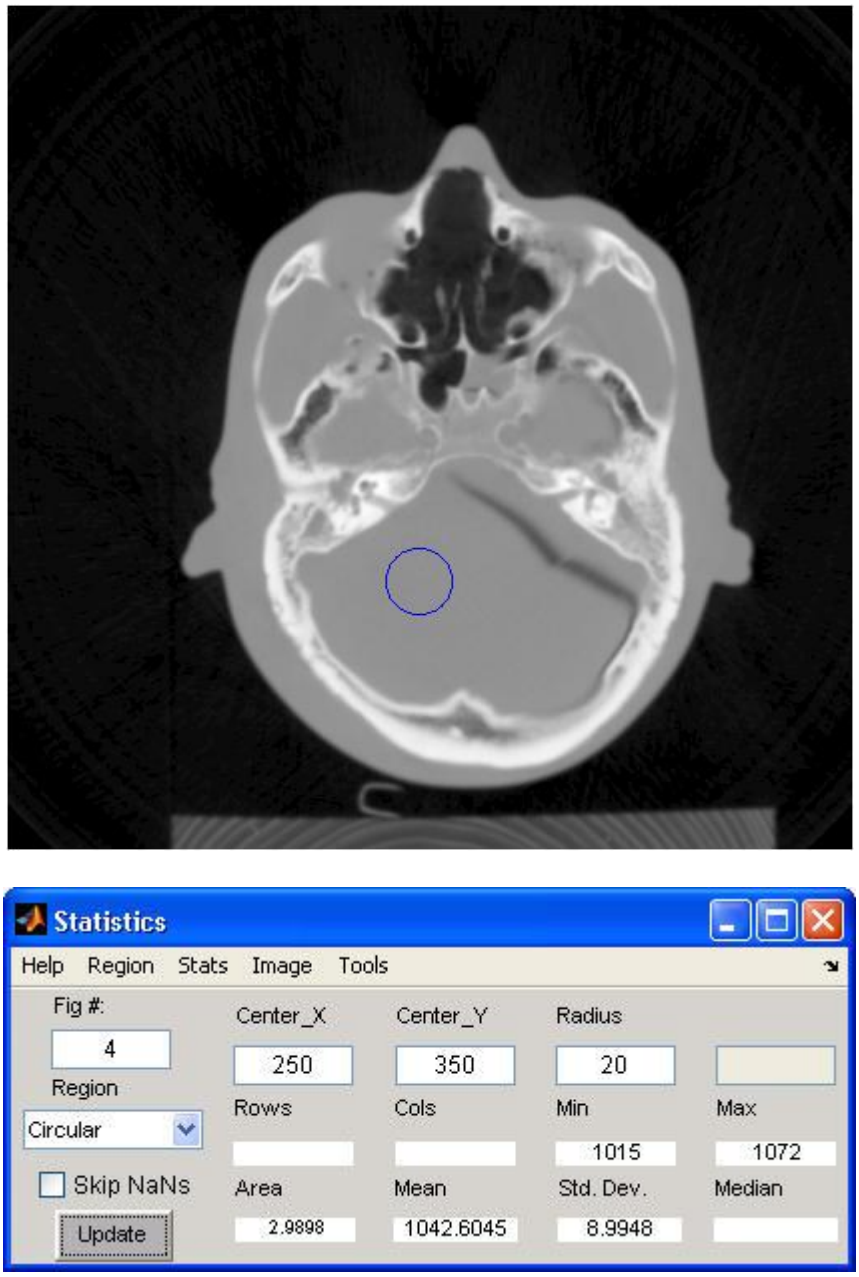

Figure 32: Head Phantom Using Standard Interpolation with ROI and Statistics

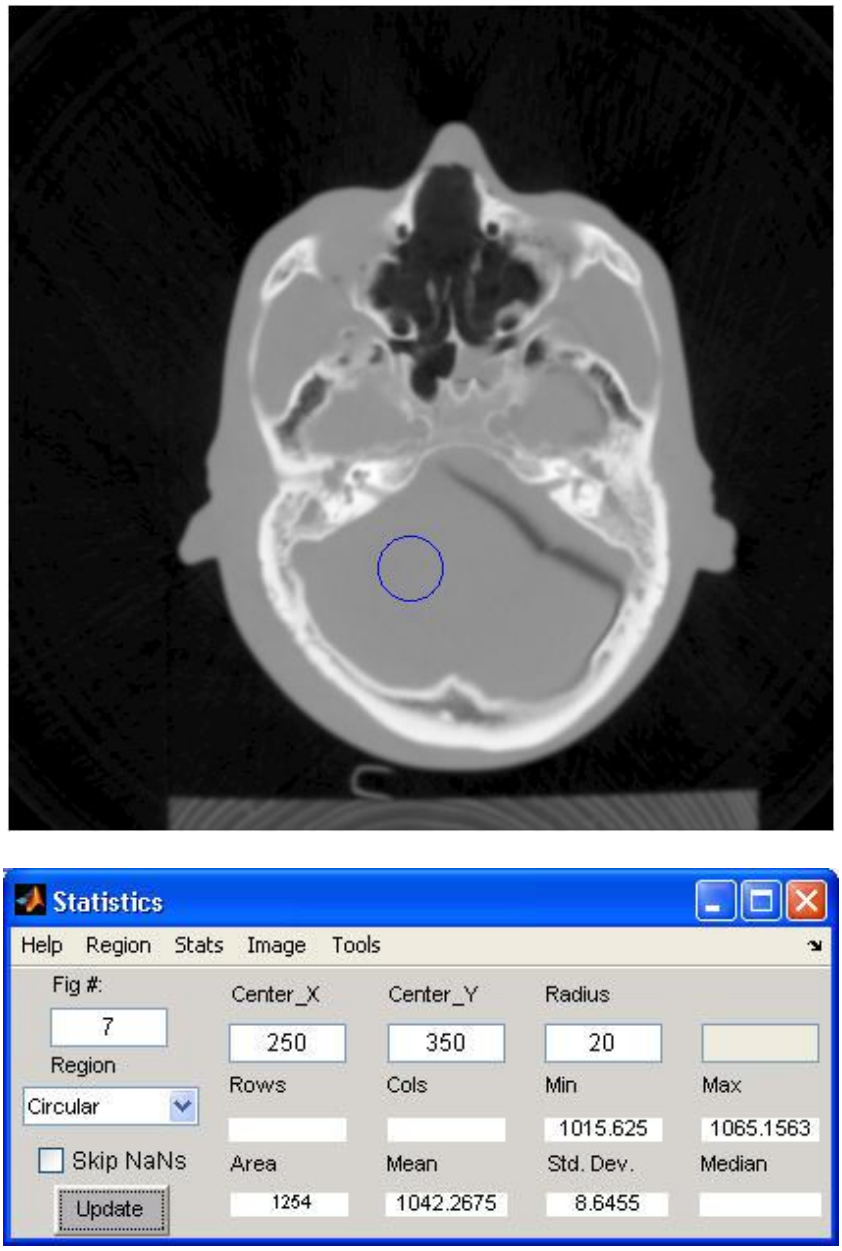

Figure 33: Head Phantom Using Partial Data Interpolation with ROI and Statistics

Note that the region of least variation in the object was chosen as the region of interest. The standard deviation in these regions show which image has the lower variation or noise level and therefore, it can be concluded that the partial data algorithm shows an improvement over the standard interpolation method. This difference is only

small in this case (8.998 vs 8.645) but it is an improvement over the interpolation method and will be even more pronounced in scanners with higher rotation speeds. The standard deviation in an image without any arcs for the same region was 5.10 HU.

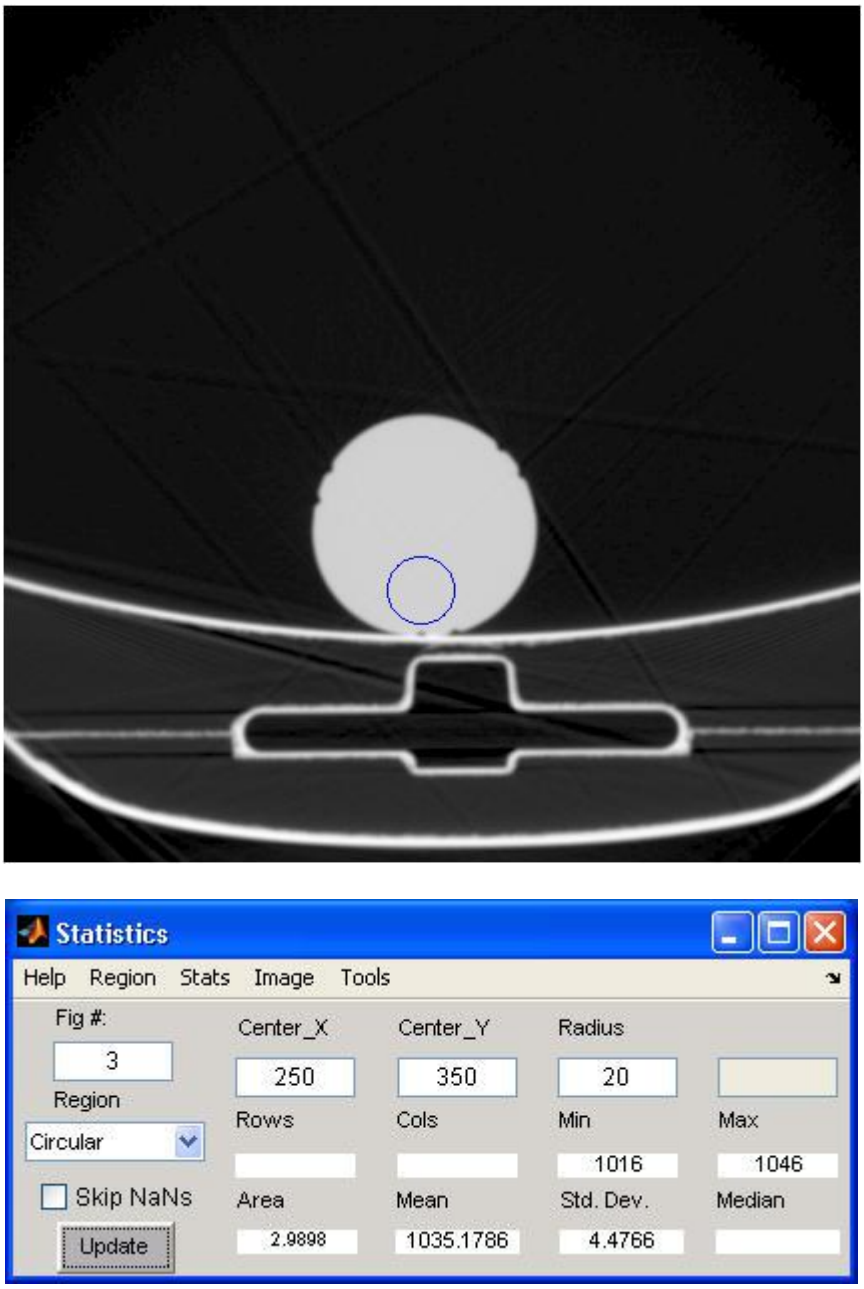

Figure 34: Water Bottle Scan Using Standard Interpolation with ROI and Statistics

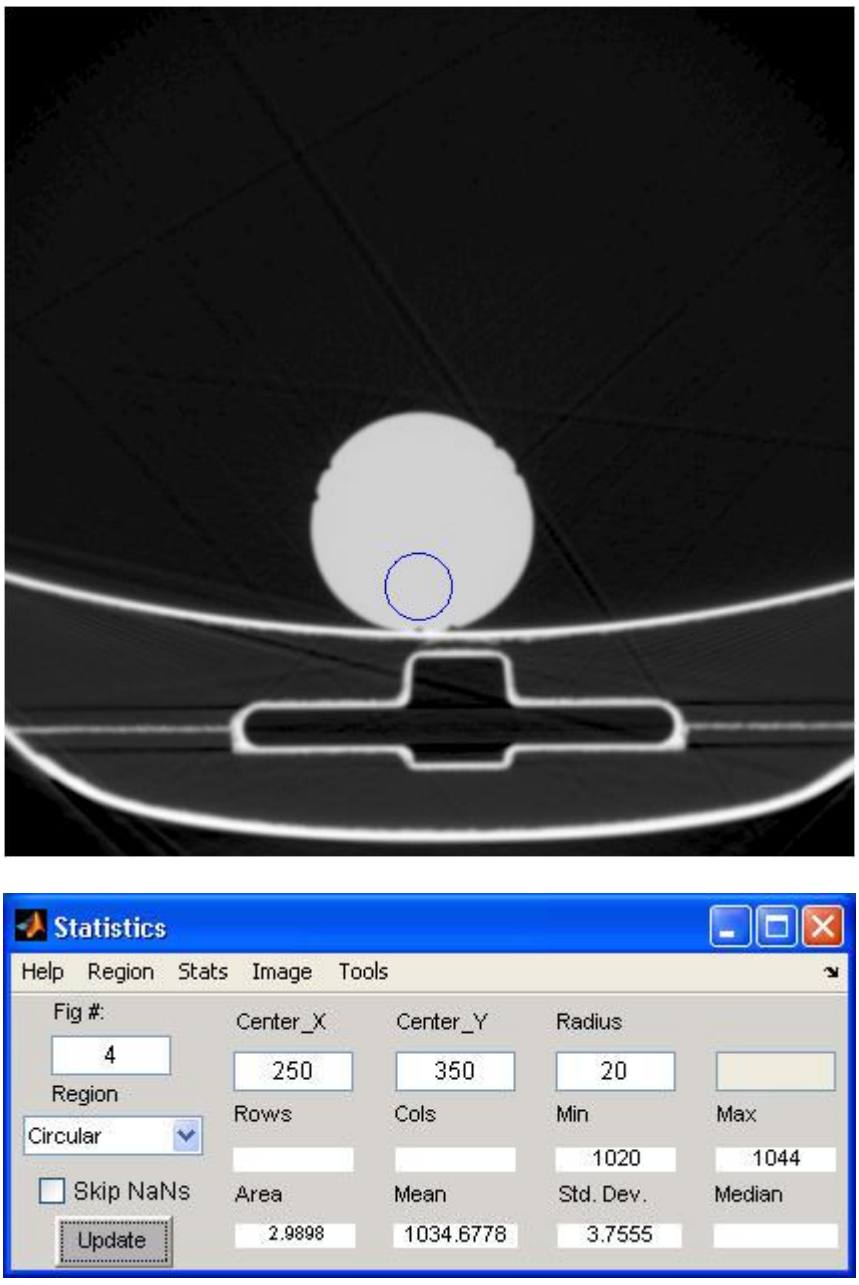

Figure 35: Water Bottle Scan Using Partial Data Interpolation with ROI and Statistics

Several repetitions of scans were done, and both methods were applied to the resulting data. Multiple sets of images were reconstructed using both methods. A head phantom and a water bottle were used to get a variation in the type of objects used to test the algorithm. Different locations for ROI's were selected. The results are shown in table 1.

Object Scanned	Std Deviation using Standard Interpolation (in HU)	Std Deviation using Partial-Data Interpolation (in HU)	Improvement of Partial Data over Standard Interpolation
Head Phantom	8.9948	8.6455	3.88%
Water Bottle	4.4766	3.7555	16.11%
Head Phantom	9.7882	9.614	1.78%
Water Bottle	2.8132	2.3316	17.12%
Head Phantom	8.1301	7.3155	10.02%
Water Bottle	3.5463	2.856	19.47%
Head Phantom	11.3338	10.5721	6.72%
Water Bottle	2.9359	2.3408	20.27%
Head Phantom	8.00	6.98	12.75%
Water Bottle	3.41	2.50	26.68%

Head Phantom	12.10	11.71	3.22%
Water Bottle	2.82	2.42	14.18%

TABLE I: Statistics from Scans Using Standard and Partial Data Methods

These differences in standard deviation values are in regions where a lower deviation is considered a better quality of image. The comparison shows that there is a lower level of noise in the partial data interpolated images, which means a better image quality. Even though there is no general acceptance of a single measure for defining image quality in CT scanning, there are several different quantitative evaluations that have been developed, one of which is known as a figure of merit which has been described in [25] as

$$Q = c.\frac{1}{(\sigma^2.\rho^{-4}.D)} \tag{6}$$

where

Q = figure of merit or image quality

c = constant

σ = standard deviation

ρ = Modulation transfer function (MTF)

D = dose, measured in milli Grays (mGy)

As we can see from equation (6), the variance (σ^2) is inversely proportional to the figure of merit in this case, which shows that the reduction in noise standard deviation

(standard deviation is defined as the square root of variance) in the images obtained with the partial data algorithm as compared to the standard interpolation leads to an improvement in image quality.

As mentioned earlier, this method provides benefit in cases where the scans are of high speeds (or short duration) that even one or two arcs will affect the image significantly. In this case, the image quality is consistently better than the standard method, which shows the benefit of using real data during arcs (in combination with interpolation) as opposed to a method that uses only interpolation. Equation (6) shows that the standard deviation is a good metric of image quality.

There are several methods to evaluate image quality such as that used in [26], where the author reviews limitations of picture quality in CT systems. He focuses on picture grain and its relationship to matrix size. In [27], the authors evaluate the correlation of radiation dose with image quality. They also measure image noise as it contributes to the overall image quality and its correlation to the CT dose index (CTDI). In practically all studies done on image quality evaluations in CT, the noise variation or standard deviation as measured here is a significant contributor to image quality.

To quantify the effect scan speed will have on how much data is lost or can be saved by this new method, I have compared some scenarios in Table 2. Assuming an arc lasts about 1 millisecond (time taken to recover from an arc in a Philips premium system today), and since one rotation is 360 degrees, we calculate the amount of data lost during one rotation in terms of the angular data.

Scanner Speed (RPM)	Rotation Time or time for one rotation (seconds)	Integration period = Rotation time/ # of views in one rotation (micro-seconds)	Angular Data Lost during 1 ms arc = 1 ms/rotation time × 360 (degrees)
120	0.5	208	0.72
180	0.33	137	1.09
200	0.30	125	1.2
220	0.27	112	1.33
300	0.20	83	1.8

TABLE II: SCANNER ROTATION SPEEDS AND THEIR EFFECTS ON DATA LOST DURING ARCING. 2400 VIEWS PER ROTATION WERE USED IN THIS CALCULATION.

Since CT images are generated using data obtained during angular acquisition during a scan, any loss of angular data is a contributor to artifacts in images [1]. In the case of, for example, the 220 RPM scan, we lose 1.33 degrees during each arc and each arc lasts at least 1 millisecond, so if we have multiple arcs we can lose several degrees of data. However, using the partial-data interpolation method we can save up to 30% (60 to 90% of rising voltage) of the data from the arc duration from being lost. If we say we have 3 contiguous arcs on the 220 RPM scan, we can save 30% of 3×1.33 degrees, which is approximately 1.2 degrees. One can see from the table that if we save the same percentage in an even faster scan, like the 300 RPM one, we can save up to 1.6 degrees of

data from being lost. This just shows the significance the rotation speed has on the amount of data being recovered. Note that 120 to 220 RPM scanners already exist in today's market. It is known from market reports that at least one CT manufacturer is currently working on a 300 RPM scanner [28] and the others will follow suit soon afterwards. This method then becomes more and more relevant in the competitive design sphere.

CHAPTER 7

CONCLUSION

A new method of interpolation has been proposed for handling arcing in an x-ray tube in a CT scanner. We collect image data while the tube voltage recovers to its programmed value after an arc, providing voltage corrected data during arcs (in combination with interpolation) as opposed to a method that uses only interpolation. Results show that this is an effective method and will enhance the performance of a high rotation speed scanner in arcing situations.

The algorithm was verified on a CT scanner during an arc event. The test was performed on a system with special software that simulates an arc condition by programming arcs into the system, which causes the voltage to switch off and turn on again after a short delay. I scanned a head phantom on a scanner with this special arc code installed. I then reconstructed both data sets, one with a standard interpolation method and the other with our partial-data algorithm. I compared the two images by selecting a region of interest in the same location in both images, and running a statistical analysis on both. The region of interest chosen was one with maximum uniformity, so the standard deviation number shows the variation or noise in a region where the lower

thee deviation, the lesser the artifacts. In this comparison, the partial-data algorithm showed an improvement over the standard interpolation method.

7.1 Benefits of Partial-Data Interpolation

- Improved image quality during tube arcing
- Improved arc handling and minimization of its effects can prove to be a competitive edge for a scanner manufacturer.
- Sometimes, scanning has to be repeated because of arc induced artifacts. This method could prevent this repeat of scan by reducing artifacts caused during a part of the scan. This could mean a 50% lower radiation exposure to a patient in such cases simply by not having to repeat the scan when arcing occurs.
- Power supply arc recovery requirements could be reduced if this method is used to reconstruct data during an arc. This could result in significant cost reductions in generator manufacture by replacing expensive design and components with a mathematical solution implemented in software.
- X-ray tube arcing rates typically increase when the tubes near end of their life. This method could help extend some of the tube life by allowing use of the scanner while a replacement is received.

7.2 Future Research

Today's scanners are limited in their rotation speeds to a maximum of around 272 milliseconds per rotation. These speeds are constantly being improved to get better resolution and lessen scan times for patients. The rotation speeds determine the duration of integration times for reconstruction and CT systems become more sensitive to any loss of data with any small increase in speed. The method proposed here will be of immense help to lessen the loss of data during arcing in such cases.

This study is only the first step to provide a preliminary implementation of the proposed method. At the time of system implementation, more work will need to be done to account for attenuation coefficient characterization of body parts like bone, tissue, fat and contrast agents. This experiment was done using water coefficients to prove that the concept works.

This research was performed with a futuristic view, and will become more and more relevant as the industry pushes towards faster rotational speed scanners, which define the need for smaller integration periods of reconstruction. Arcing during these smaller integration periods will manifest more adverse effects on images.

With an increase of scanner speeds beyond 220 RPM or 272 ms per rotation, future research could include expanding this study to possibly using data at even lower levels of voltage than those used here, which will need efforts to be made to combine different noise lowering and image quality improvement techniques with a partial data algorithm type of data translation, which will allow a lot more data recovery during arcing and even better image quality. In fact, even the method used here could benefit largely from a combination with image noise reduction techniques at the current scanner speeds.

REFERENCES

[1] Jiang Hsieh, "Computed Tomography- Principles, Design, Artifacts and Recent Advances," The International Society for Optical Engineering, SPIE Press Monograph Vol. PM 114, 2003.

[2] J. Rajwade, Emission Control System for an X-ray Tube, Master's Thesis, Cleveland State University, 2001.

http://www.csuohio.edu/engineering/ece/research/theses/2001/JaisinghThesis.pdf

[3] Guy M. Besson, "CT Image Reconstruction from Fan-Parallel Projection Data," Medical Physics, pp. 415-426, Volume 26, Issue 3, March 1999.

[4] Fathelalem F. Ali, Sachiko Yokegawa, Zensho Nakao & Yen-Wei ChenVivo "CT Image Reconstruction by Stochastic Relaxation," Third International Conference on Knowledge-Based Intelligent Information Engineering Systems, pp. 345–348, 31st Aug-1st Sept 1999,Adelaide, Australia.

[5] K.C Tam,H. Bruder, K. Stierstorfer, T. Flohr,K. Sourbelle and A. Khamene, "Improving Large Angle Cone Beam CT Image Reconstruction With Practical Supplementary Information," Nuclear Science Symposium Conference Record, pp. 998-1002, IEEE Volume 2, Issue 10-16, November 2002.

[6] Abhishek Mitra, Swapna Banerjee, "A new Interpolation Free Method for C-Ray CT Image Reconstruction," Proceedings of the 17th IEEE Symposium on Computer-Based Medical Systems, 2004.

[7] Adam M. Alessio, Paul E. Kinahan and Thomas K. Lewellen, “Improved Quantitation for PET/CT Image Reconstruction with System Modeling and Anatomical Priors,” Proceedings of SPIE 0277-786X, 2005.

[8] Paul J. Keall, Leah B. Chock, Robert Jeraj, Jeffrey V. Siebers and Radhe Mohan, “Image Reconstruction and the Effect on Dose Calculation for Hip Prostheses,” Medical Dosimetry, pp. 113-117, 2003, Vol. 28, No. 2.

[9] Jozef Pucik, Rami Oweis, “CT Image Reconstruction Approaches Applied to Time-Frequency Representation of Signals,” EURASIP Journal on Applied Signal Processing pp. 422–429, 2003:5.

[10] Per-Erik Danielsson, Maria Magnusson Seger and Johan Sunnegardh, “Basis and Window Functions in CT,” The Eighth International Meeting on Fully Three-Dimensional Image Reconstruction in Radiology and Nuclear Medicine, pp. 70–74, 6 July 2005.

[11] J. Blobel, M. Okumura, T. Ota, M. Tsuyuki, H. de Vries, J. Hall, J. Mews, “Heart-Rate Adaptive CT Image Reconstruction with automatic phase selection,” Computed Tomography Visions II-07, pp. 27-31, 2007.

[12] Asher Gringauz, Yoav Bar, “CT Image Reconstruction,” US Patent 6845143, January 18, 2005.

[13] Guy M. Besson, “Data Rebinning to increase resolution in CT Image Reconstruction,” US Patent 6411670, June 25, 2002.

[14] K. Rajan, L.M. Patnaik, J. Ramakrishna, “High-Speed Reconstruction based on CBP and Fourier Inversion Methods,” Proceedings of the High-Performance Computing on the Information Superhighway, pp. 401-406, HPC-Asia 1997.

[15] Alexei Ramotar, Jeff Orchard, “General Geometry CT Reconstruction,” The 2006 International Conference on Image Processing, Computer Vision, and Pattern Recognition, IPCV 2006.

[16] Mark A. Anastasio, Xiaochuan Pan and Eric Clarkson, “Comments on the Filtered Backprojection Algorithm, Range Conditions, and the Pseudoinverse Solution,” IEEE Transactions On Medical Imaging, Vol. 20, No. 6, pp 539-542, June 2001.

[17] Michael F. Gard, John M. Sandrik, “On-line measurement of X-ray tube voltage in a CT system,” US Patent 5530735 Issued on June 25, 1996.

[18] Jun Ni, Xiang Li, Tao He, Ge Wang, “Review of Parallel Computing Techniques for Computed Tomography Image Reconstruction,” Current Medical Imaging Reviews, Vol. 2, No 4, pp. 405-414, November 2006.

[19] M. Knaup, W. A. Kalender, M. Kachelrieb, “Statistical Cone-Beam CT Image Reconstruction using the Cell Broadband Engine,” IEEE Vol. 5, pp. 2837-2840, Oct. 29, 2006- Nov. 1, 2006.

[20] Avery D. Furbee, Lester Miller, Carl F. Bauer, “X-Ray Tube Arc Suppressor,” US Patent 5347571 Issued on September 13, 1994.

[21] Toyomasa Honda, Wataru Taguchi, "X-Ray Computed Tomography Apparatus," US Patent 6449337 Issued September 10, 2002.

[22] Jang Hsieh, Jonathan Schmidt, Clarence Gordon, Joseph Block, "Methods and Apparatus for Tube-Spit Correction," International Patent, Publication number WO 02/43451 A2, Issued 30 May 2002.

[23] R. Carrier, N. Blais, "Phantom Equivalent Thicknesses in Diagnostic Radiology," Physics in Medicine and Biology, pp. 1151-1157, September 1987.

[24] Feng Changchun, Wu Chunlong, Zhou Wei, "Relationship between X-ray attenuation coefficient and X-ray tube voltage," Trends in NDE Science & Technology; Proceedings of the 14th World Conference on Non-Destructive Testing, New Delhi, 8-13 December 1996.Vol. 3, pp 1357 – 1360.

[25] Willi A. Kalender, "Computed Tomography, Fundamentals, System Technology, Image Quality, Applications," Publicis Corporate Publishing, 2nd revised edition, 2005.

[26] G. N. Hounsfield, "Picture Quality of Computed Tomography," American Journal of Roentgentology, 127:3-8, March 1976.

[27] R.J. Scheck, E.M. Coppenrath, M.W. Kellner, K.J. Lehmann, C. Rock, J. Rieger, L. Rothmeier, F. Schweden, A.A. Bauml, K. Hahn, " Radiation Dose and image quality in spiral computed tomography: multicentre evaluation at six institutions," The British Journal of Radiology, 71: 734-744, 1998.

[28] Cheryl Hall Harris, R.N., “Road to RSNA 2008: CT Preview,” Auntminnie.com, October 29, 2008.

APPENDIX

Table III shows the simulated attenuation ratios for different thicknesses of copper. These are the values used to formulate the relationship between μ and voltage as shown in equation (3).

TABLE III: COPPER μt DATA

KV	1mm	2mm	3mm	4mm	5mm
60	2.6474	4.7224	6.6116	8.398	10.1195
65	2.2923	4.0532	5.6506	7.1603	8.6149
70	2.0142	3.5396	4.9196	6.2202	7.4693
75	1.7841	3.1225	4.3299	5.4627	6.5454
80	1.6067	2.802	3.8745	4.8743	5.8245
85	1.4675	2.5484	3.5115	4.4036	5.2474
90	1.3546	2.3408	3.2131	4.0166	4.7737
95	1.2606	2.167	2.9627	3.692	4.3772
100	1.1809	2.019	2.7499	3.417	4.0424
105	1.1129	1.8929	2.5693	3.1851	3.7617
110	1.0544	1.7848	2.4155	2.9887	3.5254
115	1.0035	1.6914	2.2832	2.8206	3.3238
120	0.9589	1.6097	2.168	2.6745	3.1489
125	0.9194	1.5376	2.0665	2.546	2.9951
130	0.8842	1.4734	1.9763	2.4319	2.8585
135	0.8526	1.4159	1.8956	2.3299	2.7364
140	0.8242	1.3642	1.8232	2.2383	2.6266

Table IV contains the simulated μt values that represent the relationship between different thicknesses of water and voltage levels. This relationship was used to formulate equations (4) and (5).

TABLE IV: SIMULATED WATER THICKNESS AND μt DATA

			Water Thickness in cm					
KV	5	10	15	20	25	30	35	40
60	1.3173	2.5	3.6703	4.8303	5.9815	7.1249	8.2616	9.3923
65	1.2726	2.4142	3.5439	4.6635	5.7745	6.8781	7.9752	9.0665
70	1.2352	2.3426	3.4384	4.5247	5.6027	6.6736	7.7383	8.7976
75	1.2021	2.2793	3.3458	4.4031	5.4528	6.4958	7.533	8.5651
80	1.175	2.2278	3.2705	4.3047	5.3316	6.3523	7.3675	8.3778
85	1.1528	2.1856	3.2088	4.2238	5.2318	6.2338	7.2305	8.2224
90	1.134	2.1498	3.1563	4.1549	5.1466	6.1323	7.1128	8.0885
95	1.1177	2.1188	3.1107	4.0947	5.072	6.0432	7.0091	7.9702
100	1.1034	2.0914	3.0702	4.0412	5.0054	5.9635	6.9162	7.864
105	1.0905	2.0668	3.0338	3.993	4.9453	5.8914	6.832	7.7676
110	1.079	2.0445	3.0008	3.9492	4.8905	5.8256	6.7551	7.6795
115	1.0684	2.0241	2.9706	3.909	4.8403	5.7652	6.6844	7.5984
120	1.0587	2.0054	2.9427	3.8719	4.7938	5.7092	6.6189	7.5232
125	1.0496	1.988	2.9168	3.8373	4.7505	5.657	6.5576	7.4529
130	1.0412	1.9717	2.8926	3.805	4.7099	5.6081	6.5002	7.3869
135	1.0334	1.9565	2.8699	3.7747	4.6718	5.5621	6.4462	7.3248
140	1.026	1.9423	2.8486	3.7461	4.6359	5.5187	6.3953	7.2662

Tables V and VI show the μt values that were measured at specific copper and water thicknesses on a CT scanner. These were used to verify and validate the accuracy or correctness of the simulated values shown in tables III and IV.

TABLE V: MEASURED COPPER DATA

Kv	1mm	2mm	3mm	4mm	5mm
80	1.5888	2.723	3.7779	4.7568	5.6547
120	0.9541	1.5699	2.1214	2.6104	3.0542
140	0.8129	1.3181	1.7712	2.1609	2.5211

TABLE VI: MEASURED WATER DATA

KV	5cm	10cm
80	1.14	2.2064
100	1.0837	2.0882
120	1.0435	2.0042
140	1.0124	1.9398

Figures 36 through 47 are the images made to compare the partial data algorithm results with standard interpolation, and are recorded in Table I.

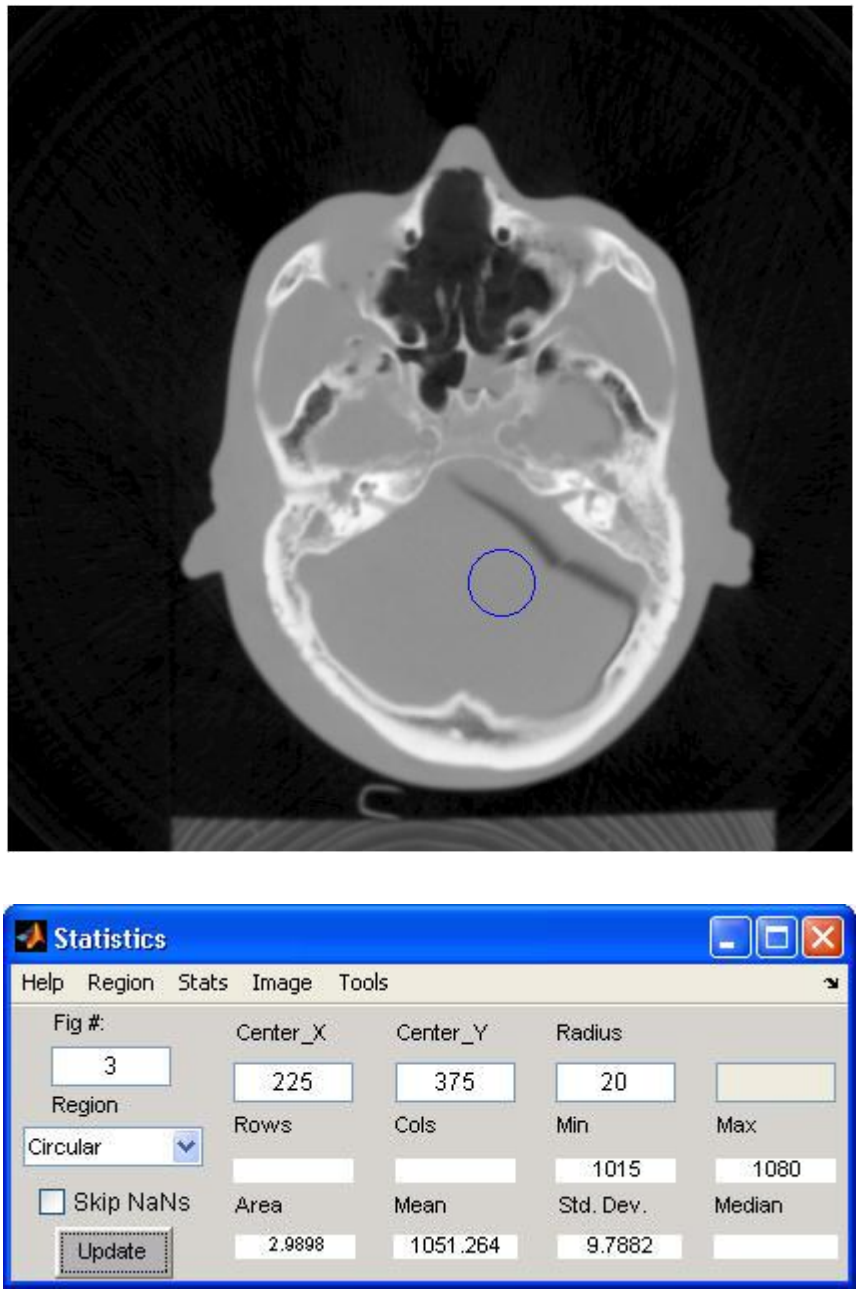

Figure 36: Head Phantom Using Standard Interpolation with ROI and Statistics (#2)

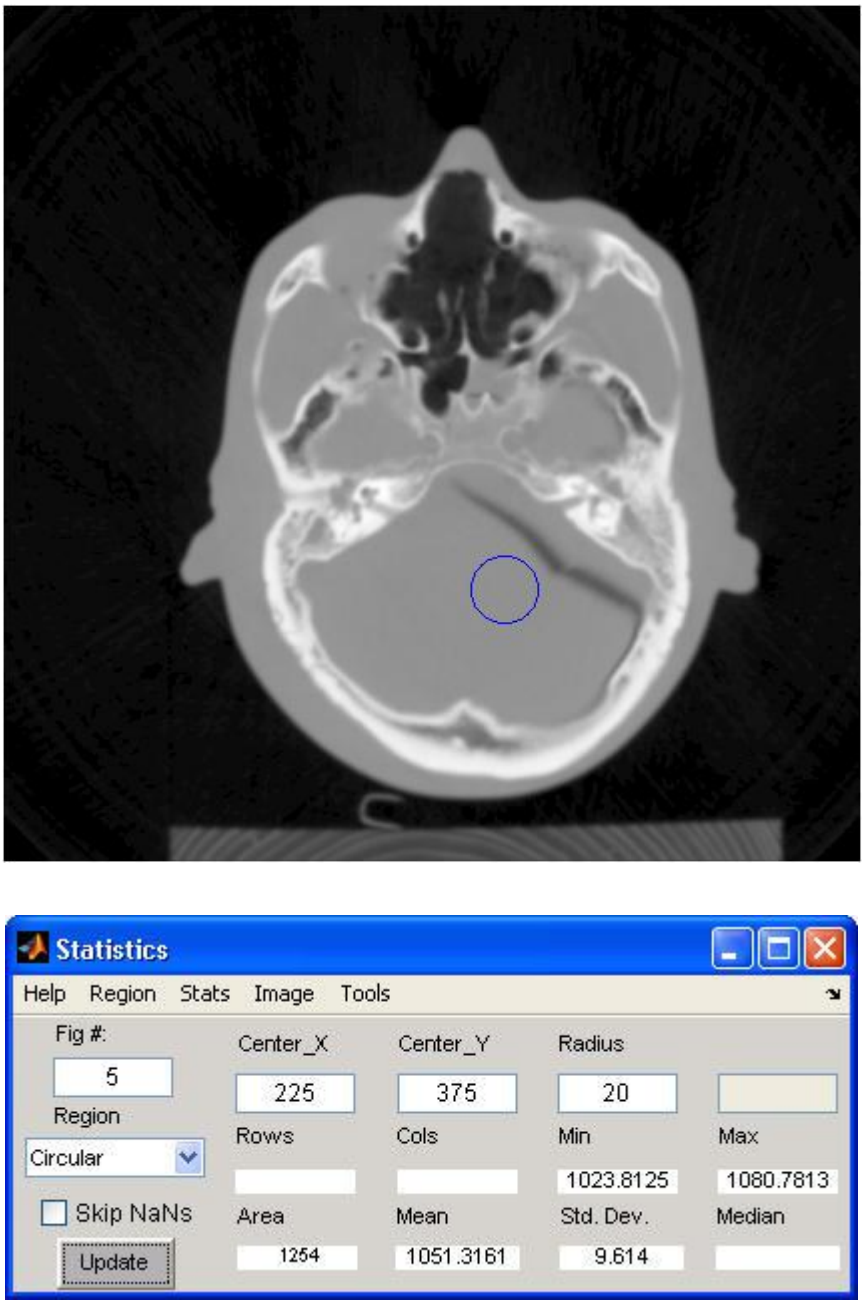

Figure 37: Head Phantom Using Partial Data Interpolation with ROI and Statistics(#2)

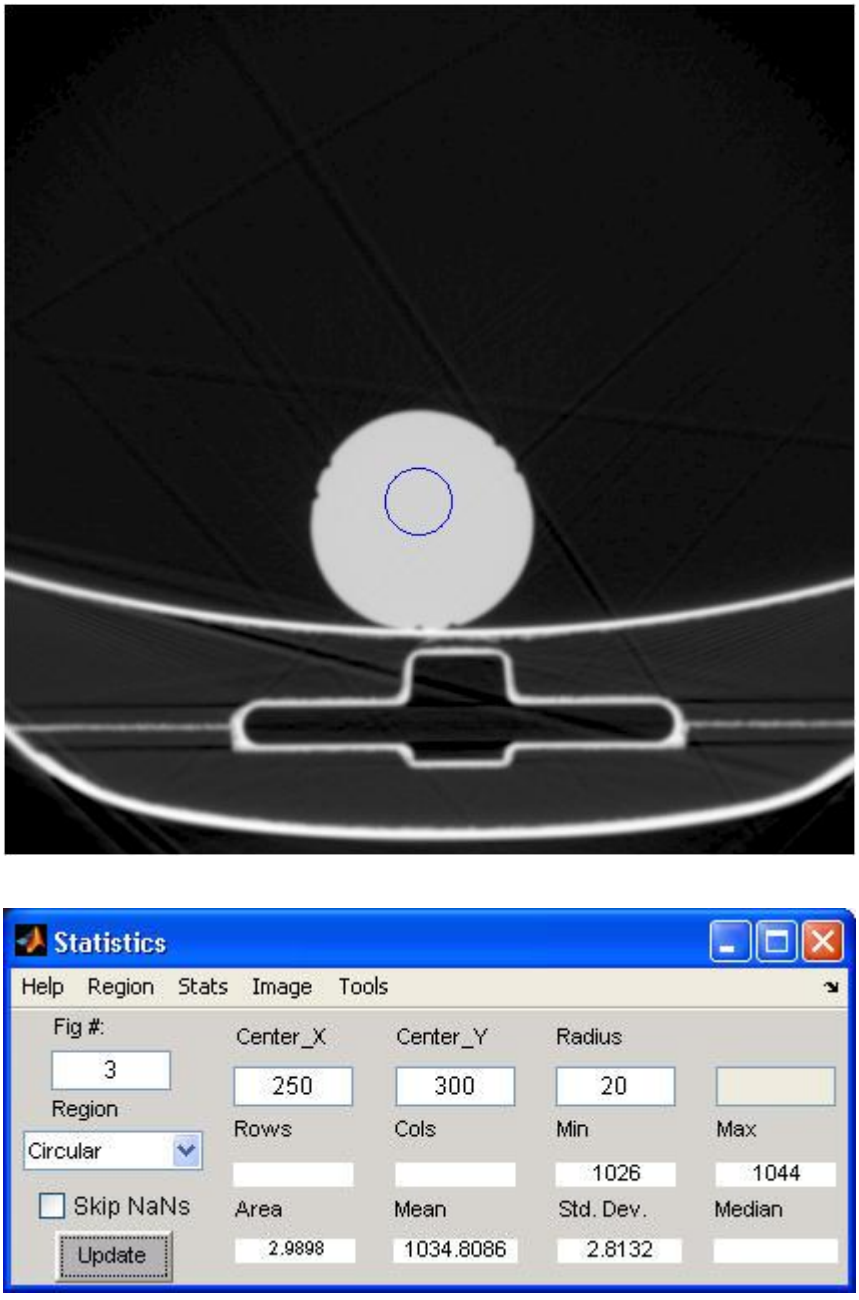

Figure 38: Water Bottle Scan Using Standard Interpolation with ROI and Statistics (#2)

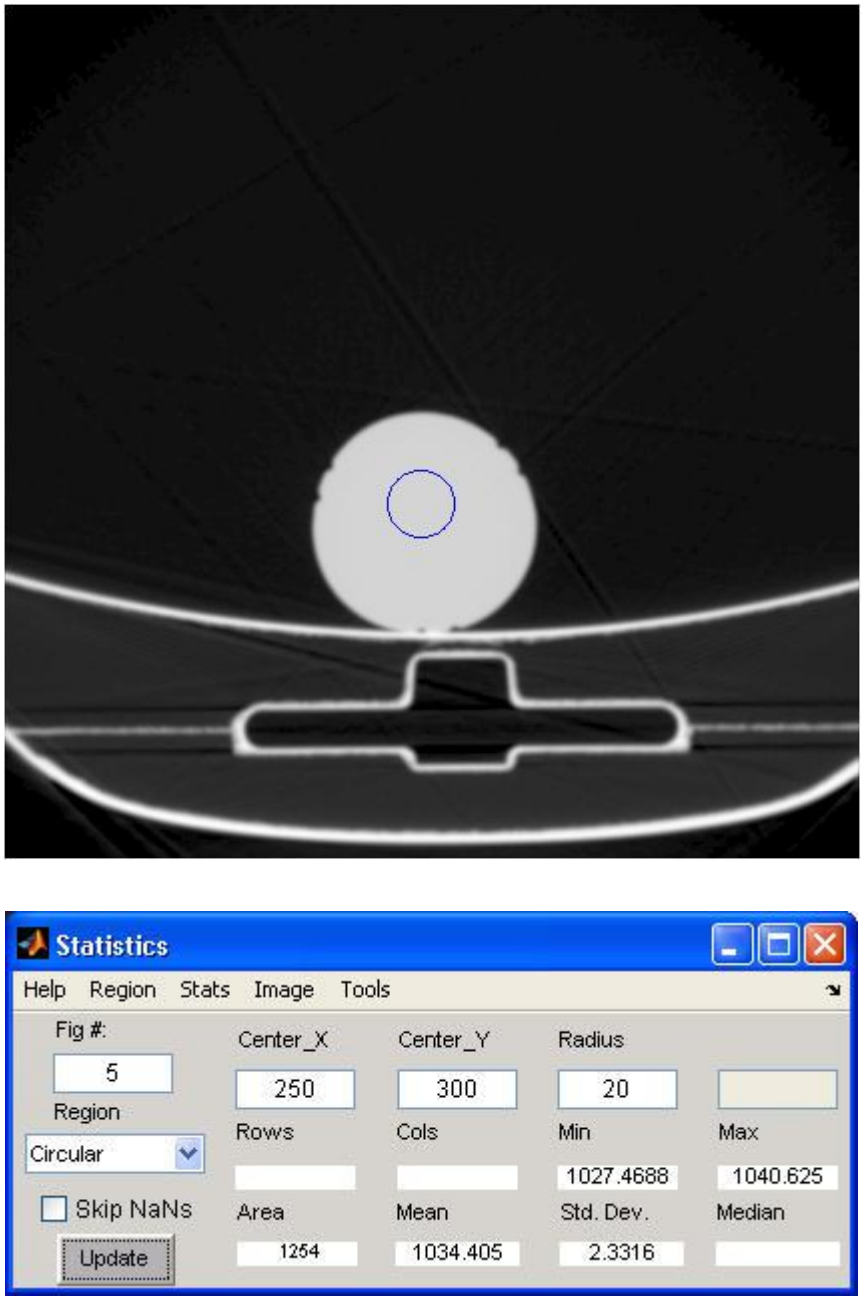

Figure 39: Water Bottle Scan Using Partial Data Interpolation with ROI and Statistics (#2)

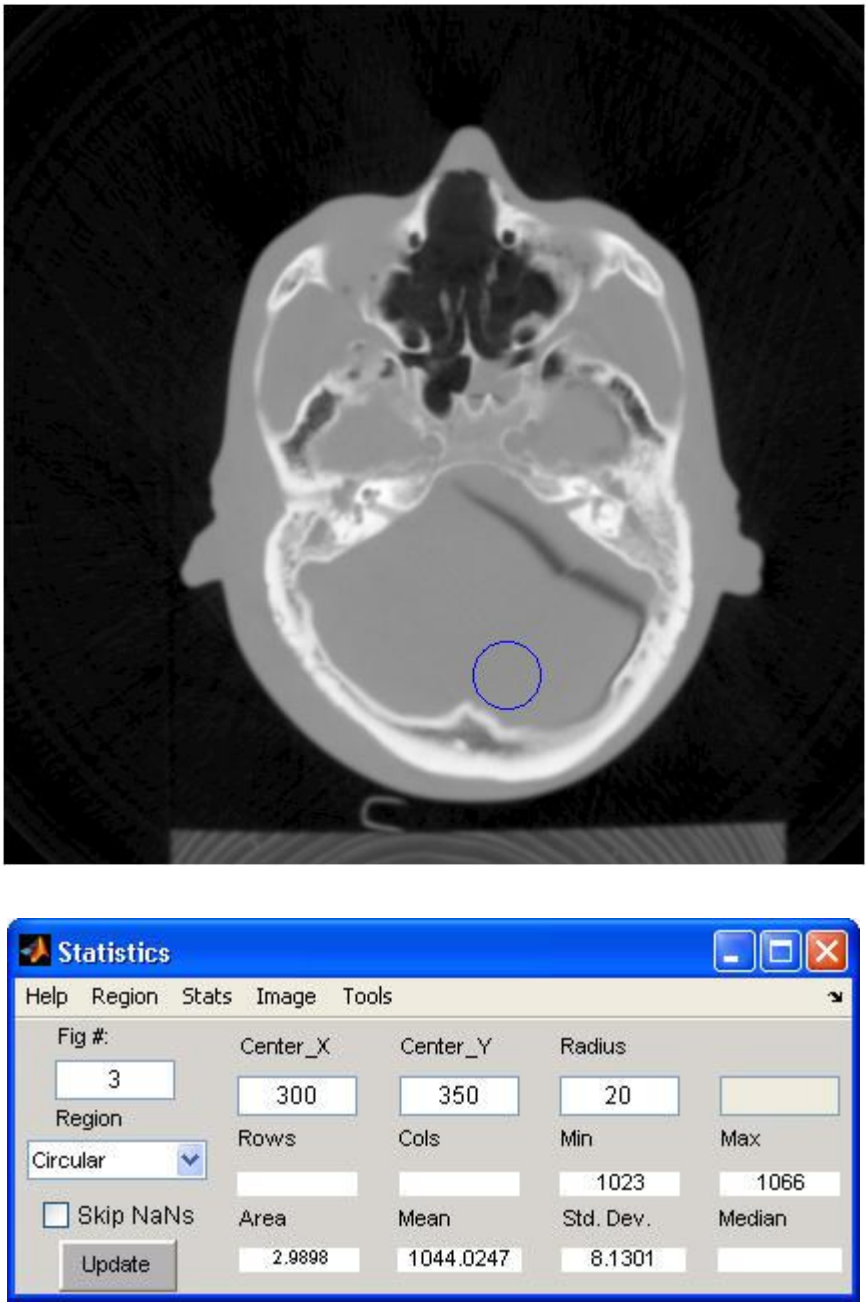

Figure 40: Head Phantom Using Standard Interpolation with ROI and Statistics(#3)

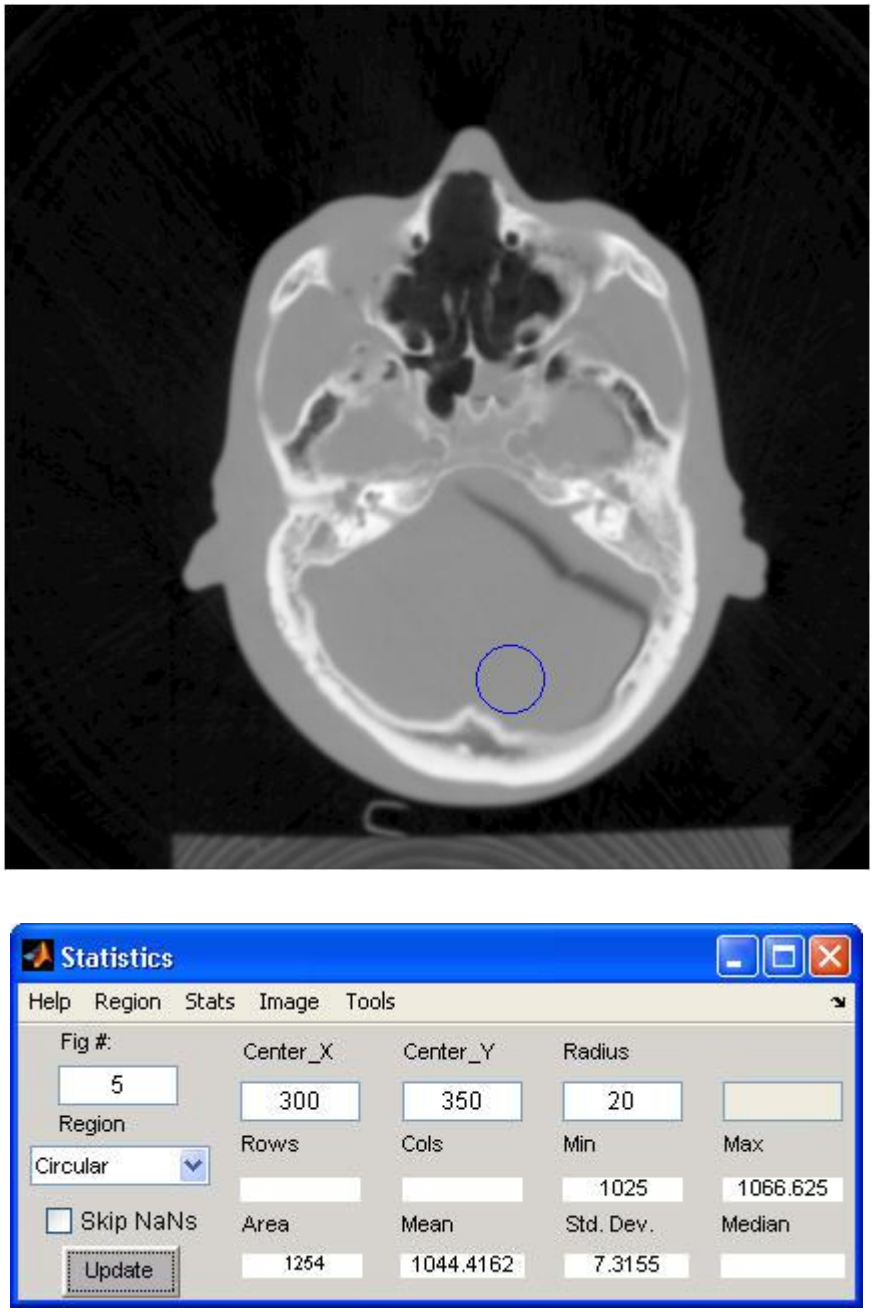

Figure 41: Head Phantom Using Partial Data Interpolation with ROI and Statistics(#3)

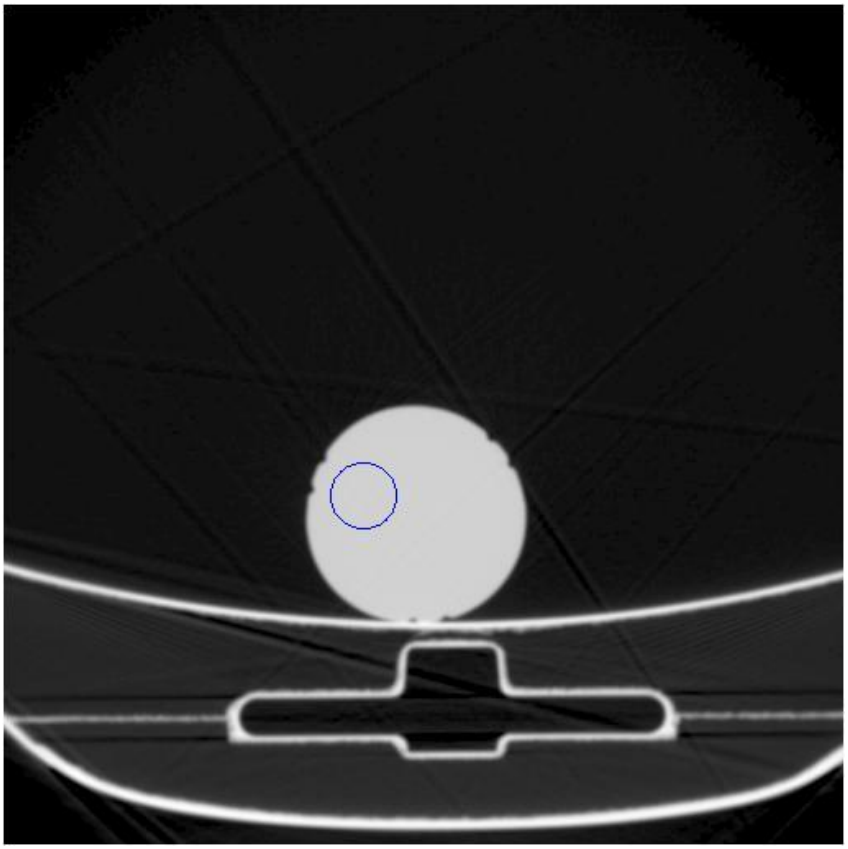

Figure 42: Water Bottle Scan Using Standard Interpolation with ROI and Statistics (#3)

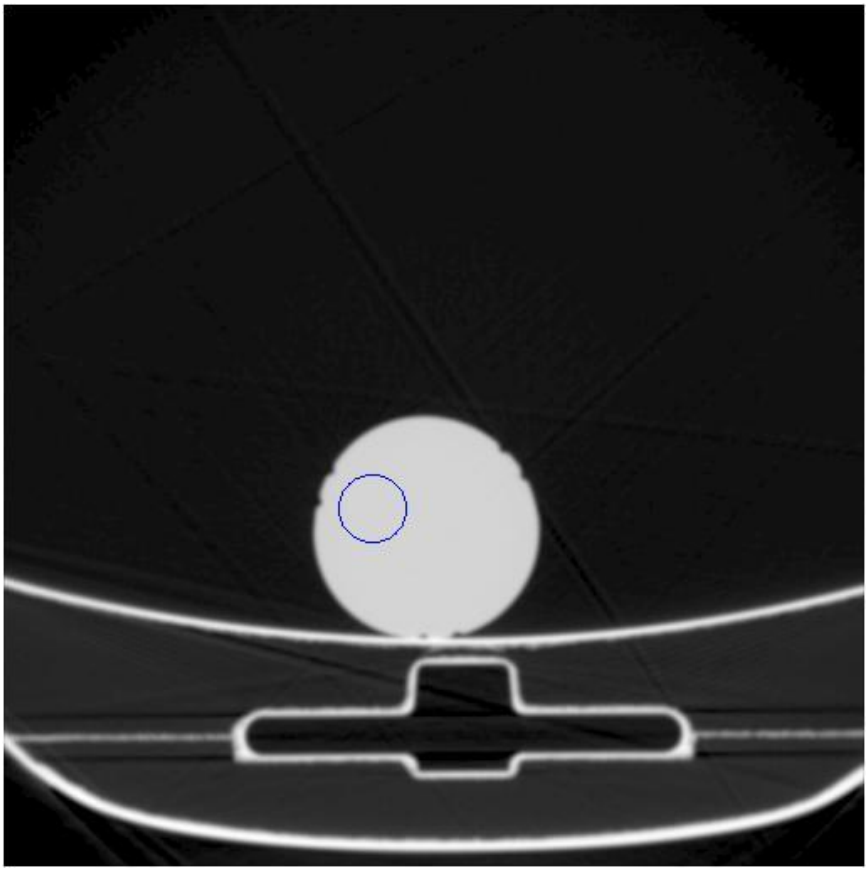

Figure 43: Water Bottle Scan Using Partial Data Interpolation with ROI and Statistics (#3)

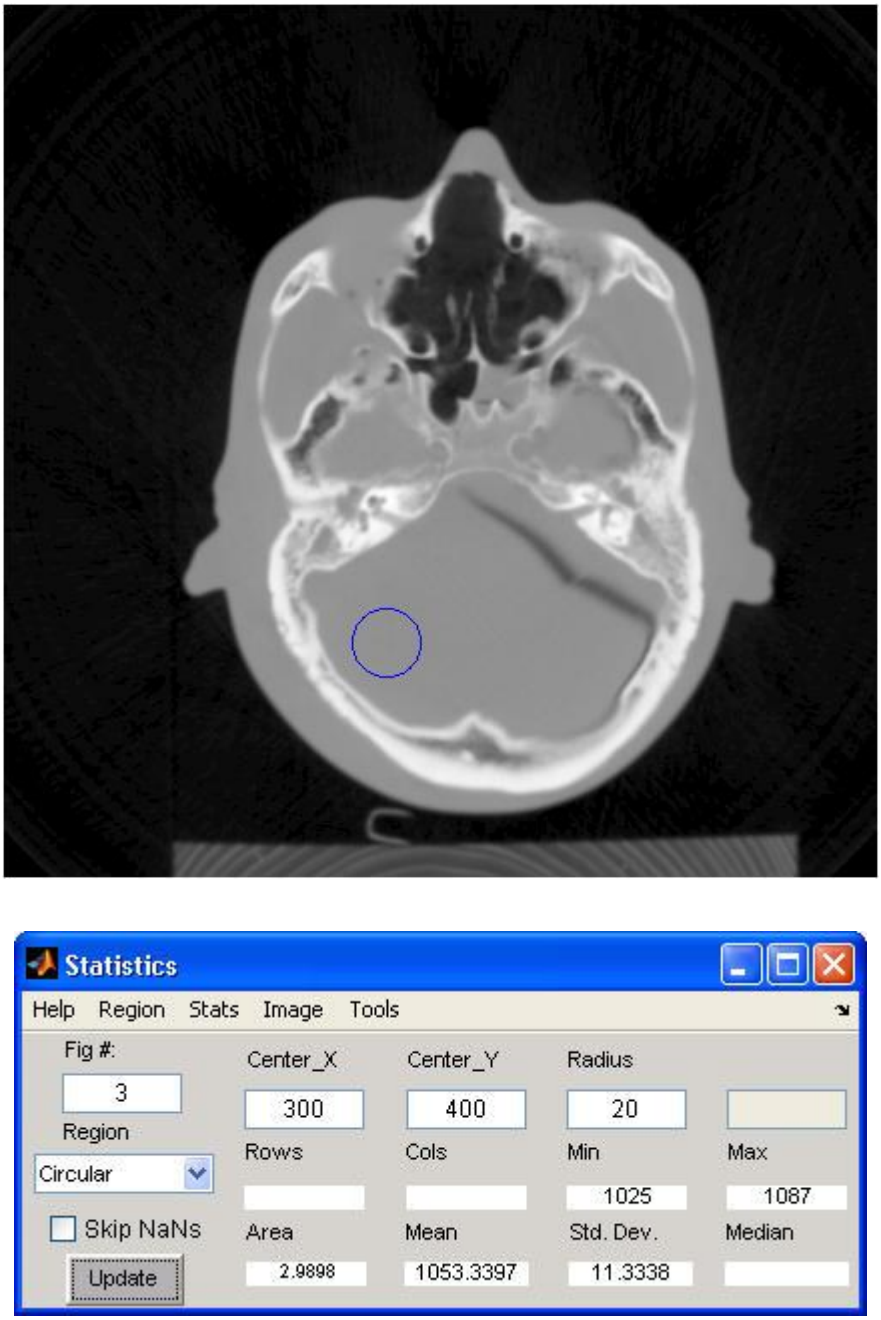

Figure 44: Head Phantom Using Standard Interpolation with ROI and Statistics(#4)

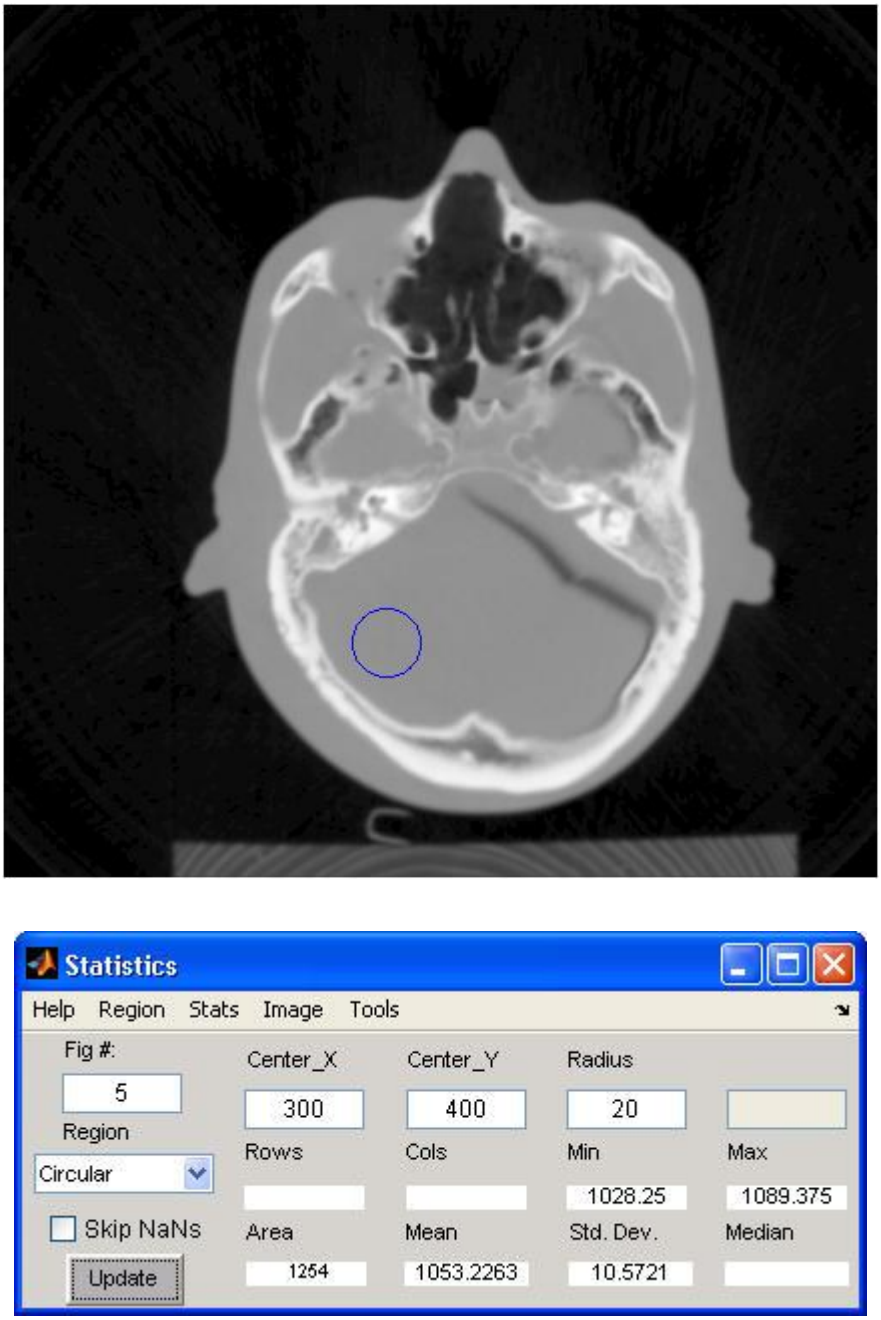

Figure 45: Head Phantom Using Partial Data Interpolation with ROI and Statistics(#4)

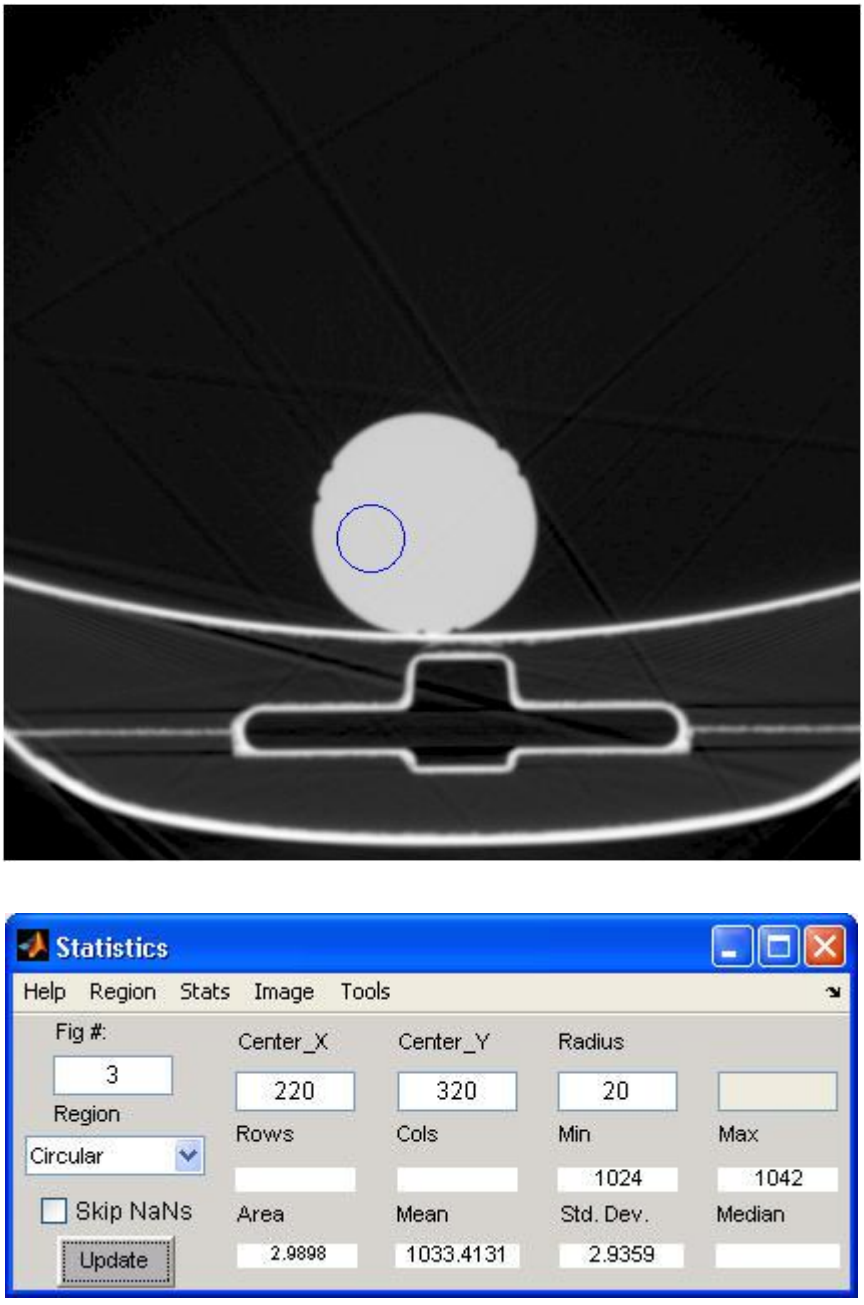

Figure 46: Water Bottle Scan Using Standard Interpolation with ROI and Statistics (#4)

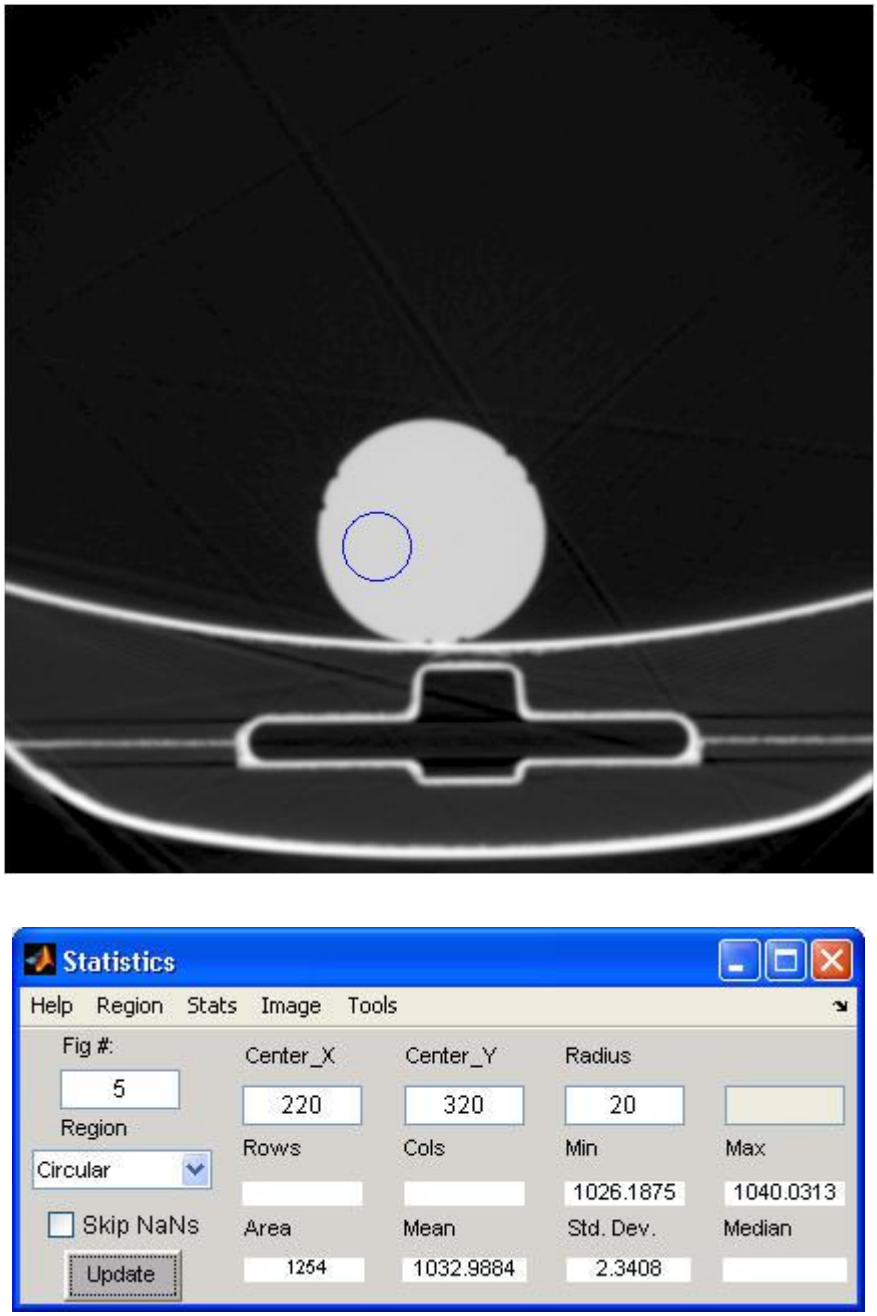

Figure 47: Water Bottle Scan Using Partial Data Interpolation with ROI and Statistics (#4)

Mathcad file for solving for *a, b* & *c* with respect to Voltage and µt

This is the one used for 5 cm of water, as an example.

5 cm

kv := 60.. 140

n

a := 1

b := 2

c := 3

Given

$$1.3173 = \frac{a}{(60 - b)^{.5}} + c$$

$$1.1034 = \frac{a}{(100 - b)^{.5}} + c$$

$$1.026 = \frac{a}{(140 - b)^{.5}} + c$$

$$\text{Find}(a, b, c) = \begin{pmatrix} 3.029 \\ 33.129 \\ 0.733 \end{pmatrix}$$

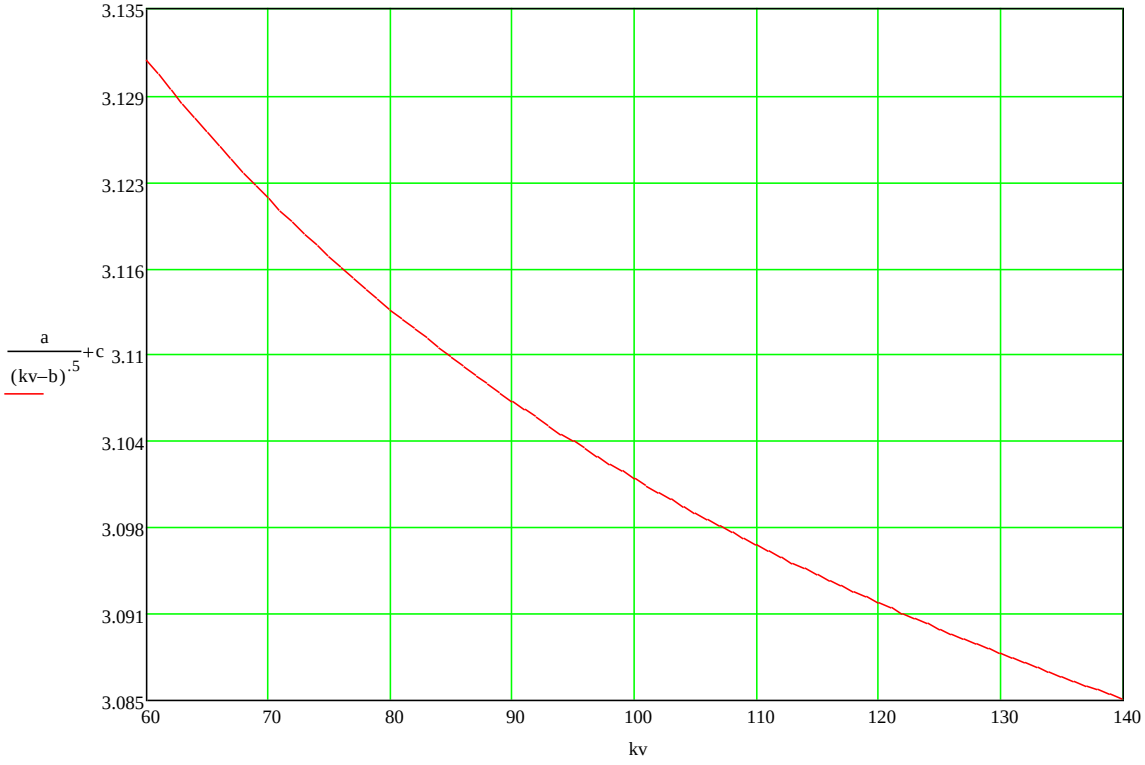
3.135
3.129
3.123
3.116
3.11
3.104
3.098
3.091
3.085
a
(kv–b)^.5 +c
60
70
80
90
100
110
120
130
140
kv

Figures 48 through 54 show pictures of various parts of the CT system used to implement the partial-data algorithm for this research.

Figure 48: Philips Brilliance® iCT Scanner with a Head Phantom

Figure 49: Close-up View of Head Phantom Placed for Scanning

Figure 50: Head Phantom Used for this Research

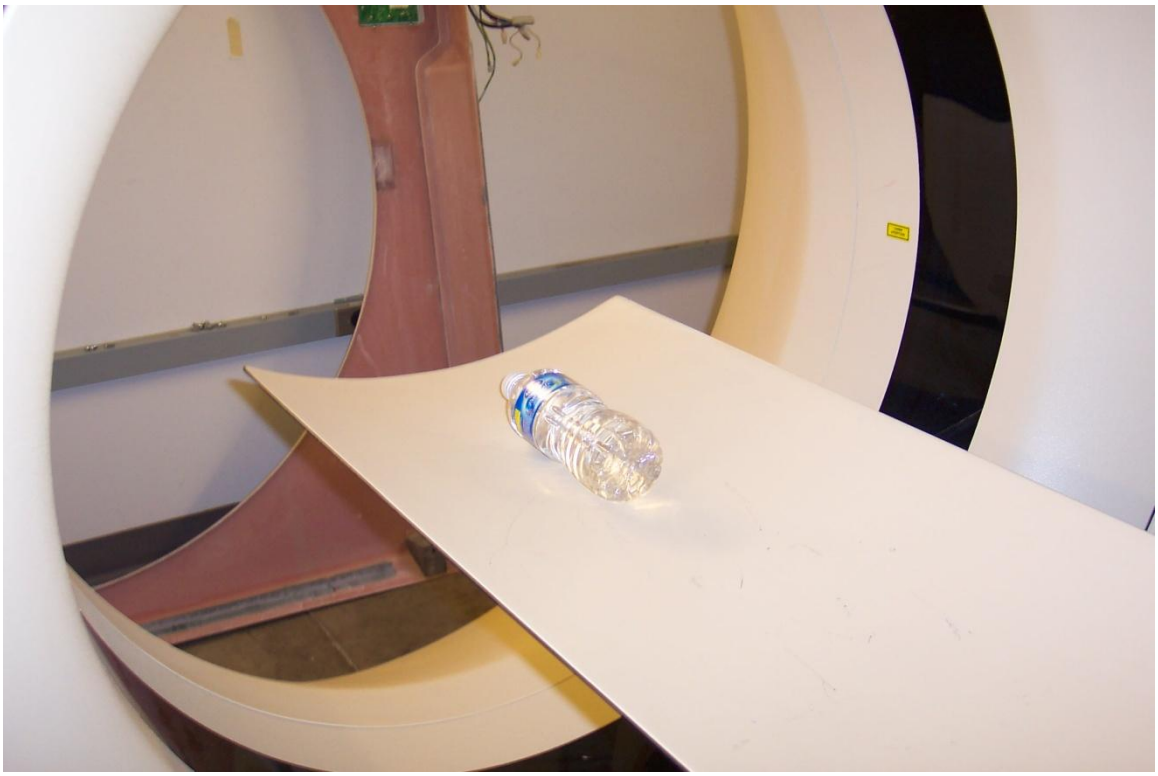

Figure 51: Water Bottle Placed for Scanning

Figure 52: Copper Strips Used for Voltage Detection (Two 1 mm Strips)

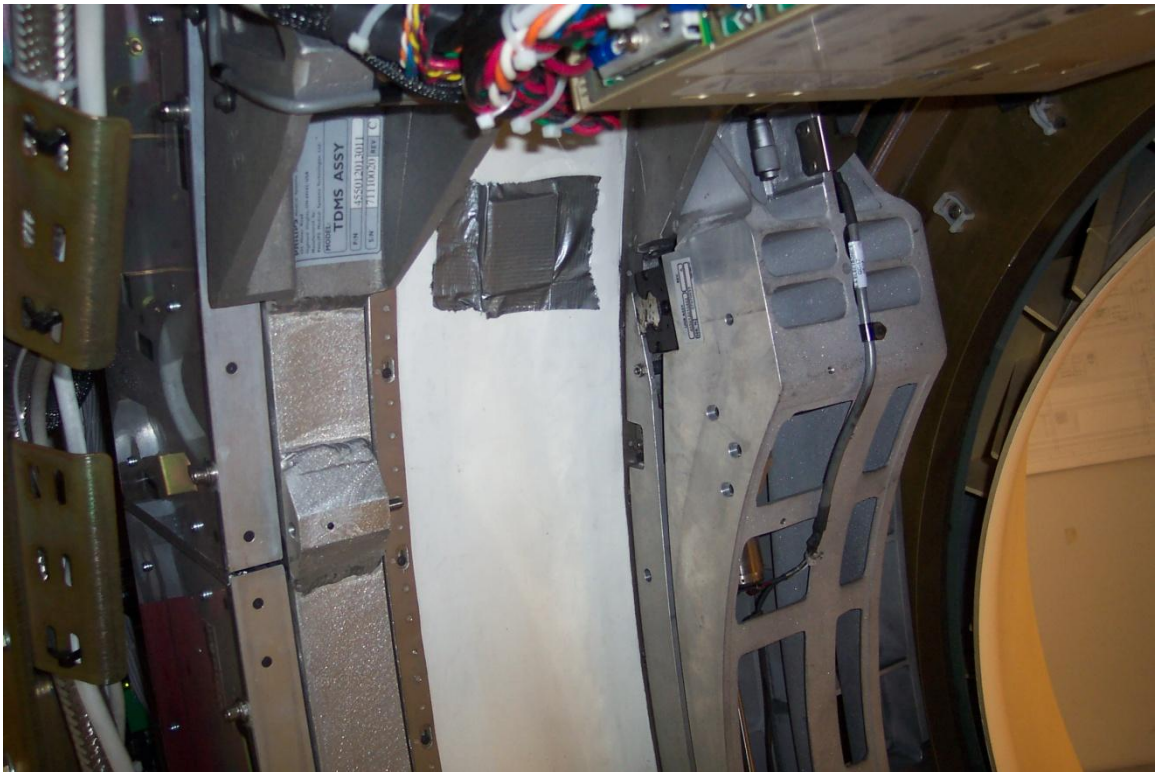

Figure 53: Copper Strips Taped to End of Detector System

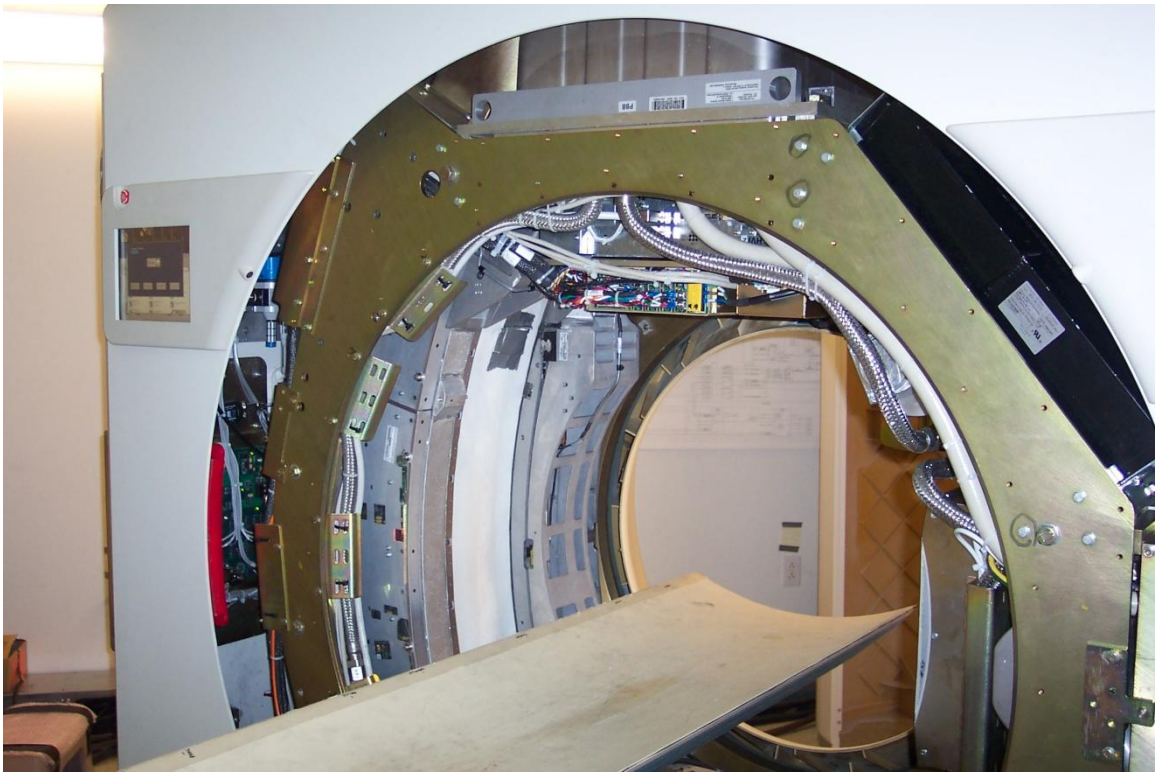

Figure 54: View of System with Copper Strips on Detector Module